UNIVERSITÀ DEGLI STUDI DI SALERNO
Dipartimento di Farmacia

Dottorato di ricerca
in Scienze Farmaceutiche
Ciclo XIV   —   Anno di discussione 2016

Coordinatore: Chiar.mo Prof. *Gianluca Sbardella*

Biomolecular and Biophysical approaches to interrogate epigenetic targets: a platform for drug discovery

Settore scientifico disciplinare di afferenza: CHIM/08

Dottorando	Tutore
Dott. *Alessandra Feoli*	**Chiar.mo Prof.** *Gianluca Sbardella*
	Co-tutore
	Chiar.mo Prof. *Alessandra Tosco*

II

INDEX

ABSTRACT

The term epigenetics refers to heritable changes in gene expression that do not involve changes in the DNA sequence. A large number of enzymes, which act mainly on histone tails and DNA, carries out epigenetic modifications, influencing several biological mechanisms.

The interplay between epigenetic enzymes and chromatin is highly complex, and despite great progress has been made in understanding the role of these proteins in biological contexts, much remains still unknown. On the other hand, it is widely reported that specific epigenetic modifications are associated with disease states, therefore epigenetic enzymes represent potential therapeutic targets. However, the lack of specific and robust screening methods to evaluate epigenetic enzyme activity limits the identification and development of epigenetic modulators.

In this scenery, this thesis is focused on the development of a robust and widely usable combined screening platform to identify small-molecule modulators of epigenetic proteins. Different biochemical and biophysical techniques were used in order to evaluate potency, selectivity, binding and mechanism of action of the modulators synthesized in the Epigenetic Medicinal Chemistry Laboratory (EMCL).

As model systems, among all the epigenetic enzymes, the attention was focused on the acetyltransferase p300, the methyltransferase SETD8 and the readers Tudor domains of PHF20. By the use of a combined approach, a set of small-molecule modulators was identified. These compounds could be used as chemical probes to further investigate the biological role of these enzymes and their implications in physiological and/or pathological processes.

1. INTRODUCTION

1.1 Epigenetics

The concept of *Epigenetics* was pioneered by Conrad H. Waddington in 1942 as "the branch of biology which studies the causal interactions between genes and their products, which bring the phenotype into being." *Epi* comes from the Greek word *over*, and thereby epigenetics is the study of the molecular, cellular, and environmental aspects of heredity, which are not explained by simple changes in the underlying DNA sequence. In fact, epigenetic processes influence the chromatin structure but not the gene sequence. Unlike somatic mutations and other genetic alterations which irreversibly alter the genes, epigenetic processes are reversible and thus provide environmental plasticity and cell adaptation to new microenvironments. Moreover, the chromatin structure has an intrinsic memory and it is transmitted over cell generations.[1]

Chromatin is made up of building blocks called nucleosomes. Each nucleosomal unit contains an octamer of four histone proteins (H2A, H2B, H3 and H4) around which genomic DNA is wound almost twice. The nucleosomes undergo recurrent structural rearrangements through DNA unwrapping, rewrapping, and histone core disassembly and assembly, and they are subject to covalent modifications. These modifications, called epigenetic marks, have been identified on both DNA and histones. Whereas DNA can primarily be methylated, histones are capable of carrying a wide array of Post-Translational modifications (PTMs). A large number of PTMs have been discovered on the histone tails that protrude from the nucleosomal core and are freely accessible to epigenetic enzymes.[2]

Histone modifying proteins have been categorized as "writers", "erasers" or "readers" (Figure 1.1). Writers are those epigenetic enzymes that lay down epigenetic marks on amino acid residues on histone tails while erasers catalyse

the removal of these marks. Readers are those proteins that contain domains that recognize these histone marks and bind to them.
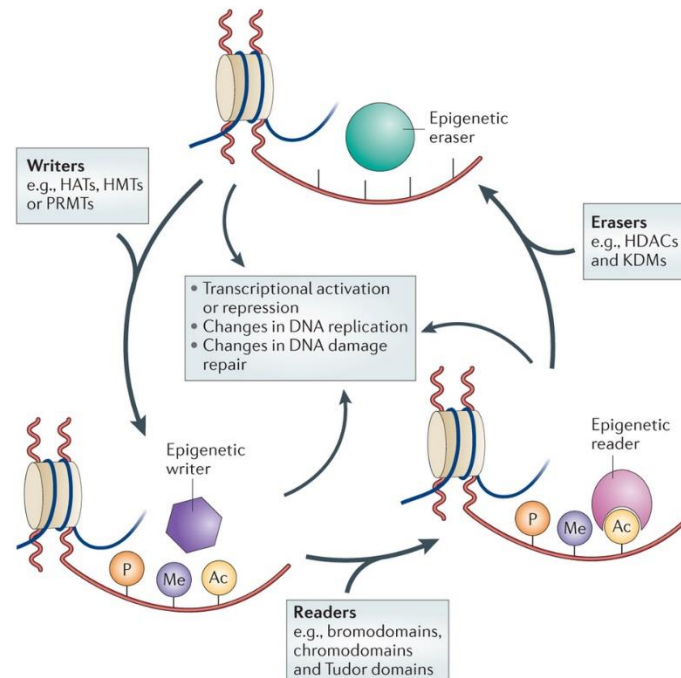
Figure 1.1: Schematic representation of the main mechanisms for epigenetic modifications.

1.2 Epigenetic Writers

Epigenetic writers are chromatin-associated proteins that catalyse the deposition of the PTMs mainly on histone tails and introduce dynamic modifications that respond rapidly to environmental changes.[3]

Among all the possible chemical modifications that can be introduced (methylation, acetylation, phosphorylation, ubiquitination, sumoylation, propionylation, butyrylation, crotonylation, ADP-ribosylation, citrullination), histone acetylation and methylation are the most abundant and widely studied. These modifications are carried out by Acetyltransferases and

Methyltransferases respectively, which are able to modify both histone and non-histone substrates.

1.2.1 Lysine Acetyltransferases (KATs)

Lysine Acetyltransferases (KATs) mediate the transfer of an acetyl group from acetyl coenzyme A (acetyl-CoA) to the ε-amino groups of lysine residues in histones and other proteins. After the acetylation, the positive charge of lysine is neutralized and, in the case of histones, the interaction with the negatively charged DNA backbone is diminished, producing an open chromatin status that is responsible for the promotion of gene expression.[3]

KATs have been classified into type A, which are nuclear proteins that acetylate chromatin-associated proteins and histones, and type B, which are located both in the nucleus and in the cytoplasm and acetylate newly synthesized cytoplasmic histones to promote their nuclear localization and deposition onto nascent DNA chains. While KAT1 is the only KAT in the type B group,[3] type A KATs can be classified into different families by structural homology and biochemical mechanism of action. Despite several KAT families have been identified, only four have been extensively studied: the Gcn5-related N-acetyltransferase (GNAT) family (KAT2),[4] the E1A-associated 300 kDa protein (p300)/CREB-binding protein (CBP) family (KAT3), the MYST family (KAT6)[5] and the regulation of Ty1 transposition gene product 109 (Rtt109) family (KAT11).

Among all the above-mentioned acetyltransferases, one of the most interesting protein is p300, which is a key enzyme in higher eukaryotes where it acts as an effector in several signalling pathways. Because of its fundamental role in different biological functions, this protein is the first target on which this thesis has been focused.

1.2.1.1 p300/CBP

p300 and CBP are two acetyltransferase enzymes expressed in humans and most higher eukaryotes. p300 (also called EP300 or KAT3B) is so-named because it

is about 300 kDa in size (with 2414 amino acids). p300 was firstly reported in 1985 and 1989 in studies looking for proteins that bind E1A, an adenoviral oncogenic transcription factor. Meanwhile, CBP (also called CREBBP or KAT3A) is composed of 2441 amino acids and was reported for the first time in 1993 in a study of proteins that bind CREB, a transcription factor that binds cAMP response elements (CREs). Because of the high sequence homology between CBP and p300, together with the little sequence homology between them and other acetyltransferases in the human genome,[6] the two proteins are now collectively referred to as p300/CBP and classified as a separate family class of KATs.

Despite they were first identified for their binding to E1A (p300) and CREB (CBP), it has been later demonstrated that these two proteins contribute to transcriptional regulation through their histone acetyltransferase activity.

p300 and CBP contain several protein interaction domains (Figure 1.2); in particular, the structure of their HAT domain suggests a "hit and run" (Theorell-Chance) catalytic mechanism in which, after binding of acetyl-CoA, the lysyl residue of the substrate peptide snakes through the p300 tunnel and reacts with the acetyl group. Interacting with a large number of transcription factors, CBP and p300 are involved in different cellular processes and misregulation of their activity is frequently implicated in many human diseases.
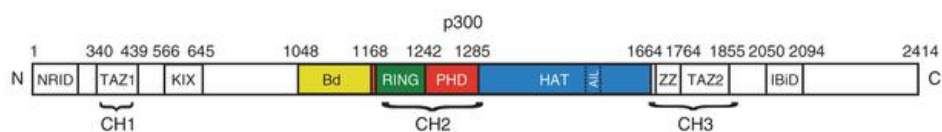
Figure 1.2: Domain architecture of p300. NRID, nuclear receptor interaction domain; TAZ1, transcriptional adaptor zinc-finger domain 1; KIX, kinase-inducible domain of CREB-interacting domain; Bd, bromodomain; RING, really interesting new gene; PHD, plant homeodomain; HAT, histone acetyltransferase domain; ZZ, ZZ-type zinc-finger domain; TAZ2, transcriptional-adaptor zinc-finger domain 2; IBiD, IRF3-binding domain.

Modifications to histone lysines associated to p300/CBP have been studied as a major factor in cancer pathogenesis, but they also play a role in neurodevelopmental disorders, neurodegenerative, autoimmune and cardiovascular disease, metabolic and psychological disorders. [7, 8]

For instance, mutations in the CBP (rarely p300) gene causes Rubinstein-Taybi syndrome, characterized by a short stature, moderate to severe intellectual disability, distinctive facial features, and broad thumbs and first toes. Moreover, CBP and p300 were demonstrated to be involved in hematopoietic homeostasis, such that mutations in the CBP/p300 interaction domain of different transcription factors were found in hematologic malignancies and chromosomal translocations involving CBP or p300 genes are associated with leukemia and lymphomas. CBP and p300 promote prostate cancer progression by activating androgen receptor-regulated transcription and colon cancer progression by microsatellite instability and they are involved in the development of drug resistance. [8]

The inhibitors of CBP/ p300 described so far are of two types: the compounds that inhibit the binding of other proteins targeting the interacting domains and the derivatives that directly affect the acetyltransferase activity. To the first class belong the bromodomain-interacting molecules, such as the 5-isoxazolylbenzimidazoles recently reported as potent and selective ligands, those targeting the TAZ1 domain, such as chetomin, and those (namely sekikaic acid and lobaric acid) targeting the KIX domain. The second class inhibits the enzymatic activity of the HAT domain; in addition to many non-selective inhibitors (e.g., the natural products anacardic acid,[9] garcinol,[10] curcumin,[11] plumbagin,[12] and their analogues or semisynthetic derivatives), the only selective p300 HAT inhibitors described to date are the bisubstrate inhibitor Lys−CoA conjugate,[13] which is not cell permeable, the pyrazolone C646,[14] described as competitive versus acetyl-CoA and noncompetitive versus a

histone substrate, and the isogarcinol derivative LTK14,[15, 16] again not very cell permeable and hardly optimizable due to its structural complexity.

For all the above considerations, there is still need for selective modulators of CBP/p300 activity not only as useful tools to dissect the role of their physiological and pathological role but also as potential leads for the development of drug candidates for specific diseases.[17-19]

1.2.2 Protein Methyltransferases (PMTs)

The protein methyltransferases (PMTs) catalyse methyl transfer from their universal methyl donor, *S*-adenosyl-L-methionine (SAM), to a nitrogen atom of lysine or arginine side chains forming *S*-adenosyl-L-homocysteine (SAH) as a byproduct of their mechanism.

In contrast to acetylation, histone methylation does not affect chromatin structure directly because this chemical modification does not change the charged state of an amino acidic residue. Depending on each specific residue, methylation is associated with activated euchromatic genes or with silenced heterochromatic genes. Moreover, each type of methyl mark represents a specific modification that is recognized as a docking site for chromatin-associated proteins that maintain chromatin architecture or regulate gene expression.[3]

The PMT enzyme class is composed of two distinct families of enzymes, based on their active site structure and on the amino acid to which they transfer methyl groups: the protein arginine methyltransferases (PRMTs) and the protein lysine methyltransferases (PKMTs). There is one exception to this general structural bifurcation of the PMT class: the enzyme DOT1L acts as a lysine methyltransferase, but its active site structure is most closely aligned with that of the protein arginine methyltransferases.[20]

1.2.2.1 Arginine Methyltransferases (PRMTs)

Arginine methylation is a common post-translational modification that has been implicated in signal transduction, gene transcription, DNA repair and mRNA splicing, among others.

Three types of methyl arginine species exist: ω-NG-monomethyl-arginine (MMA), ω-NG,NG-asymmetric dimethyl-arginine (ADMA) and ω-NG,N'G-symmetric dimethyl-arginine (SDMA).

Protein arginine methyltransferases are classified into type I or type II, according to modification types: although all PRMTs catalyse the formation of a monomethyl-arginine intermediate, type I PRMTs (PRMT1, 2, 3, 4, 5, and 8) can catalyse the production of asymmetric dimethyl-arginine, and type II PRMTs (PRMT5 and 7) are able to catalyse the production of symmetric dimethyl-arginine.[21]

1.2.2.2 Lysine Methyltransferases (PKMTs)

Histone lysine methylation is a marker of both transcriptionally active and inactive chromatin, depending on the residue that is methylated, its degree of methylation (mono-, di-, or trimethylation), and its position within the gene and in the genome. Except for DOT1L and WRAD complex,[22] all known PKMTs contain a conserved SET (Su(var)3-9, Enhancer of Zeste, Trithorax) domain harbouring the enzymatic activity.[23] To date, more than 50 PKMTs have been identified and characterized. On the basis of sequence homology, SET-containing KMTs can be divided into different subfamilies: the SUV39 family, the EZH family, the SET2 family, the PRDM family and the SMYD family.[24]

Several studies demonstrated that many SET domain PKMTs catalyse site-specific methylation of lysine residues in non-histone proteins, including transcription factors and other chromatin modifying enzymes, illustrating that lysine methylation is a widespread post-translational modification in signal transduction.[25]

Among the several PKMTs identified so far, SETD8 is the second enzyme on which this thesis is focused. In the following paragraph there will be a brief description of its mechanism of action and its implication in biological processes.

1.2.2.2.1 SETD8

SETD8 (also known as PR-Set7, SET8, or KMT5A) is the sole mammalian enzyme known to catalyze the monomethylation of histone H4 Lys20 (H4K20me1). SETD8 protein expression is tightly regulated during the cell cycle, being highest during G_2/M and early G_1 and nearly absent during S phase. SETD8 activity is essential in cell cycle progression and in the DNA damage response and it has been associated with mitotic chromosomes during cell division. SETD8 promotes transcriptional repression and mediate transcriptional activation. Recently, a direct involvement of H4K20me1 modification in the assembling of the pre-replication complex (pre-RC) on the replication origins of metazoans was demonstrated, highlighting the important role of SETD8 in this process. Besides H4K20, SETD8 methylates p53 at lysine residue 382, preventing p53 promoter binding and thereby inhibiting apoptosis. In regard to its function and role in human diseases, SETD8 is overexpressed in different types of cancer tissues and cancer cell lines including bladder cancer, non-small cell and small cell lung carcinoma, chronic myelogenous leukemia, hepatocellular carcinoma and pancreatic cancer. Furthermore, SETD8 is implicated in cancer invasiveness and metastasis through its interaction with TWIST, a master regulator in epithelial-mesenchymal transition (EMT). [26-28]
Selective SETD8 inhibitors would serve as useful chemical probes to further investigate the cellular effects of SETD8 inhibition in both normal and diseased cells and as lead structures for the development of anticancer therapeutics. However, only few inhibitors have been reported so far for this enzyme.[29-33]

Very recently, three quinone-containing inhibitors endowed with cellular activity were identified from a high-throughput screening campaign, yet they irreversibly inhibit the enzyme, probably by a covalent bond with a Cys residue.[29] These consideration prompted the research to the development of new small-molecule scaffolds for SETD8 inhibition.

1.3 Epigenetic Erasers

The erasers are enzymes responsible for the specific removal of epigenetic marks deposited by writers. Epigenetic erasers are classified in several groups of enzymes and the most studied ones are histone demethylases (HDMs) and histone deacetilases (HDACs).

1.3.1 Histone Demethylase (HDMs)

Until a decade ago, histone methylation, together with DNA methylation, was considered a stable chemical modification. This view changed with the discovery of lysine-specific demethylase 1 (LSD1) and the identification of the JMJC domain-containing lysine demethylase family. Several members of the histone demethylase family appear to be genetically amplified and overexpressed in some human tumours and these findings make the histone demethylases very interesting targets for drug discovery.

1.3.2 Histone Deacetylase (HDACs)

HDACs are enzymes responsible for the removal of the acetyl group of lysine residues in histones. After histone deacetylation, the positive charge of lysine is restored, promoting the condensation of chromatin and consequently transcriptional repression. HDACs are divided into five classes based on their phylogenetic comparison with yeast enzymes. Class I comprises HDAC1, HDAC2, HDAC3 and HDAC8; class IIa consists of HDAC4, HDAC5, HDAC7 and HDAC9; class IIb includes HDAC6 and HDAC10; class III comprises the

sirtuins from SIRT1 to SIRT7; and class IV contains only HDAC11. Enzymes from classes I, II and IV require a zinc ion for catalysis, whereas sirtuins are NAD^+ dependent enzymes with protein deacetylase and ADP ribosylase activity.[3]

More than 10 years ago, it was discovered that deregulation of HDAC activity in association with chromosomal translocation was involved in the stimulation of leukemogenesis. To date, several studies have provided evidence of aberrant acetylation and altered expression of HDACs in cancer cells and tumour tissues. Therefore, using HDAC inhibition to reverse epigenetic aberrancies in cancer cells is a powerful approach for the treatment of several tumour types and four HDAC inhibitors are now approved: vorinostat[34] is used for cutaneous T-cell lymphoma and is being explored for treatment of other cancers, romidepsin[35] is used for peripheral and cutaneous T-cell lymphoma, belinostat[36] is used for the same lymphomas but can be used in combination with other drugs to treat ovarian cancer and panobinostat[37] is used for the treatment of multiple myeloma.

1.4 Epigenetic Readers

Epigenetic readers are specialized domains able to recognize and bind to specific epigenetic marks produced by the writers and erasers. Chromatin readers are able to identify not only different modified amino acids, but also different modification states of the same amino acid.

The most known reader domains of histone PTMs can be divided in different families able to recognize acetyl (Bromodomains) and methyl marks (Tudor, Chromo, MBT, PWWD and *plant agenet* domains, which belong to the "Royal Superfamily").

1.4.1 Bromodomains

Bromodomains bind to acetylated lysine and they are probably the best-characterized epigenetic readers. The structure of these readers is highly conserved. More than 50 bromodomain proteins are encoded by the human genome and they can be clustered in nine subfamilies according to sequence homology.[3]

A well-known example of a bromodomain family is the BET (Bromodomain and extraterminal domain family) that includes four protein members (BRD2, BRD3, BRD4 and BRDT), which contain a tandem bromodomain at the N-terminal.[38] These proteins play a decisive role in the regulation of transcription and cell growth; in addition, BET proteins are usually part of large nuclear complexes that are involved not only in transcription processes, but also in chromatin remodelling, replication and DNA damage. Hence, dysregulation of BET proteins has been reported in several diseases.[39]

1.4.2 The Royal Superfamily

The royal superfamily includes Tudor, Chromo, MBT, PWWD and *plant Agenet* domains; all the members of this superfamily possess a structurally related barrel-like protein fold, which is composed of 3 to 5 antiparallel β-sheets and forms the core structure. This conserved structure probably originated from a common ancestor that specifically recognized protein methylation. In distinct royal subfamilies, additional structural elements flanking the core structure contribute to the binding properties of its members. Members from each subfamily recognize either methylated lysine or methylated arginine residues in target proteins using a common binding mode, in which an aromatic binding pocket in the barrel accepts the methylated side chain. The pocket is usually composed of 2 to 4 aromatic residues, which provide electrostatic and hydrophobic contacts to accommodate the inserting methylated ligand.[40]

1.4.2.1 Tudor Domains

Among all the methyl readers of the Royal Superfamily, particularly interesting are the Tudor domains. Mammalian Tudor proteins can contain a single Tudor domain alone, multiple tandem Tudor domain repeats or one or more Tudor domains in conjunction with other types of domain. The Tudor protein family can be largely divided into two groups, one containing methyl-arginine binding Tudor domains and the other containing methyl-lysine binding Tudor domains. Most methyl arginine binding Tudor proteins are predominantly involved in RNA-related processes while methyl-lysine binding Tudor proteins are often implicated in chromatin biology, a general feature of the other royal superfamily members.[41]

Specifically, this thesis is focused on the recently identified Tudor domains of PHF20, which have a crucial role in the stabilization and activation of the tumour suppressor protein p53.[42]

1.4.2.1.1 Tudor Domains of PHF20

The PHD finger protein 20 (PHF20/GLEA2/HCA58) was initially described as an immunogenic antigen that elicits a strong antibody response in glioblastoma and adenocarcinoma patients. Later, it was shown that PHF20 can transcriptionally activate p53 and be downregulated through phosphorylation by the Akt kinase. PHF20 was also identified as a component of the "male absent on the first" (MOF) lysine acetyltransferase, which together with O-linked β-N-acetylglucosamine transferase, isoform 1 (OGT1) form the nonspecific lethal (NSL) complex.[42]

This protein is a component of some mixed-lineage leukemia (MLL) methyltransferase complexes with the core components MLL, ASH2L, WDR5 and RBBP5. PHF20 is a multidomain protein and it comprises two N-terminal Tudor domains, a central C2H2-link zinc-finger domain and a C-terminal zinc-binding PHD domain (Figure 1.4).
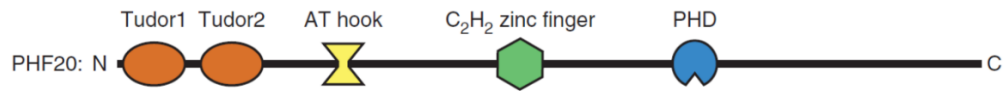
Figure 1.4: Domain architecture of PHF20.

Although little is known about its cellular role, the domain organization of PHF20 and its association with MLL core complexes suggest it to function as a transcription factor. Previous studies have indicated that the second Tudor domain is capable of binding methylated residues (preferentially dimethylated ones, one of the most common is H4K20me2) on histone tails, while no such function has been ascribed to the first Tudor domain.[43] Moreover, the second Tudor domain of PHF20 interacts specifically with p53 peptides monomethylated or dimethylated at Lys370 or Lys382.

Whether by mutation or overexpression, Tudor domains of PHF20 were found to be implicated in cancer and other diseases through aberrant binding of chromatin, which results in aberrant activation or repression of genes.

1.5 Epigenetics and Drug Discovery

Over the last decade, the cellular machinery that creates the epigenetic modifications has been the subject of intense scientific investigation. As previously discussed, epigenetics play a fundamental role in all the biological processes and modulating epigenetic mechanisms is highly relevant for many diseases. Because of the importance of epigenetic proteins in physiological and pathological processes, great efforts have been done in the discovery and development of small molecule modulators of chromatin modifying proteins. Despite all these efforts, to date only six *epi-drugs* are available in therapy (four inhibitors of HDACs and two of DNA methyltransferase) and few other modulators of some specific epigenetic proteins (EZH2, BRD4, LSD1, DOT1L) are currently in clinic phases. On the other hand, there is a large number of

enzymes for which no modulators have been reported. Therefore, despite recent advances in epigenetic modulators development, the challenge of identifying potent and selective molecules remains still open.

One of the main reasons that led to the lack of modulators is that not all the epigenetic enzymes are druggable, because of unfavourable pocket features as well as the competition with cofactors for targeting the active site.[44]

Proteins belonging to the families of HDACs, HDMs, HMTs and bromodomains are druggable, indeed robust and selective chemical probes are available to study these enzymes. On the other hand, for example, it has been very difficult to find potent, selective, and drug-like small molecule inhibitors of HATs. Beside the druggability, the identification and development of epigenetic modulators is also affected by the lack of specific and robust screening methods to evaluate their activity.

From a practical standpoint, developing assays to screen compound libraries for the identification of small-molecule modulators of epigenetic enzymes is not straightforward. In most cases, the primary screening is based on biochemical assays, which allow to evaluate the effect of the compounds on the activity of the enzyme. An ideal biochemical assay should reproduce the activity of the protein in the cellular context. However, many epigenetic targets exist as large complexes of proteins and, in some cases, these complexes are necessary for their activity, so the use of isolate proteins may be misleading. In addition, the substrates used are not always canonical histones (often peptides are preferred) and this choice could affect the results.

Cellular assays for epigenetic proteins have also proven to be somewhat complex. For many epigenetic targets, the effects of inhibitors in cell culture often take several days to see histone mark changes or effects on target genes, while phenotypic responses may require up to 7 to 10 days to be observed. In

addition, there is a lack of antibodies to detect effects on target proteins and even fewer for specific sites.[45]

In the following paragraphs, there will be an overview of the most widely used biophysical and biochemical methods in the drug discovery process for identification of epigenetic modulators.

1.6 Biophysical Methods

Biophysical methods are well-established in many areas of drug discovery. Application of these methods was once restricted to a relatively small number of scientists using specialized, low throughput technologies and methods. Now, automated high-throughput instruments are available in a growing number of laboratories.

Many biophysical methods are capable of measuring the equilibrium binding constants between pairs of interaction partners including protein-protein, protein-small molecule, and protein-nucleic acid interactions, and they can be used to measure the kinetic and/or thermodynamic components controlling biological processes in which they are involved. For a full characterization of a binding process, the determination of stoichiometry, the binding mode and any conformational change associated with such interactions are issues that should be addressed. The biophysical methods that are now available represent a powerful toolbox of techniques that can effectively deliver this full characterization. Biophysical methods are increasingly considered as a primary approach for hit finding. Among all, thermal-shift assay (mainly Differential Scanning Fluorimetry), calorimetry assays, optical biosensors and thermophoresis are techniques that have been recently successfully employed at this stage.[46]

1.6.1 Surface Plasmon Resonance (SPR)

Surface plasmon resonance (SPR) is a label-free detection method that has emerged during the last two decades as a suitable and reliable platform for biomolecular interactions. The technique allows the measurement of interactions in real-time with high sensitivity and without the need of labels, immobilizing target biomolecules on the sensor surface while a solution of ligand is flowed over the surface. Since it was first introduced in the early 1990s, SPR has been proven to be one of the most powerful technologies to determine specificity, affinity and kinetic parameters of a protein-ligand interaction.

Surface plasmon resonance occurs when a photon of incident light hits a metal surface (typically a gold surface). At the incidence angle of total internal reflection, a portion of the light energy couples with the electrons of the metal surface layer, which then oscillate with the light wave. The electrons moving are called plasmons, and they propagate parallel to the metal surface. The plasmon oscillation in turn generates an electric field whose range is around 300 nm from the boundary between the metal surface and sample solution. The defined SPR angle, at which resonance occurs, is dependent on the refractive index of the material near the metal surface. Consequently, when there is an interaction between the target biomolecules immobilized onto the surface and the analyte solution, a small change in the reflective index occurs and it is detected (Figure 1.6.1).[47]

Nature Reviews | Drug Discovery
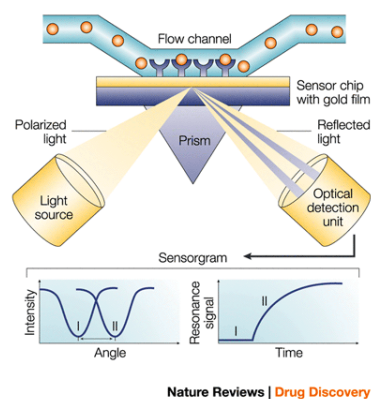
Figure 1.6.1: Typical set-up for a Surface Plasmon Resonance biosensor[48].

The main advantages of this technique are:

- Real time analysis.
- Kinetic information derived.
- Label free technique: no need for radioactive, fluorescent or any other labelling.

On the other side, operator have to face with several problems:[49]

- Mass transport can affect kinetic analysis.
- Any artefactual refraction index change (other than from the interaction) can also give signal.
- One of the interacting molecules must be immobilized on the surface.
- Lack of sensitivity when monitoring low molecular weight ligands.

1.6.2 Differential Scanning Fluorimetry (DSF)

Differential Scanning Fluorimetry (or Thermofluor assay) belongs to a class of technologies that investigate the interactions between a biological target and its binding ligand. This assay use the well-established thermodynamic principle that the thermal stability of a protein, often quantified as the midpoint of thermal denaturation or melting point (Tm, the temperature at which both native and unfolded states are equimolar), can be altered by a binding ligand in a

concentration and potency-dependent manner. In a Thermofluor assay, a compound with a low fluorescence signal in a polar environment (such as in aqueous solution) but with high fluorescence in a non-polar environment is added to a protein solution. The fluorescence of the solution is monitored while the solution is heated. When the protein chain begins to unfold, the hydrophobic core becomes exposed and the signal increases until the protein is completely denatured. Thus, the temperature of hydrophobic exposure at which half of the protein population is unfolded, is determined (Figure 1.6.2).[50, 51]
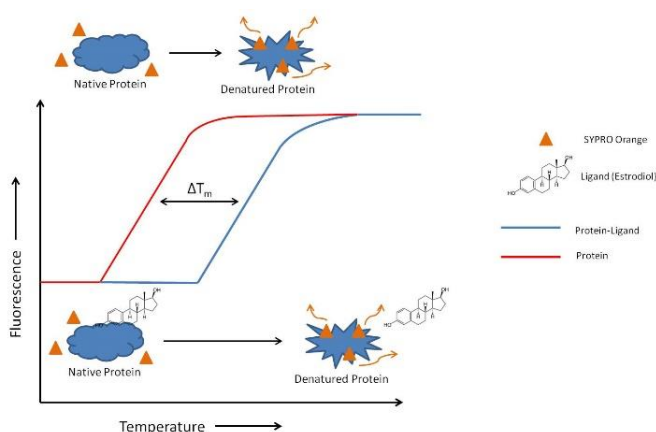
Figure 1.6.2: Typical recording of fluorescence intensity versus temperature for the unfolding of protein with and without the ligand in presence of SYPRO orange.

The commonly used fluorescent reporter dyes in thermal shift assays include Sypro Orange, Nano Orange and Sypro Red. Sypro Orange is usually the preferred choice because of its large intensity change upon binding to unfolded proteins. Intrinsic fluorescence from buried aromatic residues can also report protein unfolding as in the case of the nanoDSF. The basis of label-free fluorimetric analysis of protein unfolding lies in the properties of the fluorescent amino acid tryptophan. Since tryptophan is a hydrophobic amino acid, it is mostly located in the hydrophobic core of proteins where it is shielded from the surrounding aqueous solvent. Upon unfolding, tryptophan is exposed, and its

photophysical properties are altered. By detecting changes in tryptophan fluorescence intensity and its emission peak shift, the transition of a protein from the folded to the unfolded state can be precisely determined (Figure 1.6.3).[52]
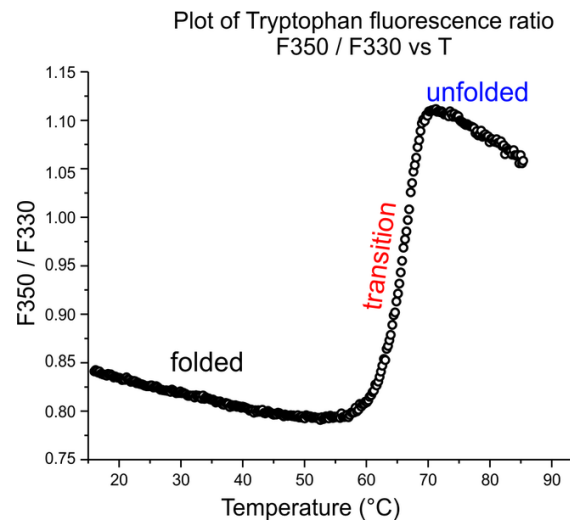
Figure 1.6.3: nanoDSF principle.

DSF is a useful screening method for the following reasons:

- Use of small amount of protein.
- Label-free and no-immobilization required.
- Easy optimization of assay conditions.
- Fast assay preparation and data analysis.

Likewise any other type of assay, this method has also intrinsic limitations:

- Not all biomolecules are responsive to fluorescence based thermal shift assays. In general, proteins with large hydrophobic surfaces, such as membrane-embedded, lipophilic, complex-forming or misfolded proteins, produce high background of fluorescence as a result of dye binding before melting.

- The assay is adversely affected by false positive or negative results: a weak binder that associates promiscuously to multiple sites on the protein surface may appear as a more potent hit.
- Interference by many detergents in the assay buffer.
- Possible competition of the reporter dye with the ligand.

1.6.3 Microscale Thermophoresis (MST)

MicroScale Thermophoresis (MST) is a powerful technique to quantify biomolecular interactions. It is based on thermophoresis, the directed movement of molecules in a temperature gradient, which strongly depends on a variety of molecular properties such as size, charge, hydration shell or conformation. Thus, this technique is highly sensitive to virtually any change in molecular properties, allowing for a precise quantification of molecular events independent of the size or nature of the investigated sample. During a MST experiment, a microscopic temperature gradient is induced by an infrared laser: the directed movement of molecules through this microscopic gradient is detected and quantified using either covalently attached or intrinsic fluorophores (Figure 1.6.4).[53, 54]
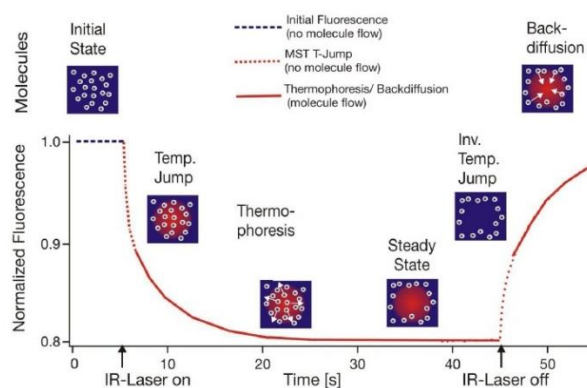
Figure 1.6.4: Typical signal of a MST experiment. Initially, the molecules are homogeneously distributed and a constant ''initial fluorescence'' is detected. Within the first second after activation of the IR laser, the ''T-Jump'' is observed, which corresponds to a rapid change in fluorophore properties due to the fast temperature change. Subsequently, thermophoretic movement of the fluorescently labelled molecules out of the heated sample volume can be detected.

MST not only allows for a precise determination of binding constants, but can also be used to derive additional information about the molecular mechanism of the investigated interaction.

From different points of view, MST technology is superior to other methods in determining the parameters of molecular interactions. The advantages of MST technology are:

- Low sample consumption.
- Robust and sensitive detection (broad concentration and size range).
- Rapid analysis.
- No surface immobilization required.
- Close to native protein conditions (possibility to work without labelling).
- Live detection of aggregation, sticking and precipitation effects.

On the other side, the technique suffers of the following drawbacks:

- For a label-free analysis, at least one Tryptophan in the protein sequence is needed.
- Absorption or Emission phenomena of small molecule compounds can interfere with protein signal.
- Target and substrate must be soluble in the same buffer conditions.

1.7 Biochemical Methods

Biochemical methods are the most common techniques used for the study and characterization of small molecule compounds activity in drug discovery. While biophysical methods allow interaction studies between the compound and the target, biochemical assays give a quantitative measure of the ability of the compound to influence target activity. Biochemical assay development begins

with a purified enzyme preparation that demonstrates catalytic activity on a specific substrate in a cell-free context. Usually, procedures for enzyme assays are well documented or cited in literature, but even accurate observance gives no guarantee of an unequivocal outcome: the same assays performed independently may yield quite different results. In fact, the enzyme activity depends on multiple factors and the understanding of particular features of each enzymes is required. The enzyme activity depends decisively on defined conditions with respect to temperature, pH, nature and strength of ions and enzyme assays can only be reliably compared, if such conditions are strictly observed.[55]

Many different approaches are available to measure enzymatic activity and can be differently classified. The most commonly used assays are based on the measurement of radioactivity and fluorescence.

1.7.1 Radioactivity Based Assays

Traditionally, assays based on radioactive probes (usually tritiated or iodinated ligands) have been successfully used to determine enzymatic activity because of the high sensitivity of the technique and the possibility to perform experiments on unmodified receptors expressed in native tissues and even in transfected cells. However, the use of radioactive ligands as tracers in these assays presents several drawbacks, both technical and financial. Technically, a classic radioactivity assay cannot be performed in a homogeneous format. Consequently the assay requires multiple washing steps before reading the radioactivity. This need adds complexity to the procedure and makes these assays more difficult to perform in high-throughput screening leading to extra cost. Additionally, the washing steps prevent any possibility of carrying out kinetics experiments on a single sample. Over the past decade, strategies such as scintillation proximity assays (SPA), which can be performed in homogeneous conditions, have been developed. SPA utilize microscopic beads containing scintillant: the interaction of these beads with β-particles, generated

by the radioactive decay of tritium or iodine, releases photons that may be measured with scintillation counters or charge-coupled device (CCD) imagers. A variety of SPA bead formats allows utilization of various substrates, but these assays are still expensive due to the production cost of beads.

A second technical drawback rely on the nature of the radioactive probe: it is difficult, in part for health reasons, to perform saturation assays that necessitate high concentrations of radioactive ligand. Furthermore, due to the hazardous nature of the compounds, the use of radioactive probes has some restrictions in term of radioactive waste disposal, delimitation of working area and staff medical follow-up. As a result, other techniques have been introduced to replace the use of radioactive assays, such as fluorescence techniques, without completely supplanting them.[56]

1.7.2 Fluorescence Based Assays

Among the most popular enzyme assays, the fluorescence-based ones are largely used in screening campaigns. These assays are commonly based on synthetic substrates that incorporate a chromophore, whose fluorescence properties change as a result of the enzyme reaction. The key advantage of these substrates is that the assay is simple and the signal produced is directly related to the enzyme-catalysed reaction. If the fluorescent product is soluble, the assay is well-suited for microtiter plate based assays. To date, almost all examples of fluorescent substrates focus on a small family of fluorophores and chromophores, in particular umbelliferones, nitrophenols, fluoresceins, rhodamines and BODIPY dyes, all of which are relatively large aromatic groups which tend to influence both substrate binding, catalytic turnover, and solubility.[57]

With the aim to overcome the limitations of traditional fluorescence-based assays, in the last few decade there was the introduction of other new

luminescence based techniques. Among all of them, one of the most widely used is the Alphascreen technology.

1.7.2.1 AlphaScreen Technology

An AlphaScreen assay utilizes proximity-based fluorescence detection through the tethering of donor and acceptor beads by a protein-ligand interaction (Figure 1.7.1).
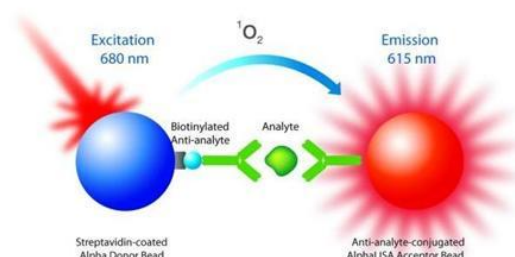
Figure 1.4.1: Principle of the Alphascreen assay technology.

Initially developed underneath the name LOCI® (Luminescent Oxygen Channeling Immunoassay), the reagents and bead technologies for drug discovery are currently exclusively commercially available under the name AlphaScreen by Perkin Elmer. In this assay, the photosensitizer phthalocyanine is dissolved on a polystyrene donor bead. Excitation with 680 nm light induces phthalocyanine to convert ambient oxygen to singlet oxygen molecules with a 4 µs half-life. These molecules can diffuse 200 nm freely through solution. If a polystyrene acceptor bead is within the lifetime of the singlet oxygen species, the singlet oxygen will react with thioxene derivatives on the bead, resulting in a dioxetane product followed by a diester fluorescent product. If the emission is at 615 nM, the assay is called AlphaLISA: both assays rely on the same Donor beads but use different Acceptor beads. AlphaScreen Acceptor beads are embedded with three dyes: thioxene, anthracene, and rubrene. Rubrene, the final fluorophore, emits light detectable between 520-620 nm. In the AlphaLISA Acceptor beads, anthracene, and rubrene are substituted with an Europium

chelate. The Europium (Eu) chelate is directly excited by the 340 nm light resulting from the conversion of thioxene to a di-ketone derivative following its reaction with singlet oxygen. The excited Europium chelate generates an intense light detectable within a much narrower wavelength bandwidth centred around 615 nm. In contrast to the AlphaScreen, the AlphaLISA emission is therefore less susceptible to interference by either artificial or natural compounds that absorb light between 500-600 nm.

In both cases, the detection of the chemiluminescent readout depends on binding of the protein and its related ligand. Typically, the donor bead captures substrates (by the biotin-streptavidin interaction) while the acceptor bead interacts with the modifications on the substrate, after the enzymatic reaction. The interaction of protein and substrate results in chemical energy transfer of acceptor and donor beads, culminating in a luminescent signal. Lack of binding fails to bring acceptor and donor beads into sufficiently close proximity and the singlet oxygen decays without the production of light. Since the beads are coated with hydrogel, non-specific interactions are minimized, providing a large signal-to-background assay window.[58, 59]

However, Alphascreen may be sensitive to different types of interferences. For example, antioxidants or other quenchers of reactive oxygen species like metal ions can strongly affect the emitted signal, as well as biotin-like compounds can compete for the interaction of biotinylated substrate with Donor beads. Moreover, since the Alphascreen detection is only based on a fluorescence intensity measurement, coloured compounds absorbing in the 500-600 nm wavelength range can artificially decrease the signal and therefore may be detected as false positives in HTS.[60]

2. AIM OF THE WORK

Epigenetic enzymes are involved in the development of several diseases and, as previously discussed, they are considered very interesting targets for drug discovery. The complexity of these proteins, together with the lack of a complete understanding of their biological role, are responsible for the limited number of currently identified modulators.

Different methodologies are available for the identification of epigenetic modulators (Chapters 1.6 and 1.7), nevertheless to date there is not a gold standard approach for the evaluation of their activity. It is worth mentioning that in a drug discovery programme it is necessary to use different technologies. The reasons of this need are different. First, each technique suffers of intrinsic limitations that could affect the outputs, as previously reported, so it is necessary to validate data. In addition, a single method is not suitable to deeply characterize the modulators activity (for example binding, mechanism of action, potency and so on). Furthermore, the use of different methodologies allow the identification of pan-assay interference compounds (PAINS), which encompass some 400 structural classes (for example enones, catechols, isothiazolones and so on). Usually, during the screening of compounds libraries, the activity of 5-12% of compounds does not depend on a specific, drug-like interaction between molecule and protein. PAINS can give false readouts in a variety of ways. Some are fluorescent or strongly coloured. In certain assays, they give a positive signal even when no protein is present. Other compounds can trap the toxic or reactive metals used to synthesize molecules in a screening library or used as reagents in assays. These metals then give rise to signals that have nothing to do with a compound's interaction with a protein. Other PAINS coat a protein or sequester metal ions that are essential to a protein's function, or they may alter proteins chemically without fitting specifically into a binding site.

All of these mechanisms prevent further attempts to improve the biological activity of a molecule by modifying its structure. The only method to discover PAINS is to use orthogonal assays that can give different readouts, so it is possible to define "true hits".

In this scenery, the aim of my phD project was to develop a robust and widely usable combined screening platform to identify small-molecule modulators of epigenetic enzymes (Figure 2.1). To overcome the limitations of each technique and with the aim to identify "true hits", different biophysical and biomolecular techniques were exploited to interrogate three epigenetic proteins (p300, SETD8 and Tudor domains of PHF20) and we validated the outputs. It is important to highlight that the use of multiple technologies enabled also a deep characterization of modulators activity, allowing the determination of binding, mechanism of action and potency.
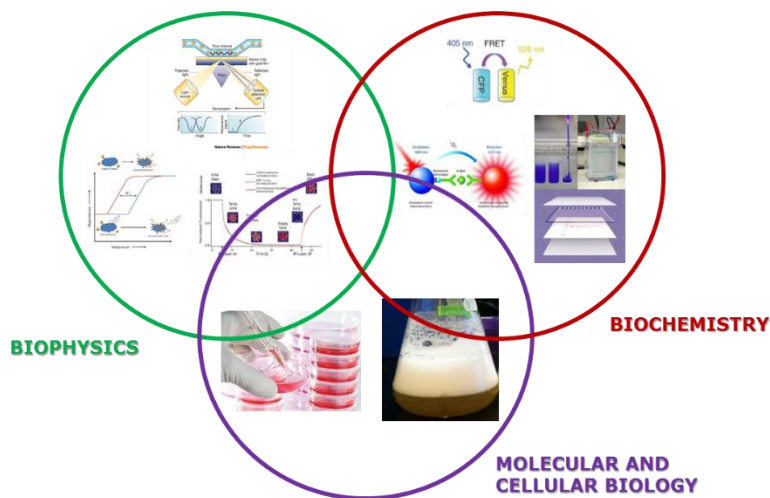
Figure 2.1.: Combined approach to interrogate epigenetic enzymes.

3. RESULTS AND DISCUSSION

3.1 p300

3.1.1 SPV106 analogues as modulators of acetyltransferase activity

Different approaches have been used to identify p300 modulators, but only a limited number of small molecule inhibitors have been described, with various degrees of selectivity and cell permeability. Ethnomedicine has inspired the identification of a few natural products, including anacardic acid,[9] garcinol,[10] curcumin,[11] plumbagin,[12] and guttiferone A[61] as inhibitors of different classes of KATs. Among them, in the Epigenetic Medicinal Chemistry Laboratory (EMCL) we focused our attention on anacardic acid. Anacardic acid, a small molecule compound extracted from cashew nut shell liquid which is known to have antitumor activity, inhibits acetyltransferase activity of p300, but it's not a selective inhibitor.[9]

In 2008, EMCL reported on the activity of a series of long-chain alkylidenemalonates (LoCAMs) as protein acetyltransferases modulators. The design of LoCAMs was inspired by the structural simplification of anacardic acid (Figure 3.1.1).[62, 63]

Figure 3.1.1: From anacardic acid to LoCAMs.

One of these compounds, the diethyl pentadecylidenemalonate **1** (**SPV106**), has a unique activity profile. This compound exhibits inhibitory properties against p300 with a potency comparable to that of anacardic acid, and it simultaneously enhances the acetylating activity of PCAF. Therefore, it is the first mixed activator/inhibitor of protein acetyltransferases.[62, 63]

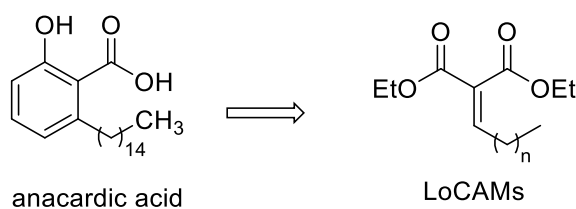As a result of its peculiar activity profile, derivative **1** was successfully used as a chemical probe in a study that correlated Duchenne cardiomyopathy with PCAF-mediated lysine acetylation levels of connexin 43.[64] It was also examined during investigations of the role of KAT enzymes in the regulation of the extinction of conditioned fear and neuronal plasticity.[65] More recently, treatment with compound **1** has been shown to reverse alterations in human cardiac mesenchymal cells obtained from diabetic patients and restore cellular function.[66]

The uncommon biological properties of derivative **1** prompted us to explore the structure-activity relationships of LoCAMs. First, we focused on the alkyl chain and the flexibility of the scaffold:[62] we found that variations in the alkyl chain length influenced the activity profile of KAT modulators, whereas all other modifications, such as variations in flexibility/rigidity of the core structure and the introduction of substituents, were detrimental.[62] Indeed, not only the selectivity toward different KAT enzymes, but also the inhibitory and activating properties, varied depending on the substitution pattern.[62]

As a further exploration of the structure-activity relationships of this class of KAT modulators, and with the aim of identifying potential structural features that differentially affect the activity of acetyltransferases, my project started with the synthesis of a number of 1,3-dicarbonyl derivatives (Figure 3.1.2). The synthesized compounds formally derived by the replacement of one or both ester functions with keto- or carboxylic acid groups while the alkyl chain length was kept constant. In addition, because it was previously found that the diketo-analogue of compound **1** (derivative **2d**, Figure 3.1.2) retained inhibitory activity against p300,[62] a few shorter and longer-chain homologues of **2d** were also prepared.
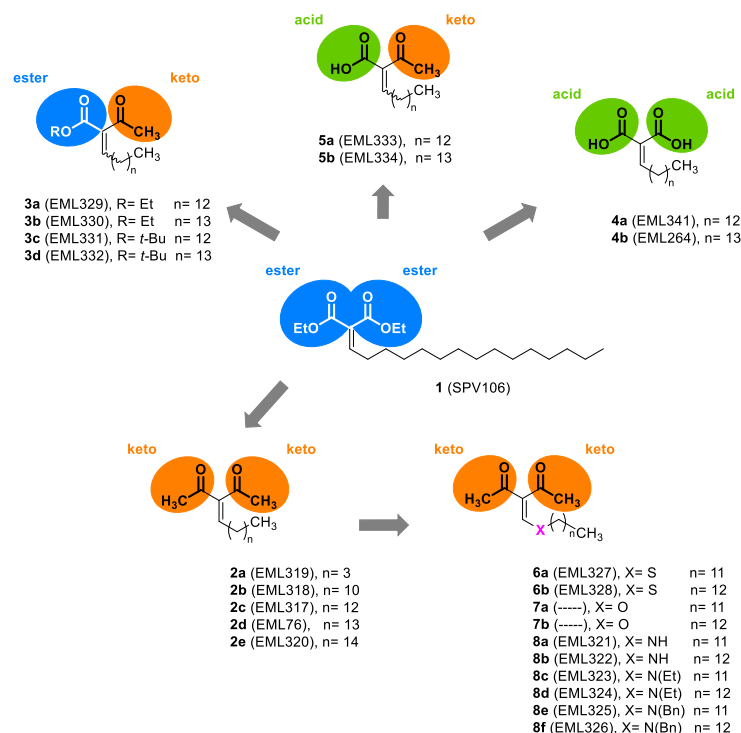
Figure 3.1.2: 1,3-Dicarbonyl derivatives **2a-e**, **3a-d**, **4a,b**, **5a,b**, **6a,b**, **7a,b**, and **8a-f**.

3.1.1.1 Chemistry

Novel **SPV106** derivatives **2**-**5** were prepared by Knoevenagel condensation of a 1,3-dicarbonyl derivative with the appropriate alkyl aldehydes. The aldehyde used, if not commercially available, were prepared from the corresponding alcohol by oxidation with 2,2,6,6-tetramethylpiperidine 1-oxyl (TEMPO),[67] (Scheme 3.1.1). Derivatives **2a**-**e**, **3a**-**d**, and **4a**,**b** were prepared by reacting, respectively, pentane-2,4-dione, ethyl 3-oxobutanoate, *tert*-butyl 3-oxobutanoate, or malonic acid with the appropriate aldehyde in dichloromethane using piperidine and acetic acid as the catalysts (Scheme 3.1.1).
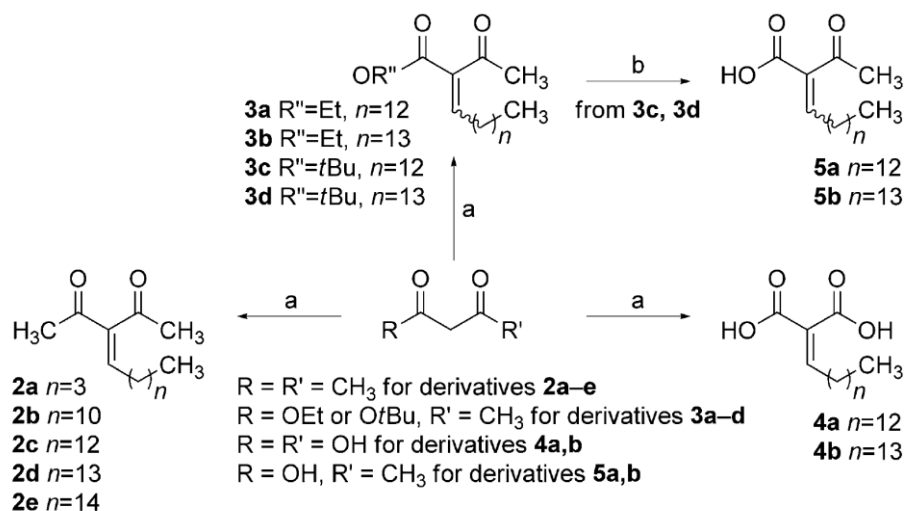
Scheme 3.1.1: Reagents and conditions: a) alkyl aldehyde, AcOH, piperidine, CH_2Cl_2, RT, 2–12 h; b) TFA/CH_2Cl_2 (5:95), RT, 30 min.

The hydrolysis of *tert*-butyl esters **3c,d** was performed with trifluoroacetic acid (TFA), yielding the corresponding 2-alkylidene-3-oxobutanoic acids **5a,b**. By Knoevenagel condensation of ethyl 3- oxobutanoate and *tert*-butyl 3- oxobutanoate with alkyl aldehydes, derivatives **3a,b** and **3c,d** were obtained, as mixtures of E and Z isomers. After the separation of the two isomers by silica gel chromatography, it was observed a spontaneous interconversion of the compounds. For this reason, compounds **3a**-**d** and the corresponding acids **5a,b** were tested as the E/Z mixtures. Alkylthiomethylidenepentane-2,4-diones **6a,b** and alkylaminomethylidenepentane-2,4-diones **8a**-**f** were obtained in high yield (Scheme 3.1.2) by reacting, respectively, the appropriate alkyl amine or alkyl thiol with 3-(ethoxymethylene)-2,4-pentanedione **9** in THF at reflux.[68]
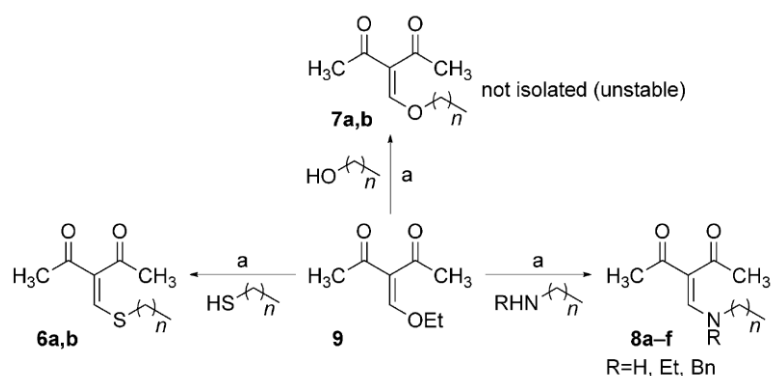
Scheme 3.1.2: Reagents and conditions: a) alkyl amine, thiol, or alcohol (n=11, 12), THF, reflux, 2 h.

Alkyloxymethylene-2,4-pentanediones **7a,b** were obtained in good yield under the same conditions from the corresponding alkyl alcohols. Unfortunately, compounds **7a,b** were unstable even in presence of low amount of water. Therefore, any attempt to purify these derivatives by chromatography was unsuccessful. Moreover, because an aqueous medium is required for biological screening, any further purification efforts was abandoned.

This pool of **SPV106** analogues synthesized was used to develop a screening strategy, using biophysical and biochemical techniques.

3.1.1.2 Biophysical Screening: Surface Plasmon Resonance Assay

To avoid time-consuming, expensive assays, all compounds were preliminarily screened using a Surface Plasmon Resonance (SPR)-based binding assay. As discussed in the introduction section, this biophysical technique is well suited for a primary screening.[69] Recently, at EMCL, an SPR-based binding assay was established and successfully employed to study the real-time interactions between small-molecule derivatives and p300[62, 63] as well as other epigenetic targets.[70]

In this project, SPR was used for the identification of compounds able to bind to at least one of the acetyltransferase enzymes (p300 and/or PCAF). Thus, the

human recombinant p300 (aa 1284-1673) and PCAF (aa 492-658) catalytic domains were immobilized (up to ⁓10 000 response units (RU)) on the flow cells of the biosensor chip, and 1,3-dicarbonyl derivatives **2-8** were injected at various concentrations (from 25 to 100 µM) over the protein surface. To decrease false positives related to detergent-sensitive and aspecific aggregation-based binding, 0.005% of Surfactant P20 was added to the running buffer in all experiments. In addition, to evaluate potential non-specific binding, all compounds were injected on an immobilized myoglobin. The binding of each compound was read in real time as the change in mass at the sensor surface. After injection, running buffer was allowed to flow over the surface, and the dissociation of compounds from the surface was observed.

These experiments showed that tetradecylidene- and pentadecylidene-substituted pentane-2,4-diones, malonic acids, and 3-oxobutanoic acids (**2c,d**, **4a,b**, and **5a,b**, respectively) efficiently interact with the immobilized proteins, as demonstrated by the concentration-dependent responses and the clearly evident exponential curves during both the association and dissociation phases (the sensorgrams for compounds **2d**, **4b**, and **5b** are displayed in Figure 3.1.2).

For the compounds **2d**, **4b** and **5b** equilibrium dissociation constant (KD) values were derived from the ratio between kinetic dissociation (kd) and association (ka) constants, obtained by fitting data from all injections at different concentrations of each compound, using the simple 1:1 Langmuir binding fit model of the BIAevaluation software. The compound **2d** showed a KD of 5.85 x 10^{-5} against p300 and of 2.74 x 10^{-5} against pCAF, while for the compound **4b** the KD obtained was of 4.32 x 10^{-7} against p300 and of 1.53 x 10^{-5} against pCAF. Regarding the compound **5b**, the KD against p300 was of 3.05 x 10^{-6} while the one reported against pCAF was of 1.52 x 10^{-4}.

On the other hand, both 3-oxobutanoates **3a-d** and derivatives **6-8**, which are characterized by the presence of a heteroatom in their aliphatic chains, showed negligible interaction. In addition, in agreement with what was previously

reported for LoCAMs,[62] it was shown that variations in the alkyl chain length influenced the binding profile of the tested pentane-2,4-diones **2a-e**. In fact, their superior (**2e**) and inferior (**2a** and **2b**) homologues also produced good sensorgrams but showed low and/or concentration-independent responses.
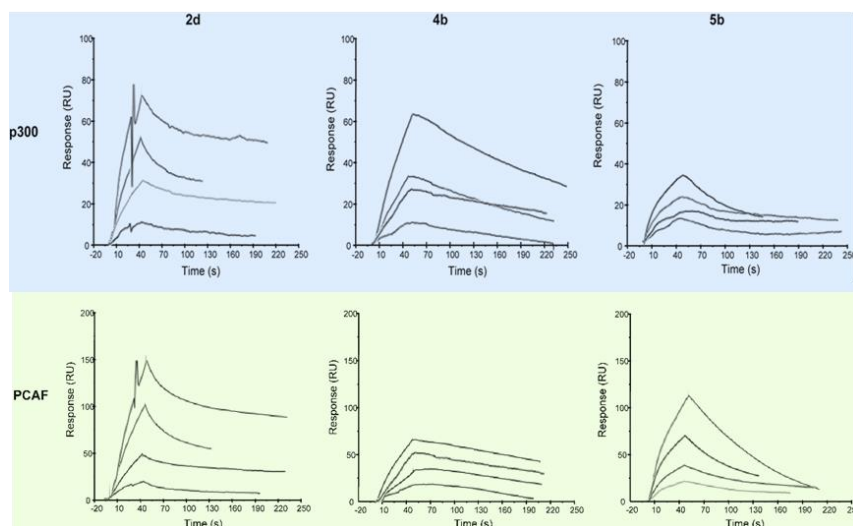
Figure 3.1.3: Sensorgrams obtained from the SPR interaction analysis of compounds **2d**, **4b**, and **5b** binding to immobilized p300 (catalytic domain, aa 1284-1673, top row) and PCAF (catalytic domain, aa 492-658, bottom row). Each compound was injected at four different concentrations (25, 50, 75, and 100 μM).

3.1.1.3 Biochemical Screening: Radiometric Assay

SPR, used as a filtering method, gives information about the interaction of the molecules with targets and explain the modulatory activity, but cannot be used to define the potency of molecules. For this reason, the effect of the selected derivatives (SPR+) **2c**,**d**, **4a**,**b**, and **5a**,**b** on the catalytic activity of the human recombinant acetyltransferase enzymes p300 and PCAF was determined in radiometric activity assays, which were performed by Reaction Biology Corporation (Malvern, PA, USA), using curcumin and anacardic acid as reference compounds. Two negative controls (SPR-, **6b** and **8b**) were also tested to cross-validate the selection method.

As shown in Table 3.1.1, all the SPR+ derivatives substantially affected the activity of one or both the HAT enzymes.

compd	IC$_{50}$ (µM) or % activity at 100 µM	
	p300/KAT3B	PCAF/KAT2B
2c	no inhib	229.1%
2d	no inhib	389.3%
4a	1.3	50.3
4b	1.1	21.1
5a	2.4	345.9%
5b	4.7	497.3%
6b	no inhib	no inhib
8b	no inhib	no inhib
curcumin	6.5	NT
AA	NT	33.9

Table 3.1.1: Effects of compounds **2c**,**d**, **4a**,**b**, **5a**,**b**, **6b**, and **8b** on the activity of p300 and PCAF. Compounds were tested in 10-dose IC$_{50}$ mode with threefold serial dilutions starting at 100 µM. Data were analyzed with GraphPad Prism software (version 6.0) for IC$_{50}$ curve fits. Enzyme activity percentage was determined at 100 µM with respect to DMSO. Histone H3 was used as substrate (5 µM), and [acetyl-^{3}H]acetyl coenzyme A (3.08 µM) was used as an acetyl donor.

In particular, pentane-2,4-diones **2c,d** induced a marked dose-dependent increase in the enzymatic activity of PCAF (HAT activity at 100 µM: 229% and 389%, respectively; Table 3.1.1), while they did not affect the activity of p300. In contrast, malonic acids **4a,b** strongly inhibited both enzymes, with IC$_{50}$ values in the low micromolar range (1.3 and 1.1 µM, respectively, for p300, and 50.3 and 21.1 µM, respectively, for PCAF; see Table 3.1.1), which are similar to or more potent than the reference compounds (IC$_{50}$: 6.5 µM and 33.9 µM for curcumin and anacardic acid, respectively; Table 3.1.1). Notably, 3-oxobutanoic acids **5a,b** efficiently inhibited p300 (IC$_{50}$ values of 2.4 µM and 4.7 µM, respectively) but also caused strong amplification of PCAF enzymatic activity in a dose-dependent manner (HAT activity at 100 µM: 346 and 497%, respectively; Table 3.1.1). This effect was even more significant than that

observed for pentane-2,4-diones **2c**,**d**. In accordance with the SPR experiments, the negative controls negligibly affected the enzymatic activity of p300 and PCAF (see **6b** and **8b** in Table 3.1.1).

3.1.1.4 Evaluation of Cellular Activity

After the characterization of the enzymatic activity of compounds **2c**, **2d**, **4a**, **4b**, **5a** and **5b** using a biophysical and a biochemical method, the screening approach continued with the aim to evaluate their effect on cells. Cellular assays were carried out on three different cell lines, namely human leukemic monocyte lymphoma U937 cells and human cervical carcinoma C33A and HeLa cells. First, an MTT assay was performed after the treatment with selected derivatives to assess the maximum concentration of compounds that could be used without significantly affecting cell viability. For solid C33A and HeLa tumor cell lines, it was observed no significant decrease in the number of metabolically active cells after 24 h of treatment with concentrations up to 200 μM for derivatives **2c**,**d** and **4a**,**b** and up to 50 μM for compounds **5a**,**b**.

On the other hand, in the case of the more sensitive U937 cell line (Figure 3.1.4a), it was registered a significant decrease in cell viability starting from lower concentrations of tested compounds (100 μM for **2c**,**d** and **4a**,**b** and 10 μM for **5a**,**b**, respectively). Therefore, the derivatives were evaluated on U937 cell line for their effects on the cell cycle. After 24 h of treatment, compounds **4b**, **5a**, and **5b** were able to arrest the cell cycle in the G_1 phase (Figure 3.1.4b). In the case of the latter two compounds, this occurred at concentrations as low as 10 μM. This result is consistent with the importance of acetylation for control of the G_1/S transition.[71-74] Under the same conditions, the other derivatives had no significant effects on the cell cycle.
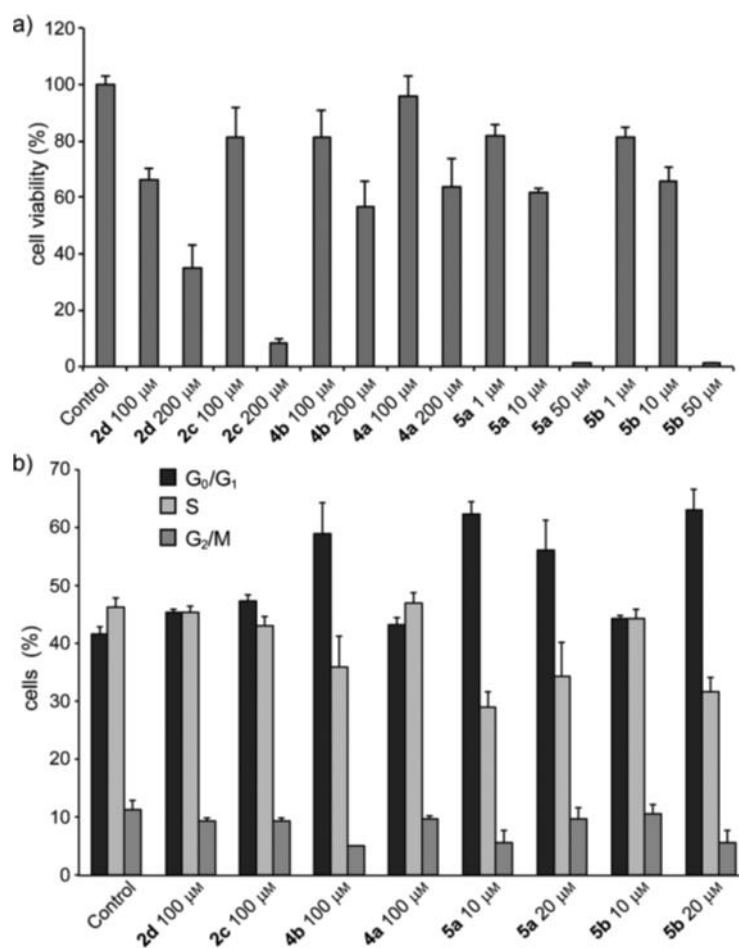
Figure 3.1.4: Cell viability and cell-cycle analysis in U937 cells by fluorescence-activated cell sorting (FACS). a) Cell viability was assessed by measuring the mitochondrial-dependent reduction of MTT to formazan. b) U937 cells were treated with compounds **2c,d**, **4a,b**, and **5a,b** at the indicated concentrations for 24 h, stained with propidium iodide, and subjected to flow cytometric analysis to determine the distribution of cells in each phase of the cell cycle. Data are reported as the mean ±SD of at least three independent experiments.

Finally, the effects of compounds **2d**, **4b**, and **5b** were determined on the acetylation levels of specific lysine residues of core histones H3 (K9) and H4 (K5) in the three cell lines. Cells were incubated for 24 h with vehicle and tested with compounds at the indicated concentrations, using as reference compound the suberoylanilide hydroxamic acid (SAHA; 5 µM).[75] The histone extracts were then immunoblotted with antibodies to specific histone acetylation sites

(Figure 3.1.5). Consistently with the different patterns of acetylation recently described by Garcia and co-workers,[76] it was observed that the tested compounds differentially affected the H4K5ac and H3K9ac levels in the three cell lines. This observation is not surprising, considering that in the cellular context, acetyltransferases are similar to other enzymes by not being isolated; they participate in complex pathways and actively crosstalk with each other and with other proteins.

Specifically, the effect of pentane-2,4-dione **2d** on both markers was negligible in U937 cells (Figure 3.1.5, left and middle panels), whereas a decrease was observed in both cervical carcinoma cell lines, which was more evident for H4K5ac (Figure 3.1.5). Both malonic acid **4b** and 3-oxobutanoic acid **5b** induced a marked decrease in the acetylation of lysine H4K5 in C33A cells (Figure 3.1.5, left panel), whereas no appreciable effect on the same marker was detected in HeLa cells, and an increase was observed in U937 cells (Figure 3.1.5).

In contrast, derivative **4b** induced a moderate decrease in the acetylation of H3K9 in C33A and HeLa cells (Figure 3.1.5, middle panels), and there was no appreciable variation in U937 cells (Figure 3.1.5, middle panel). The compound **5b** induced a decrease in the acetylation of H3K9 in C33A and HeLa cells (Figure 3.1.5, middle panels) and a marked increase in the acetylation level in U937 cells (Figure 3.1.5, middle panel). As expected, treatment with the reference compound SAHA reliably showed a significant increase in the lysine acetylation level (Figure 3.1.5).
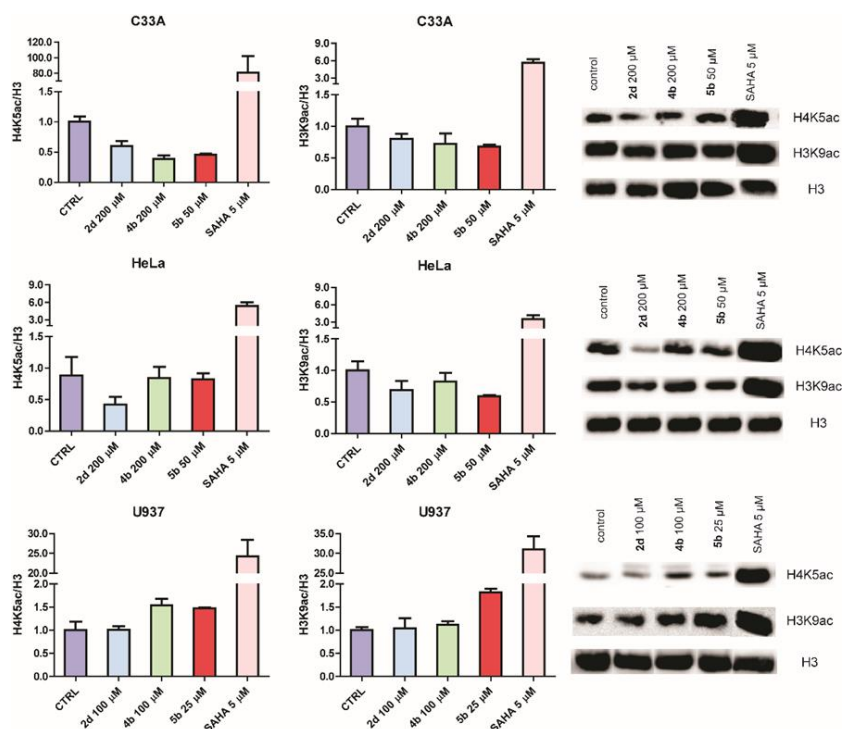
Figure 3.1.5: Western blot analyses performed with compounds **2d**, **4b**, and **5b** at the indicated concentrations for 24 h on the acetylation of the specific lysine residues H4K5 (left column) and H3K9 (middle column) in histone extracts from a) C33A and b) HeLa carcinoma cells, and c) U937 leukemic monocyte lymphoma cells. Acetylation was detected by immunoblotting with antibodies specific for histone acetylation sites as indicated. Total histone H3 was used to check for equal loading. SAHA (5 μM) was used as a reference compound. Signals were detected with the ImageQuant LAS 4000 digital imaging system and quantified by ImageQuantTL software (version 8.1); total histone H3 levels were used for normalization. The results are reported as the mean ±SD of three independent experiments.

The differences observed in the activity profile of the structurally related compounds **2c,d**, **4a,b**, and **5a,b** against the two acetyltransferases could have a number of explanations, and the mechanisms underlying their biological effects remain unclear. However, it has been previously reported that small modifications in structurally related compounds lead to dramatic differences in terms of selectivity between PCAF and p300.[15] Moreover, is worth mentioning that the catalytic mechanisms of the two enzymes are different, with PCAF

using a ternary complex mechanism,[77] and a Theorell–Chance "hit and run" model proposed for p300.[19]

In conclusion, the application of this screening strategy allowed the identification of some analogues of **SPV106** (**2d**, **4b**, and **5b**) characterized by different activity profiles against PCAF and p300 (pure PCAF activator, pan-inhibitor, or mixed PCAF activator/p300 inhibitor). The compounds described may be useful chemical tools for mechanistic studies of lysine acetylation and its implications in physiological and/ or pathological processes.[7]

3.1.2 From Garcinol to 5-Benzylidenebarbituric Acid Derivatives

As exemplified by the discovery of **SPV106**, structural simplification represents a drug design strategy to simplify the structure and shorten synthetic routes while keeping or enhancing the biological activity of a natural bioactive compound.[62, 63, 78]

Prompted by these successful results, we decided to apply a molecular pruning approach to the molecular scaffold of garcinol that is a non-selective inhibitor of p300 extracted from *Garcinia Indica.* From this compound, in the last few years, two molecules have been developed. Isogarcinol and its derivative LTK-14 are two semisyntethic garcinol derivatives that, even if characterized by improved potency and selectivity, they still retain the synthetic complexity of garcinol that limits studies on structure-activity relationships.

To rapidly gain access to the compounds and promptly achieve a comprehensive SAR framework, the lead structure of garcinol was simplified step-by-step to identify the minimal structural elements required for p300 inhibitory activity.

Our molecular simplification strategy applied to the garcinol structure is schematically depicted in Figure 3.1.5.

First, the pruning of the condensed cyclohexanone ring turned the bicycle core into the simple cyclohexanetrione. Then the isosteric replacement of nitrogen

for carbon provided the easily synthesizable barbituric acid moiety, providing the first series of analogues (compounds of type A in Figure 3.1.5). The removal of the benzoyl carbonyl group and the introduction of unsaturation yielded the second (B) and third (C) series of derivatives, respectively. Subsequently, we decided to explore the importance of the nature of the carbon chain on the two nitrogen atoms and the significance of the substitution pattern on the phenyl ring. Therefore, we introduced an aliphatic saturated (*i*-butyl), unsaturated (allyl), or aromatic (benzyl) chain in place of the prenyl substituent on the nitrogens, whereas the phenyl ring was decorated with hydroxyl and/or methoxyl groups.

The three series of derivatives resulting from this approach, namely benzoylbarbiturates A, benzylbarbiturates B, and benzylidenebarbiturates C (Figure 3.1.5) were synthesized in the EMCL and were screened using different methodologies.
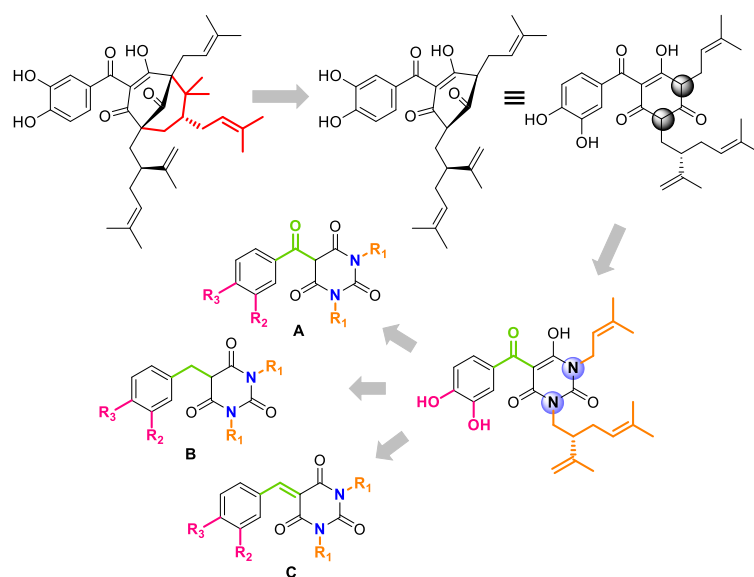

Figure 3.1.5: Flowchart of the molecular pruning approach.

First, a biochemical filter was applied: the effect on the catalytic activity of the human recombinant acetyltransferase enzymes p300 and PCAF was determined at a fixed concentration of 100 μM in a radiometric activity assay, using curcumin,[11] anacardic acid,[9] and C646[14] as reference compounds (the radiometric assays were performed by Reaction Biology Corporation, Malvern, PA, USA). The results, reported in Table 3.1.2, are summarized as heat maps in Figure 3.1.6. Firstly, it was clear that derivatives of the general structure C (Figure 3.1.6) were endowed with the highest inhibitory activity against p300: they displayed a greater than 90% inhibition of p300 activity, and therefore IC_{50} values were determined only for these compounds (Table 3.1.2).

In addition, the activity was markedly affected by the nature of the substituent on the nitrogen atoms. In fact, derivatives with benzyl substituents were always more active than the corresponding *iso*-butyl-substituted analogues and even more active than the allyl-substituted ones (compare, for example, the activity of compounds **15b** and **15c** with those of derivatives **16b** and **16c** and **17b** and **17c**, respectively). With regard to the substitution pattern on the phenyl ring, the presence of a 4- hydroxyl substituent was crucial for the inhibitory potency of the compounds, which was further increased by the presence of a second oxygen atom in position 3. In fact, derivative **15b** resulted in more potency than curcumin and derivatives **15c** and **15e** were more potent than both curcumin and C646 (Table 3.1.2). On the contrary, replacement of the 4-hydroxyl with a methoxyl group reduced the activity of the resulting derivatives (compare the activities of compounds **15b**, **15c**, and **15e** with those of compounds **15g**, **15d**, and **15f**, respectively). It is noteworthy that the inhibition activity was selective, as all the compounds were scarcely active against PCAF (Table 3.1.2).

compd	R₁	R₂, R₃	% inhibition p300 (at 100 µM, mean ± SD)	% inhibition PCAF (at 100 µM, mean ± SD)	IC₅₀ (µM) p300 (mean ± SD)
9a	Bn	H	84.8 ± 0.2	−14.5 ± 7.8	
9b	Bn	4-OH	54.4 ± 0.2		
9c	Bn	3-OH, 4-OH	48.2 ± 2.2		
10a	*i*-Bu	H	34.1 ± 1.2	19.3 ± 2. 4	
10b	*i*-Bu	4-OH	39.7 ± 0.9	3.4 ± 8.2	
10c	*i*-Bu	3-OH, 4-OH	8.4 ± 2.1	−13.2 ± 11.6	
11a	allyl	H	28.1 ± 3.8	−2.7 ± 0.1	
11b	allyl	4-OH	19.1 ± 1.8	3.6 ± 1.8	
11c	allyl	3-OH, 4-OH	4.9 ± 1.9	5.0 ± 1.7	
12a	Bn	H	83.9 ± 6.7		
12b	Bn	4-OH	60.3 ± 1.1		
12c	Bn	3-OH, 4-OH	59.9 ± 0.6		
13a	*i*-Bu	H	23.1 ± 4.0		
13b	*i*-Bu	4-OH	64.6 ± 0.5	−10.5 ± 9.6	
13c	*i*-Bu	3-OH, 4-OH	24.3 ± 2.4	−7.5 ± 7.4	
14a	allyl	H	28.9 ±10.3		
14b	allyl	4-OH	23.7 ± 0.6	−10.5 ± 9.6	
14c	allyl	3-OH, 4-OH	1.1 ± 2.3	−0.6 ± 1.6	
15a	Bn	H	NT		
15b	Bn	4-OH	99.2 ± 0.6	−2.3 ± 2.8	2.1 ± 0.2
15c	Bn	3-OH, 4-OH	96.15± 0.15	−162.4 ± 8.2	1.6 ± 0.1
15d	Bn	3-OH, 4-OMe	97.28 ± 0.22	−55.6 ± 9.1	5.9 ± 0.3
15e	Bn	3-OMe, 4-OH	97.06 ± 0.18	−25.8 ± 16.4	1.5 ± 0.2
15f	Bn	3-OMe, 4-OMe	88.25 ± 0.85	−8.2 ± 3.7	11.4 ± 0.6
15g	Bn	4-OMe	93.59 ± 1.39	−22.2 ± 1.8	8.0 ± 0.4
16a	i-Bu	H	NT		
16b	i-Bu	4-OH	94.03 ± 0.17	−34.1 ± 2.4	8.5 ± 0.3
16c	i-Bu	3-OH, 4-OH	91.85 ± 0.22	10.6 ± 2.0	5.4 ± 0.2
16d	i-Bu	3-OH, 4-OMe	84.68 ± 0.35	9.3 ± 1.0	31.4 ± 0.9
16e	i-Bu	3-OMe, 4-OH	96.43 ± 0.67	9.2 ± 0.4	4.2 ± 0.3
16f	i-Bu	3-OMe, 4-OMe	45.82 ± 2.91	3.6 ± 3.2	
16g	i-Bu	4-OMe	53.78 ± 5.01	3.1 ± 1.4	
17a	allyl	H	NT		
17b	allyl	4-OH	64.71 ± 0.71	3.3 ± 0.7	
17c	allyl	3-OH, 4-OH	61.65 ± 2.46	3.0 ± 1.2	
17d	allyl	3-OH, 4-OMe	49.48 ± 2.10	5.1 ± 1.6	
17e	allyl	3-OMe, 4-OH	67.33 ± 0.01	6.6 ± 0.5	26.4 ± 0.7
17f	allyl	3-OMe, 4-OMe	31.15 ± 0.48	11.7 ± 0.2	
17g	allyl	4-OMe	59.85 ± 1.96	3.6 ± 3.2	
curcumin			93.45 ± 0.81	-	6.5 ± 0.2
AA			-	102.9 ± 2.3	
C646			86 @10 µM	<10 @10 µM	1.6 ± 0.2

Table 3.1.2: Effects of Compounds **9-17** on the Activity of p300 and PCAF. Enzyme activity percentage determined at 100 µM with respect to DMSO. Values are the means ± SD determined for at least two separate experiments and are indicated in percentage points. Histone H3 was used as substrate (5 µM), and [acetyl-^{3}H]acetyl coenzyme A (3.08 µM) was used as an acetyl donor. The most active compounds were tested in 10-concentration IC_{50} mode with 3-fold serial dilutions starting at 100 µM. Data were analyzed with GraphPad Prism software (version 6.0) for IC_{50} curve fitting.
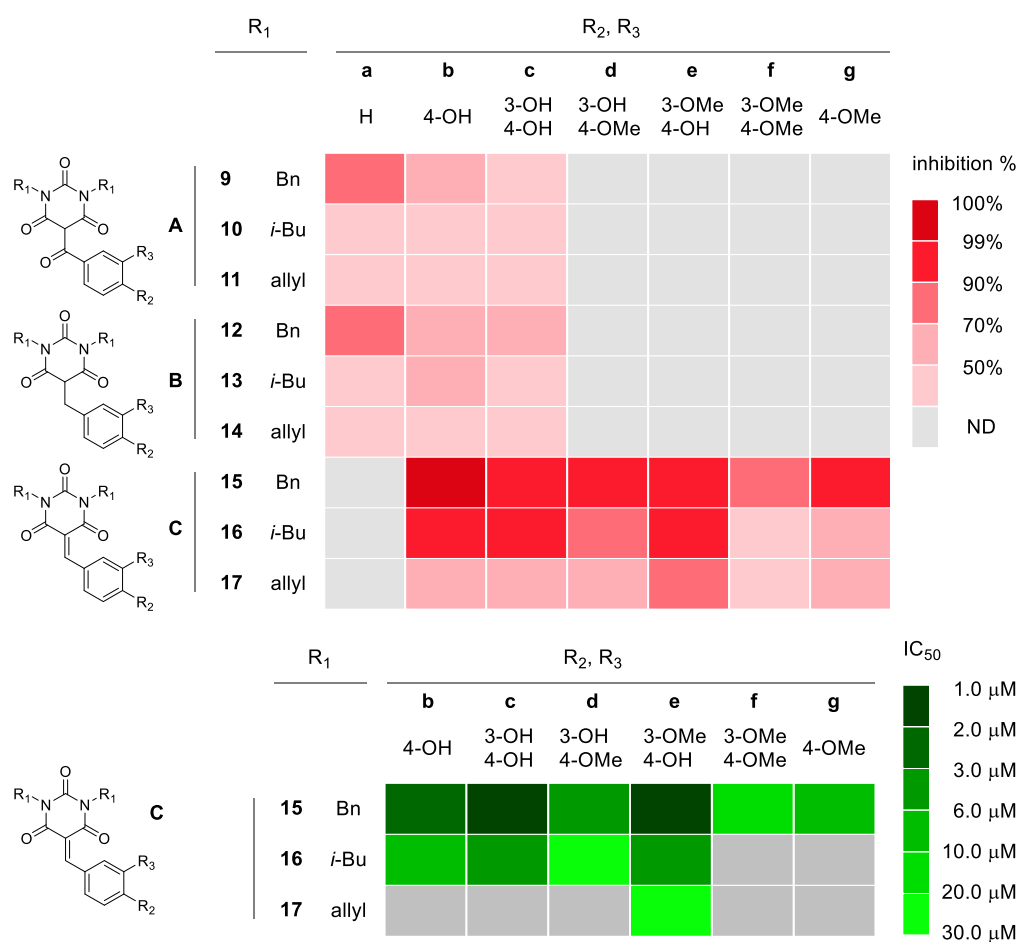

Figure 3.1.6: Inhibitory activities of compounds **9-17**. The heat maps depict the percentage of inhibition of p300 activity at 100 µM concentration of compounds **9-17** (top panel) and the IC_{50} values for selected compounds **15-17** (bottom).

3.1.2.2 Biophysical Screening: Surface Plasmon Resonance Assay

The biochemical assay allowed the selection about 20 compounds that were able to inhibit selectively p300. To further characterize the activity of the selected compounds and establish whether their inhibitor effects were due to direct binding to the target protein, SPR biophysical assay were performed. This assay was applied to Benzylidenbarbituric acid derivatives **15**-**17** (for which the IC_{50} was measured), together with compounds **9a** and **12a**, chosen as the best inhibitors among the benzoylbarbiturates A and the benzylbarbiturates B, respectively (Figure 3.1.6). Toward this aim, the human recombinant p300 (aa 1284-1673) catalytic domain was immobilized (up to approximately 10000 RU, response units) on a sensor chip, and tested ligands were injected at different concentrations over the protein surface, following the procedure reported in Chapter 3.1.1.2.

All compounds were shown to interact with the immobilized recombinant p300 HAT domain, even if a KD measurement was possible only for derivatives **12a** (KD = $(1.1 \pm 0.7) \times 10^{-6}$) and **9a** (KD = $(2.4 \pm 1.3) \times 10^{-7}$). For the benzylidenebarbituric inhibitors of type C, while setting up the injection conditions, an unexpected SPR response for subsequent injections at the same concentration was observed. Specifically, all derivatives gave a high SPR signal for the first injection immediately after dilution from the stock solution in DMSO (the time passed from the dilution to the real contact of the molecule with the sensor chip was estimated to be 2 min), while subsequent injections of the same dilution (after 10 and 15 min) gave a strongly reduced signal. On the other hand, a fresh dilution from stock produced, again, a high signal superimposable on the first injection.

The SPR response of compound **15b** binding, taken as representative of the series, to immobilized p300 is shown in Figure 3.1.7, whereas all the other 10 sensorgrams are displayed in Figure 3.1.8.

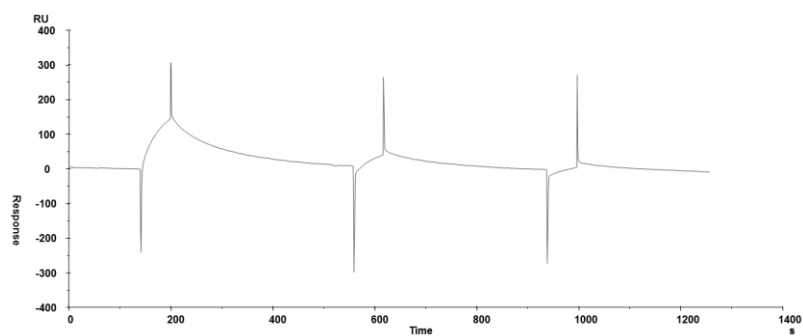**Figure 3.1.7**: Sensorgrams obtained from subsequent injections (after 2, 10, and 15 min) of a 10 µM solution of compound **15b** on immobilized p300 (catalytic domain, aa 1284-1673).

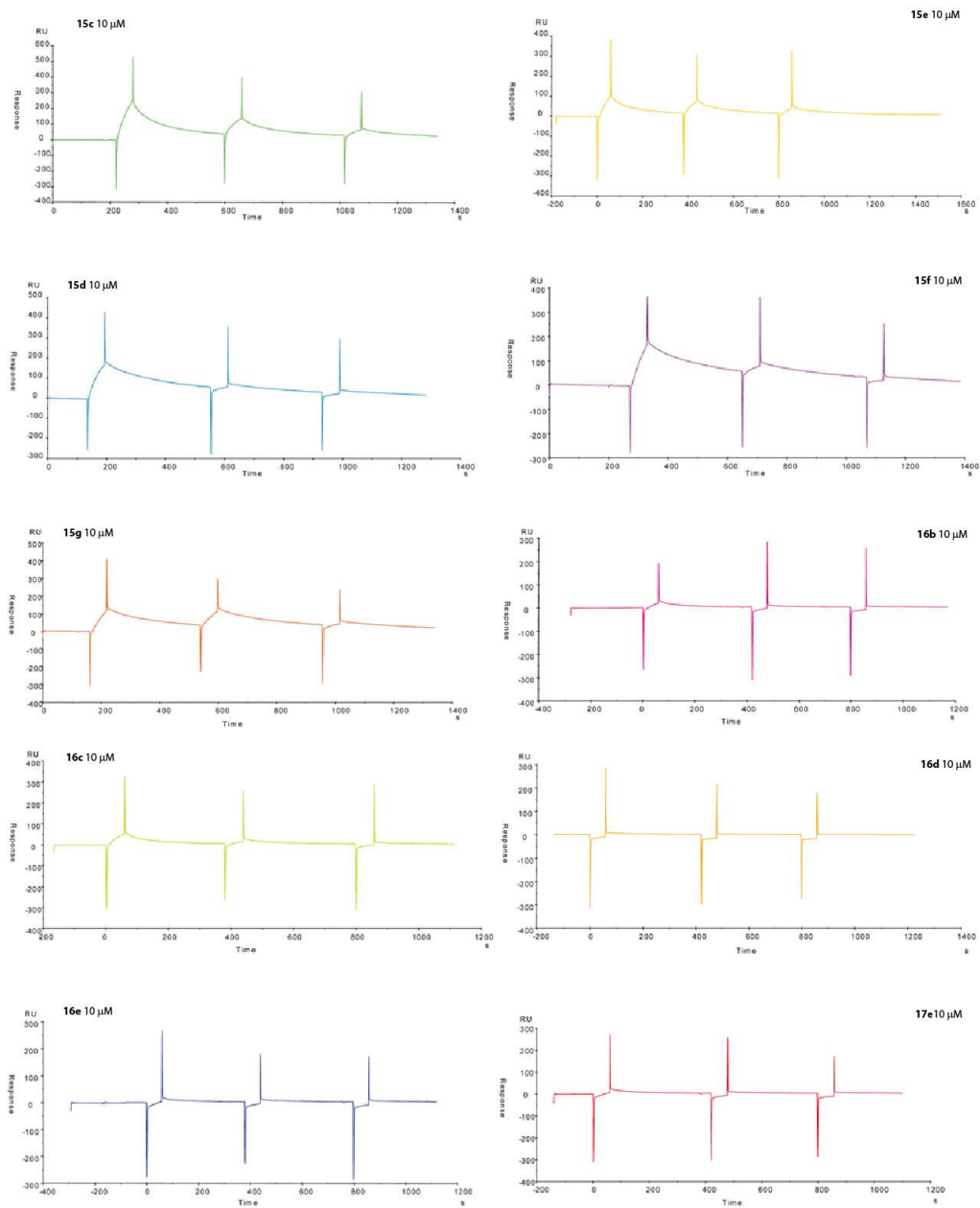**Figure 3.1.8**: Sensorgrams obtained from subsequent injections (after 2, 10, and 15 min) of a 10 μM solution of compounds **15c**-**g**, **16b**-**e** and **17e** on immobilized p300 (catalytic domain, aa 1284-1673).

3.1.2.3 Stability assays

The time-dependent outcomes of the SPR prompted the evaluation the stability of the barbituric acid derivatives in aqueous solution. Therefore, compounds **15b**-**g**, as well as derivatives **9a** and **12a**, were incubated with phosphate-buffered saline (PBS) solution at 25 °C and the stability of compounds was evaluated by HPLC analysis after 2, 10, 30, 60 min and 24 h (Figure 3.1.9). The experimental results indicated that the 5-benzoyl- and 5-benzylbarbituric acid derivatives **9a** and **12a**, respectively, were stable under the conditions routinely used in the biological assays (Figure 3.1.9). On the other hand, as hypothesized, the 5-benzylidenebarbituric acid derivatives, while stable in organic solvents, were revealed to be unstable in aqueous solutions. For almost all the compounds, degradation became evident after 10 min of incubation in an aqueous medium, and after 24 h, only the presence of hydrolysis products (aldehyde and barbituric acid) was detected. The effect was especially marked for derivatives bearing a hydroxyl group in the phenyl ring, for which degradation was almost complete after only 30 min of incubation in the aqueous medium (**15b**-**e**, Figure 3.1.9).

These findings, which are consistent with the SPR results, suggested that the IC_{50} values provided by the biochemical assays might have underestimated the potency of the 5-benzylidenebarbituric acid derivatives. The high susceptibility of benzylidenebarbituric derivatives of type C to hydrolysis appeared as a major issue to be addressed before considering any further studies, considering the incompatibility of the stability conditions with all biological assays. Therefore, we resolved to modify their structure to overcome the aqueous instability problem while preserving the activity of the parent compounds.
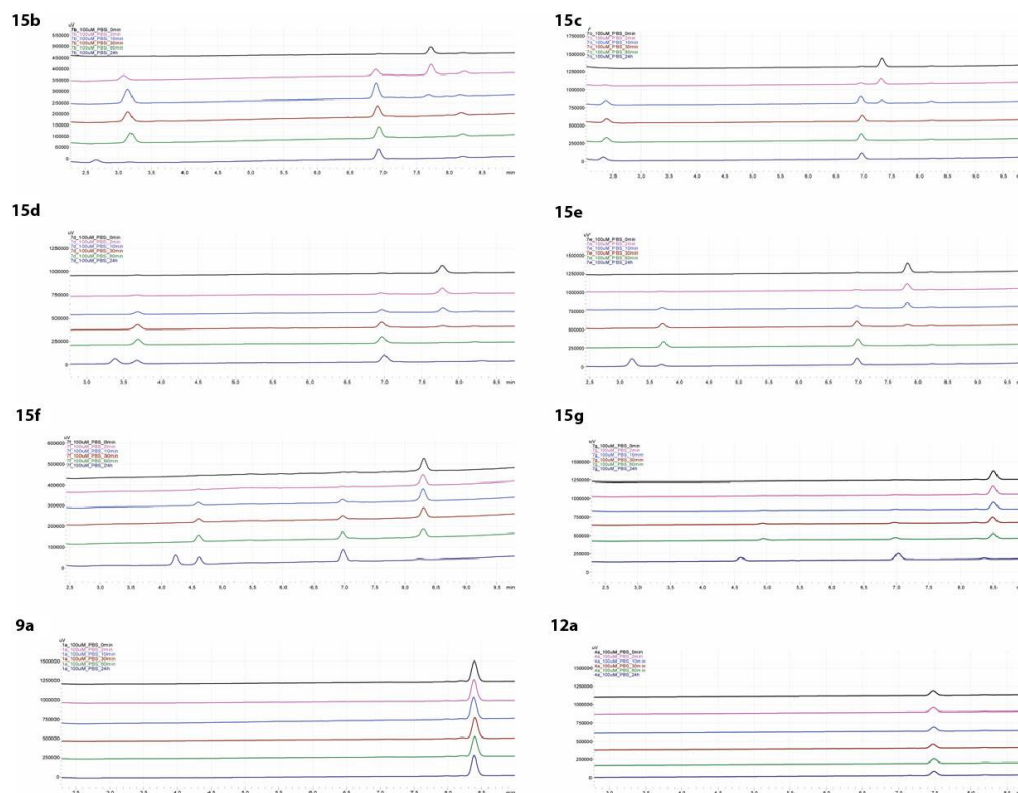
Figure 3.1.9: HPLC chromatograms obtained for compounds **15b**-**g**, **9a** and **12a** injected immediately after the dissolution in PBS, after 2, 10, 30, 60 min and 24 h. Spectra were recorded at 220 nm.

3.1.2.4 Chemical Stabilization of 15b Derivative

We supposed that the insertion of two methyl groups in the *ortho* positions of the benzylidene moiety of derivative **15b**, one of the most potent compound designed, could protect the double bond from hydrolysis. As the crucial 4-hydroxyl group was not involved, this modification was expected to not significantly affect the inhibitory potency.

Hence, in the EMCL the derivative **15h** was synthesized and its chemical stability was first evaluated. HPLC analysis revealed that the compound did not decompose after exposure to PBS buffer solution over a period of 24 h (Figure 3.1.10).
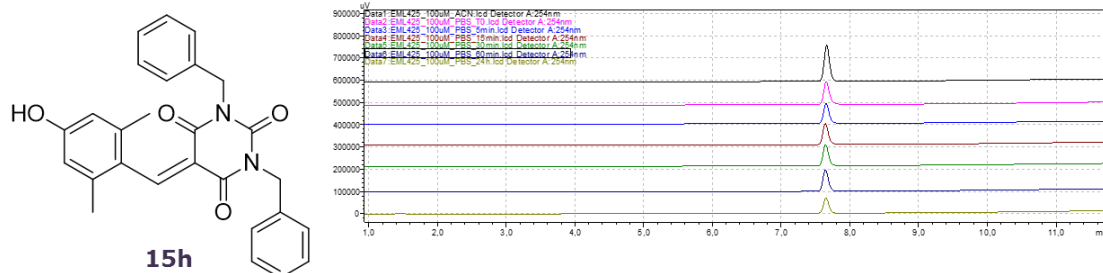
Figure 3.1.10: Chemical structure of derivative **15h** and HPLC chromatograms obtained for it, injected immediately after the dissolution in PBS, after 2, 10, 30, 60 min and 24 h. Spectra were recorded at 220 nm.

3.1.2.5 Biochemical and Biophysical Characterization of 15h Derivative

Once chemical stability was established, derivative **15h** was tested for inhibition of the recombinant acetyltransferase enzymes p300, PCAF and GCN5 (Figure 3.1.11). It was found that the introduction of two methyl groups in the structure of **15b** resulted in an analogue (derivative **15h**) endowed with potency and selectivity comparable to those of the parent compound. In fact, **15h** efficiently inhibited p300 (IC$_{50}$ value of 2.9 µM) while being practically inactive against the enzymes GCN5 and PCAF.
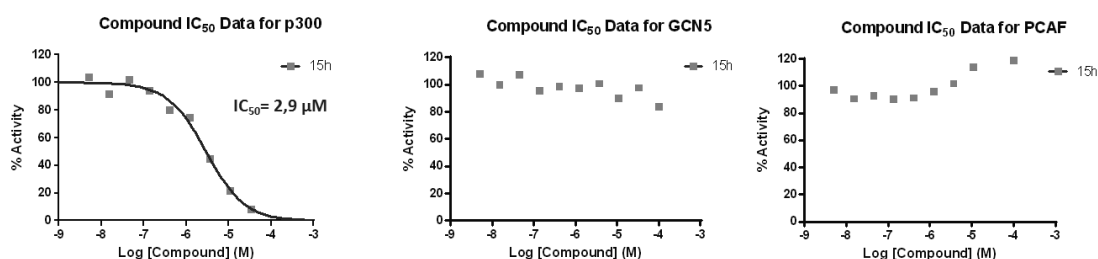
Figure 3.1.11: Concentration-response inhibition of p300, GCN5 and PCAF by compound **15h**. The compound was tested in 10-concentration IC$_{50}$ mode with 3-fold serial dilutions starting at 100 µM. Data were analyzed using GraphPad Prism software (version 6.0) for curve fitting, using a sigmoidal concentration-response with a variable slope equation.

It is important to note that, due to the time-dependent instability of aqueous solutions of 5-benzylidenebarbiturates **15b**-**g**, a direct comparison of the

acetyltransferase inhibitory potency of compound **15h** with those of derivatives **15b**-**g** might not be very meaningful.

After the biochemical characterization of **15h** derivative, to establish whether its inhibitor effect was due to direct binding to the target protein, the SPR biophysical assay was performed. As shown in Figure 3.1.12, the concentration-dependent responses and the clearly evident exponential curves during both the association and dissociation phases indicate that **15h** derivative efficiently interacts with the protein.
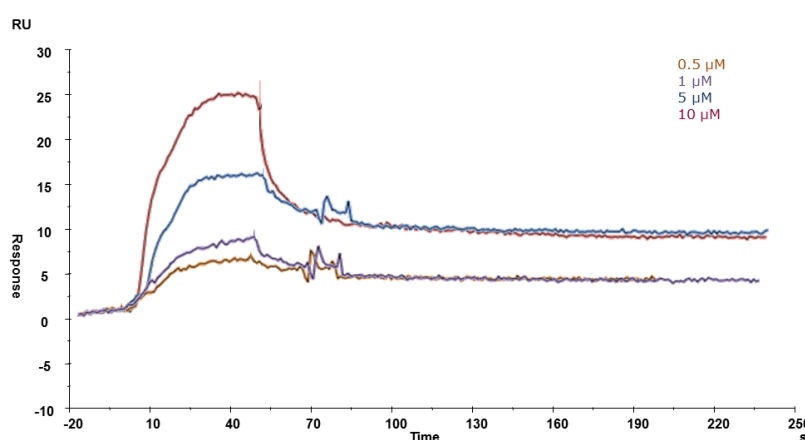
Figure 3.1.12: Sensorgrams obtained from the SPR interaction analysis of compound **15h** to immobilized p300 (catalytic domain, aa 1284-1673, top row). Compound was injected at 0.5, 1, 5, and 10 μM, giving the concentration-dependent signals shown. Using the 1:1 Langmuir binding fit model of the BIAevaluation software, the KD was determined. (KD = $6.27 \pm 1.1 \times 10^{-8}$).

The conjugated double bond in compound **15h** is potentially electrophilic and could serve as a Michael acceptor and covalently modify the target enzyme. Therefore, even if the results of the SPR experiments were not consistent with this hypothesis, it was investigated whether **15h** could generate adducts with the nucleophile β-mercaptoethanol. HPLC chromatographic analysis revealed no evidence of reaction under the buffer conditions used in the enzymatic assay (Figure 3.1.13), thus suggesting that **15h** acts as a reversible p300 inhibitor.

Figure 3.1.13: HPLC chromatograms of the mixture of compounds **15h** and 2-mercaptoethanol (β-mercaptoethanol, BME) injected immediately after the dissolution in PBS, after 30, 60, 120, 240 min and 24 h. Spectra were recorded at 220 nm.
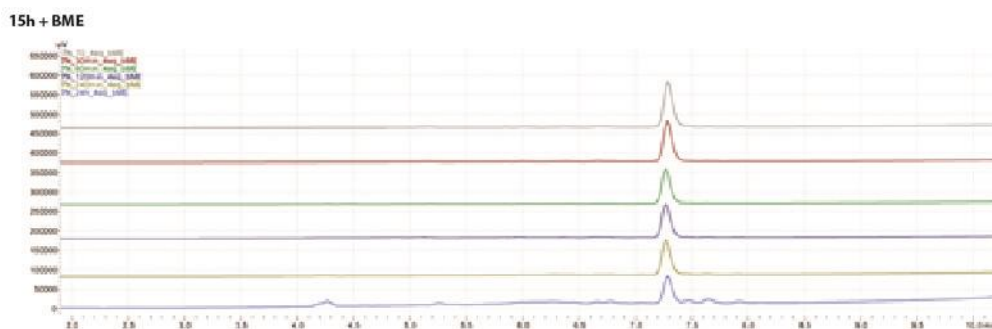
3.1.2.6 Inhibition Mechanism of **15h** Derivative

Subsequently, to better characterize the enzymatic activity of compound **15h**, the kinetic mechanism of p300 inhibition was evaluated using another biochemical method, the AlphaLISA homogeneous proximity immunoassay. This type of assay allows one to measure enzyme activity by detecting the acetylation of a biotinylated histone H3 peptide using streptavidin-coated donor beads and AlphaLISA acceptor beads conjugated to an antibody directed against the modified substrate.

The inhibitory effect of **15h** was explored by performing two sets of experiments. Firstly, enzyme activity was measured by varying the histone H3 peptide substrate concentration while keeping the acetyl-CoA concentration constant. Subsequently, the acetyl-CoA concentration was varied while keeping the H3 peptide concentration constant.

Figure 3.1.14 shows the double-reciprocal plots at three different inhibitor concentrations (0, 5, and 10 μM). From these data, derivative **15h** was shown to be a non-competitive inhibitor versus both acetyl-CoA and a histone H3 peptide, able to bind both the free enzyme and the enzyme-substrate complex, even with unequal affinity constants determined by the two secondary plots reported in Figure 3.1.15.
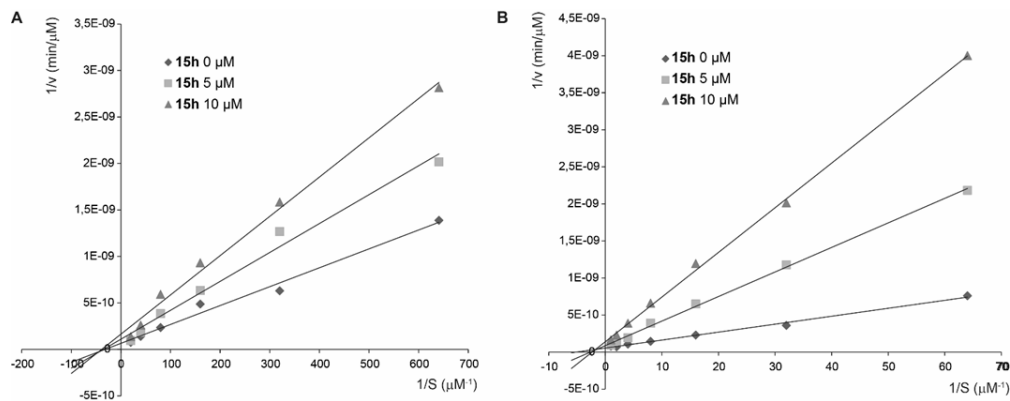
Figure 3.1.14: (A) Plot of 1/v vs 1/[H3] at a fixed acetyl-CoA concentration (3 μM) and three different concentrations of **15h** shows non-competitive inhibition. **15h** Ki = 9.4 μM, α Ki = 6.8 μM, H3 apparent Km = 30 nM. (B) Plot of 1/v vs 1/[acetyl-CoA] at a fixed H3 concentration (0.05 μM) and three different concentrations of **15h** shows non-competitive inhibition. **15h** Ki = 2 μM, α Ki = 5.7 μM, acetyl-CoA apparent Km = 194 nM.
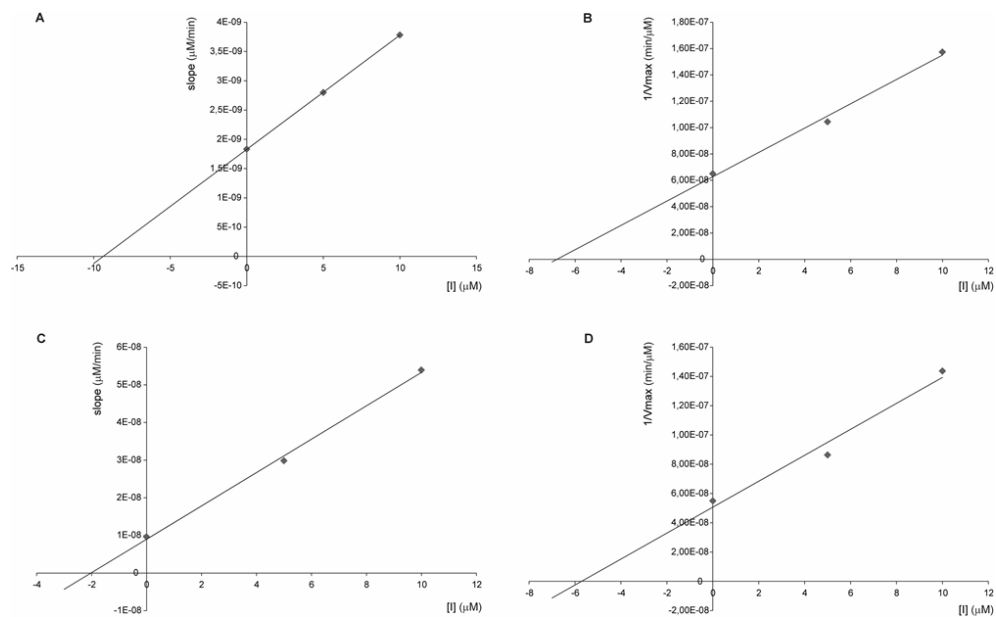
Figure 3.1.15: Kinetic assays. (**A**, **C**) The slope of the double reciprocal plot was plotted against inhibitor concentration ([I] in μM). K_i was obtained from the negative x intercept of the slope replot. **A** (H3) K_i= 9,4 μM, **C** (AcetylCoA) K_i= 2 μM. (**B**, **D**) The reciprocal of Vmax was plotted against inhibitor concentration ([I] in μM). αK_i was obtained from the negative x intercept. **B** (H3) αK_i= 6,8 μM, **D** (AcetylCoA) αK_i= 5,7 μM.

3.1.2.7 Evaluation of Cellular Activity

After the identification of the stable, potent and selective p300/CBP inhibitor **15h**, its effect was evaluated in cells. Before starting with cellular assays, it was estimated the cell permeability of **15h**.

To this aim, the well-validated parallel artificial membrane permeability assay (PAMPA) technique was employed.[79, 80] The highly permeable drug propranolol and the poorly permeable drug furosemide were used as references. The compound showed an apparent permeability value (P_{app}) of 1.9×10^{-6} cm/s, similar to that of propranolol ($P_{app} = 4.1 \times 10^{-6}$ cm/s), and very different from furosemide ($P_{app} = 0.09 \times 10^{-6}$ cm/s).

These positive findings prompted the evaluation on the effect of **15h** on cells. Similarly to what was carried out in the previously reported **SPV106** analogues screening, it was evaluated the effect of **15h** on the cell cycle progression and the percentage of sub-G_1 hypodiploid nuclei in the human leukemia U937 cell line. After 72 h of incubation with **15h** at 100 μM, the compound induced a marked arrest in the G_0/G_1 phase and a significant increase in hypodiploid nuclei percentage (Figure 3.1.16).
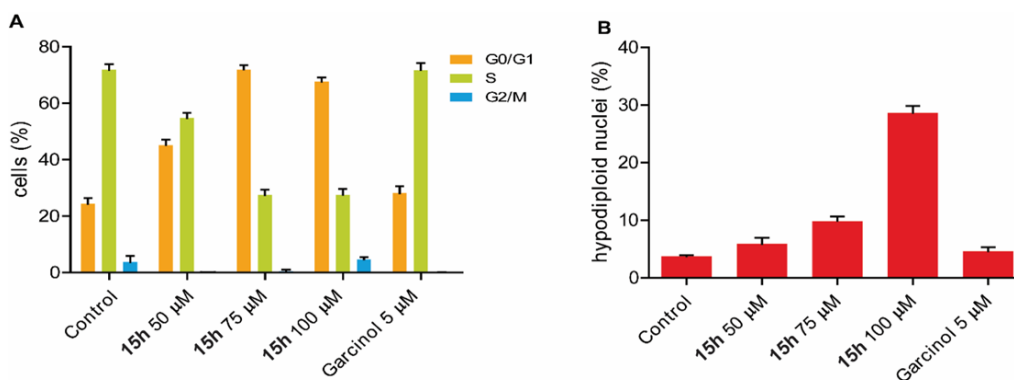
Figure 3.1.16: Cell cycle analysis (A) and percentages of cells with hypodiploid nuclei (B) in U937 cells by fluorescence-activated cell sorting (FACS). The U937 cells were treated with the compounds **15h** and garcinol at the indicated concentrations for 72 h, stained with propidium iodide, and subjected to flow cytometric analysis to determine the distribution of cells in each phase of the cell cycle. Data are reported as the mean ± SD of at least three independent experiments.

Subsequently, the effects of compound **15h** on cellular histone acetylation were investigated, using modification-specific antibodies against H3K9ac and H4K5ac (Figure 3.1.17). Cells were incubated for the indicated times (24, 48, or 72 h) with **15h** (100 μM) or the reference compound garcinol (5 μM),[10] and the histone extracts were then immunoblotted with antibodies to specific histone acetylation sites. As represented in Figure 3.1.18, it was observed that compound **15h** induced a marked and time-dependent reduction in the acetylation of lysine H4K5 and H3K9 in U937 cells.
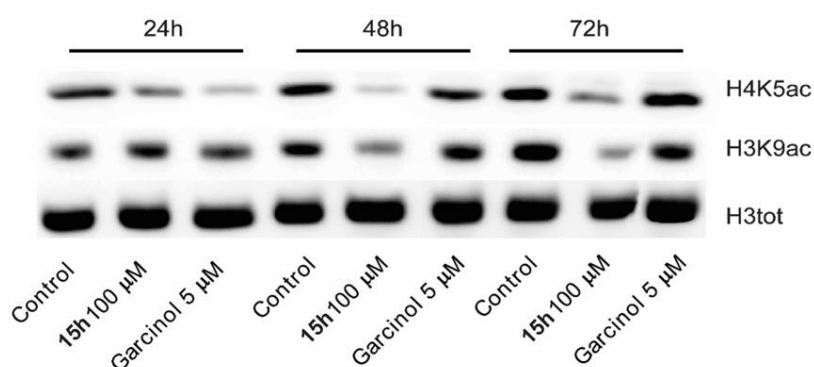
Figure 3.1.17: Western blot analyses performed with compound **15h** at 100 μM for 24, 48, and 72 h on the acetylation of the specific lysine residues H4K5 (upper lane) and H3K9 (middle lane) in histone extracts from U937 leukemic monocyte lymphoma cells. Acetylation was detected by immunoblotting with antibodies specific for histone acetylation sites as indicated. Total histone H3 was used to check for equal loading. Garcinol (5 μM) was used as a reference compound.

Taken together, all these findings corroborate the inhibitory effect of **15h** on the intracellular histone acetylation mediated by p300 and are consistent with the importance of this enzyme for control of the G_1/S transition. In fact, p300 is required for the orderly G_1/S transition in human cancer cells, and selective inhibitors, such as C646, induce cell cycle arrest in the G_1 phase and apoptosis.[14, 71, 81-83]

In conclusion, this screening method allowed the discovery of the derivative **15h**, more potent and selective than the reference compounds curcumin and anacardic acid; it is a reversible inhibitor and non-competitive versus both substrate and cofactor, endowed with good cell permeability ($P_{app} = 1.9 \times 10^{-6}$ cm/s), as assessed by the PAMPA technique. Furthermore, in human leukemia U937 cells, it induced a marked and time-dependent reduction in the acetylation of lysine H4K5 and H3K9, a marked arrest in the G_0/G_1 phase and a significant increase in hypodiploid nuclei percentage.

Therefore, **15h** may be an invaluable chemical probe not only for mechanistic studies of p300-mediated lysine acetylation but also to further investigate the biological role of this KAT enzyme and its implications in physiological and/or pathological processes.[8] Moreover, in the last few months, compound **15h** became commercially available (Xcessbio™) and was recently used in a research article of Simola D. F. *et al.* as CBP/p300 *in vivo* chemical probe to study the synaptic plasticity in the ant *Camponotus floridanus.*[84]

3.2 SETD8

SETD8 is the sole protein lysine methyltransferase (PKMT) known to monomethylate lysine 20 of histone H4 *in vivo* (Chapter 1.2.2.2.1). As SETD8 is implicated in many essential cellular processes, the identification of specific modulators is of great importance to further clarify the biological role of this methyltransferase. Despite such need, few modulators of high quality have been reported so far for SETD8.[29, 85]

A few years ago, a high-throughput screening campaign of ChemBridge's diversity library (DIVERSet, 10000 compounds) led Bedford and coworkers to the identification of small molecule modulators of protein methyltransferases.[86] On the basis of our observation that two different dye-like scaffolds, namely a xanthenic moiety and an aminohydroxynaphthalene sulfonic moiety, were recurrent as privileged structures in the hits selected, in the EMCL a small focused library containing the two dye-like scaffolds was prepared to identify hits for the development of modulators of arginine methyltransferases (PRMTs).[70, 87, 88]

Interestingly, a few compounds were able to inhibit both arginine and lysine methyltransferases and among them, the compound EPI-009 (Thymolphthalein) (Figure 3.2.1) showed low IC_{50} values against SETD8 ($IC_{50}= 9$ μM) in a radioactive assay.[89]
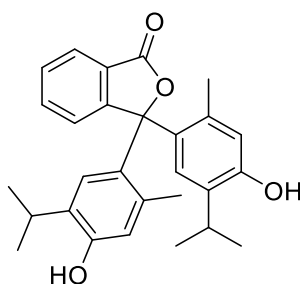
Figure 3.2.1: EPI-009 structure.

To further investigate its activity profile and with the aim to develop selective SETD8 inhibitors, a screening approach for this epigenetic enzyme was developed.

3.2.1 His-SETD8-FLAG expression and purification

The development of different biochemical and biophysical assays requires large amount of protein. To reduce the costs of the assays, the first issue to be addressed was the "in house" production of SETD8. Therefore, a pET-28 b (+) vector containing SETD8 (residues 51-383) was generously provided by Dr. D. Reinberg (Department of Biochemistry and Molecular Pharmacology, Howard Hughes Medical Institute, New York (USA)) and allowed the expression of a double tagged His-FLAG human SETD8 protein. The vector was transformed into BLR(DE3)*pLysS* competent cells and the protein was overexpressed in LB, optimizing the induction conditions at 1 mM IPTG for 6 h at 25 °C. The expressed protein was purified by affinity chromatography using an AKTA FPLC system and a 1-mL HisTrap HP column (Figure 3.2.2).

The activity of the protein was determined in AlphaLISA assay, which was previously optimized using a commercially available protein (His-SETD8). It was not possible to use the expressed SETD8 in the same concentration of the commercially available one (20 nM) because of an unsuitable signal/noise ratio. It was necessary to increase the concentration of the expressed protein (1 μM) to have a result comparable to the one got with the reference protein (Figure 3.2.3).
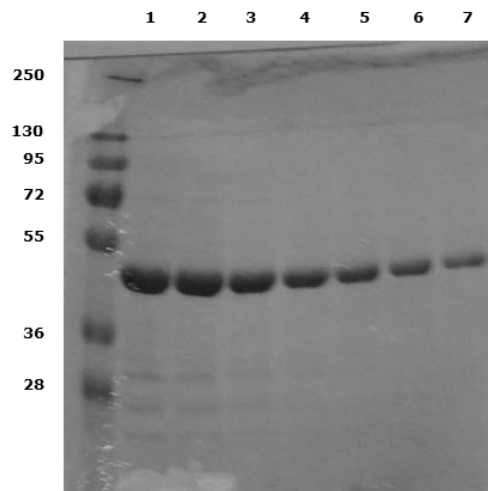
Figure 3.2.2: 1-7) Elution Fractions.
SDS-PAGE after the purification of the protein by affinity chromatography using HisTrap HP column and an AKTA FPLC at 1 mL/min.
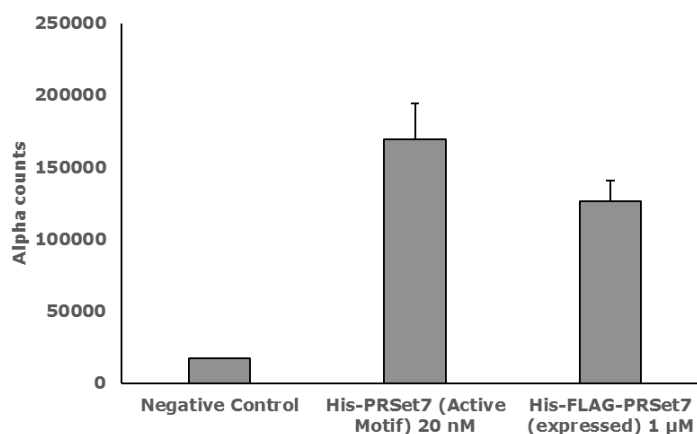
Figure 3.2.3: AlphaLISA assay performed with the commercially available His-SETD8 and the expressed His-FLAG-SETD8. The assay was performed incubating the protein with 150 nM of Histone H4 and 200 μM of SAM for 1h at room temperature. The results reported are the means ± SD determined for at least two separate experiments.

3.2.1.1 Microscale Thermophoresis (MST) experiments at LMU

After the optimization of expression and purification procedures for SETD8, I spent a period at Ludwig Maximilians Universität München (LMU) in the lab of prof. Axel Imhof, where I had the opportunity to learn the Microscale

Thermophoresis technique (MST). MST measurements are based on the physical principle of Thermophoresis, which is the directed motion of molecules in temperature gradients (Chapter 1.6.3).[53, 54]

After the labeling of human His-FLAG-SETD8 with the dye NT-647, the protein was used to perform Thermophoresis experiments in order to study the interaction of the protein with EPI-009. Unfortunately, these experiments did not allow the detection of any interaction between the protein and the small molecule compound (Figure 3.2.4).
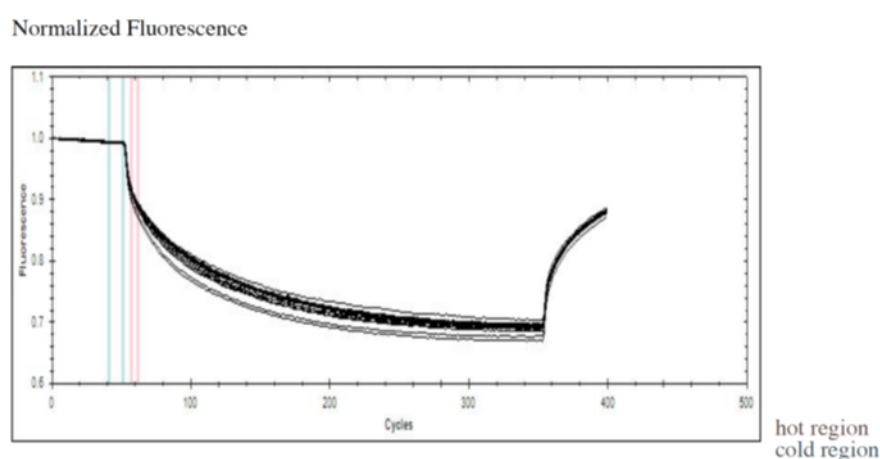
Figure 3.2.4: Microscale Thermophoresis time-traces of the interaction between human His-FLAG-SETD8 and EPI-009. The overlapping of curves showed no interaction between the two binding partners.

However, the thermophoresis experiments performed under the same conditions but using another protein, a mouse-SETD8 without any tag (characterized by 91% sequence homology compared to the human one) showed a clear interaction with EPI-009, with a KD of 1.02×10^{-4} (Figure 3.2.5).

Normalized Fluorescence
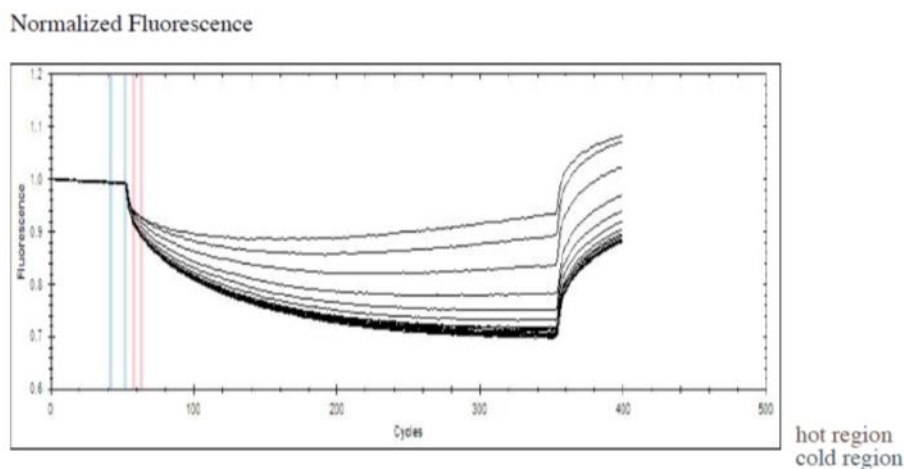
Figure 3.2.5: Microscale Thermophoresis time-traces of the interaction between mouse SETD8 and EPI-009.

The different behaviour of the two proteins let us to speculate that tags could prevent the binding with the small molecule EPI-009. It is worthwhile noting that all tags, whether large or small, could interfere with the biological activity of a protein, impede its crystallization, interfere with the proper structure or otherwise influence its behaviour. Consequently, it is usually desirable to remove them and work with a protein in a native state.[90-93] Unfortunately, in the case of this protein, the removal of both tags was not possible because of the lack of cleavage sites.

3.2.2 Cloning, Expression and Purification of GST-SETD8

With the aim to obtain a protein in a native state, the DNA sequence encoding for human SETD8 was cloned into a pGEX-4T-1 plasmid, in order to express a cleavable GST-tagged protein at the amino terminus.

The plasmid pET-28 b (+) was sequenced, afterwards primers were designed to amplify the DNA encoding for the protein. After the amplification by PCR reaction, the DNA was inserted first in the cloning vector pGEM-T and then in the expression vector pGEX-4T-1, using as restriction sites BamHI and XhoI.

The vector pGEX-4T-1 was transformed into BLR(DE3)*pLysS* competent cells and the protein was overexpressed in LB, optimizing the induction conditions at 1 mM IPTG for 2 h at 37 °C. The expressed protein was purified by affinity chromatography using an AKTA FPLC system and a 1-mL GSTrap HP column (Figure 3.2.6). Unfortunately, the protein showed instability during the purification steps. As reported in Figure 3.2.5, GST-SETD8 (66 kDa) was eluted together with some degradation products. Despite the highlighted instability, the activity of the protein was evaluated using the AlphaLISA assay.
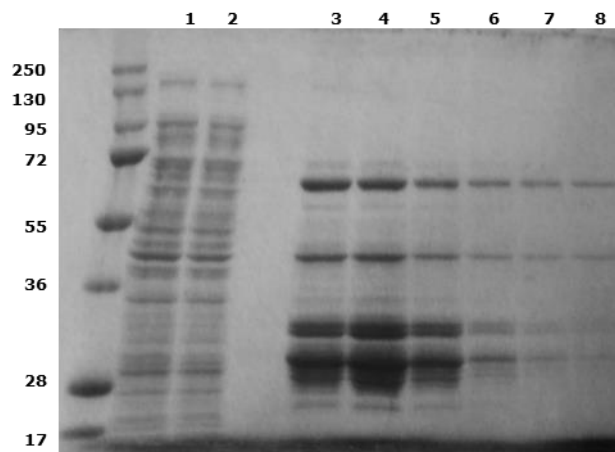
Figure 3.2.6: SDS-PAGE of the purification of GST-SETD8 (66 kDa) by affinity chromatography using GSTrap HP column and an AKTA FPLC at 1 mL/min. Lane 1: lysate; Lane 2: unbound fraction; Lanes 3-8: elution fractions

As shown in the Figure 3.2.7, the expressed GST-SETD8 (3.3 μg/mL) was active in the biochemical assay.
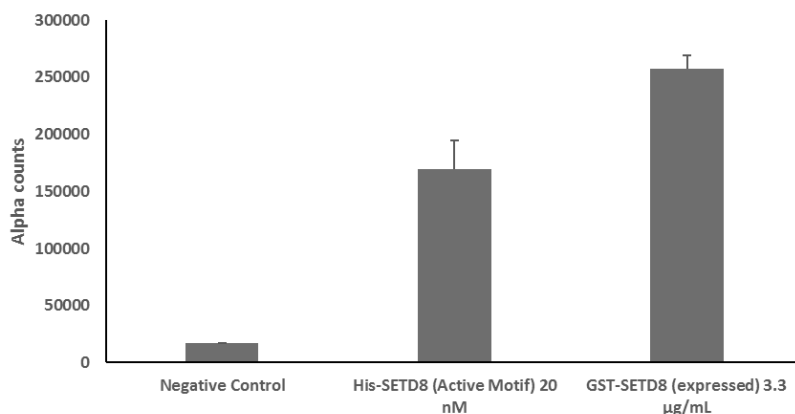
Figure 3.2.7: AlphaLISA assay performed with the commercially available His-SETD8 and the expressed GST-SETD8. The assay was performed incubating the protein with 150 nM of Histone H4 and 200 μM of SAM for 1h at room temperature. The results reported are the means ± SD determined for at least two separate experiments.

3.2.2.1 Cleavage of GST tag

Subsequently, GST cleavage was performed using the ThrombinCleanCleavage Kit. A specific cleavage site located between the tag and the protein sequence would have ensured simple removal of the tag.

Tags cleavage conditions are dependent on the protein of interest and have to be optimized for each protein separately. In the case of GST-SETD8, although different temperatures and incubation times were tested (data shown in Table 3.2.1), it was not possible to isolate the cleaved protein because of protein degradation or inactivity of the proteolytic enzyme. Therefore, also this approach has been abandoned.

Indeed, the use of Thrombin to obtain a pure "native-like" protein of interest is often associated to non-specific cleavage: even if the most common linker sequence recognized by thrombin is LVPRG or LVPRGS (which is derived from the sequence in bovine factor XIII that is cleaved by thrombin during the activation process), it is not absolute.[43, 44] Cleavage can occur at other sequence sites in the protein, causing proteolytic degradation and this was probably the case of GST-SETD8.

In order to obtain a stable and easily cleavable protein, it was selected the Halotag system, that was developed to overcome the current limitations of traditional protein tagging platforms.[94] Experiments on the optimization of expression and purification conditions of SETD8 with the Halo tag are still in progress.

#	Temperature	Digestion Time	Result
1	25 °C	360 min	Degradation
2	25 °C	240 min	Degradation
3	25 °C	120 min	Degradation
4	25 °C	60 min	Degradation
5	25 °C	30 min	Degradation
6	4 °C	360 min	Degradation
7	4 °C	240 min	Degradation
8	4 °C	120 min	Degradation
9	4 °C	60 min	No cleavage

Table 3.2.1: Summary of all the tested GST cleavage conditions.

3.2.3 Gene Reporter System

For the development of a robust screening platform for SETD8, biochemical and biophysical approaches were needed as well as cellular assays.

To address this need, the experimental conditions of a Gene Reporter System (previously reported by D. Reinberg and coworkers[28]) have been optimized.

Using a 293T-REx cell line containing a stably integrated 5xUAS site directing luciferase expression, GAL4-SETD8 was expressed under an inducible tetracycline-responsive promoter. In normal conditions, Tet repressors bound to TetO$_2$ elements keep Gal4-SETD8 expression repressed. Upon induction by tetracycline, the repressors leave the DNA and GAL4-SETD8 is expressed, resulting in binding to the GAL4 binding sites to the luciferase reporter that is

stably integrated in euchromatic DNA. SETD8 recruitment to the artificial UAS locus led to decrease in luciferase expression, due to the methylation on the gene promoter by SETD8 (Figure 3.2.8). The decrease of luciferase expression can be easily monitored by a luciferase activity assay (Dual-Light® luminescent reporter gene assay).
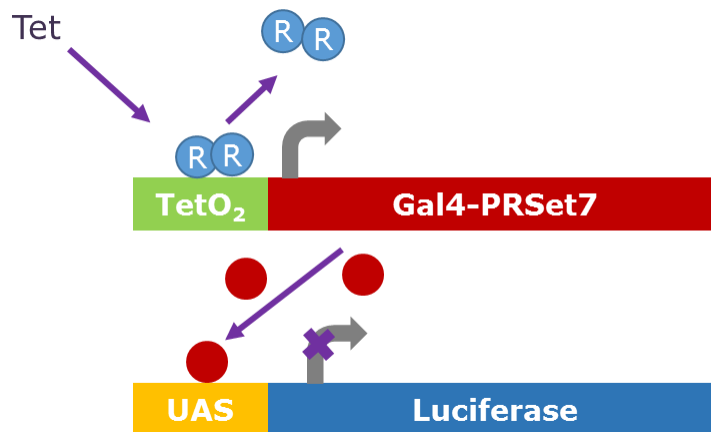
Figure 3.2.8: Gene Reporter System

The experimental conditions of the assays were optimized in order to obtain the transfection of plasmid in cells, detectable by luciferase activity variation. First, the required cell confluence was evaluated: 3000-5000-10000 cells were seeded in 96-well plate and after 48 h of incubation at 37 °C it was shown that the better confluence was obtained by seeding 10000 cells for each well. Subsequently, several transfection experiments were performed in order to establish the minimum concentration of transfecting agent needed: while the use of 0.1 µL/well of Lipofectamine was not sufficient for the transfection, good results were achieved using 0.2 and 0.4 µL of transfecting agent; accordingly, 0.2 µL of Lipofectamine was used in the following experiments. Finally, the quantity of vector to be used in the experiments was evaluated: among 100, 50 and 25 ng of DNA, the best results were achieved using 100 ng of pcDNA™4/TO GAL4-SETD8.

In Figure 3.2.9 the result of the luciferase assay, performed with the optimized transfection conditions, is reported. As expected, the addition of Tetracycline, which led to overexpression of GAL4-SETD8, is associated with a decrease in Luciferase expression, detected in a luminesce assay. The use of this system will be particularly useful, as it will allow the identification of new cell-permeable modulators of SETD8.
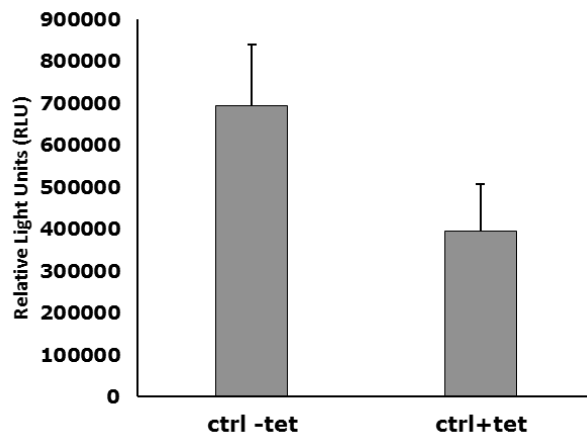
Figure 3.2.9: Dual-Light® Luminescent Reporter Gene Assay performed on 293T-REx lysate after the transfection.

3.3 TUDOR DOMAINS OF PHF20

3.3.1 UNC1215 analogues as Tudor modulators

Among different reader proteins, Tudor domains of PHF20 belong to the Royal superfamily of methyl-lysine effector proteins (Chapter 1.4.2.1.1).

UNC1215 (Figure 3.3.1) is the first in class chemical probe for the reading function of L3MBTL3, a relatively uncharacterized member of the human Malignant Brain Tumor (MBT) family of chromatin interacting transcriptional repressors. Interestingly, this is the only molecule described to interact with the Tudor domain of PHF20.[95] With the aim to discover new potent and selective inhibitors of this epigenetic reader, a small pool of UNC1215 analogues was synthesized in the EMCL (for patent reasons, I cannot show the structures of the prepared derivatives). In order to evaluate the activity of these putative modulators of this reader, a screening method for this target was established.
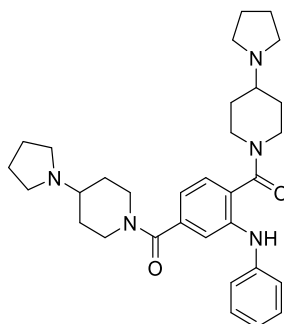
Figure 3.3.1: UNC1215 structure.

3.3.1.1 Protein expression and purification

Since Tudor domain of PHF20 is a newly identified target, the protein is not commercially available. A pGEX-4T-1 vector containing Tudor 1 and 2 (residues 1-150) was generously provided by Dr. M. Bedford (Department of Epigenetics & Molecular Carcinogenesis, Smithville, Texas, USA) and allowed the expression of a GST-tagged protein (Figure 3.3.2).
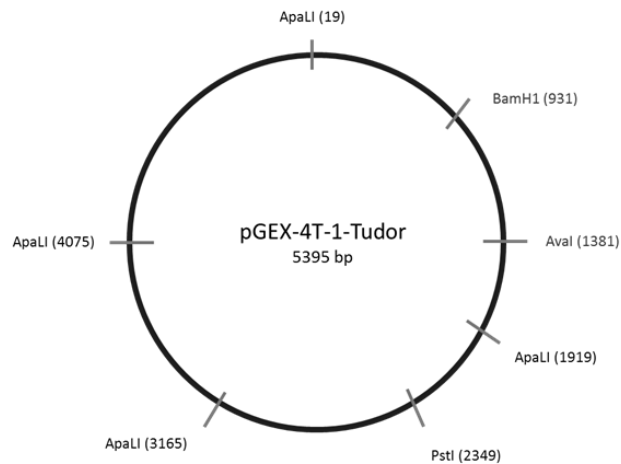
Figure 3.3.2: Plasmid map for the expression of PHF20 Tudors (aa 1-150) as GST tagged protein (44 kDa).

The vector was transformed into BLR(DE3)*pLysS* competent cells and the protein was overexpressed in LB, optimizing the induction conditions at 1 mM IPTG for 4 h at 37 °C. The expressed protein was purified by affinity chromatography using an AKTA FPLC system and a 1-mL GSTrap HP column (Figure 3.3.3).
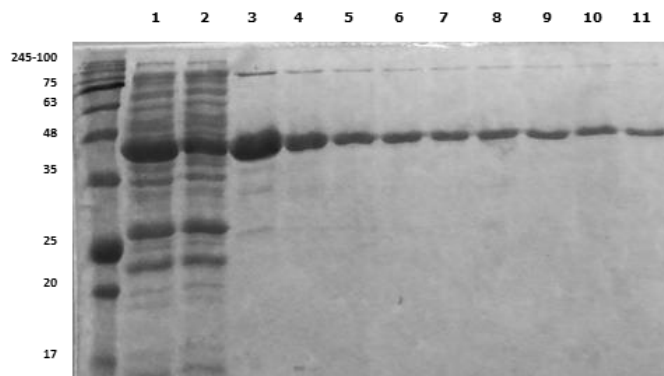
Figure 3.3.3: SDS-PAGE of the purification of the protein by affinity chromatography using GSTrap HP column and an AKTA FPLC at 1 mL/min. Lane 1: lysate; Lane 2: unbound fraction; Lanes 3-11: elution fractions.

With the aim to obtain the protein free from its fusion carrier partner, the GST tag was completely cleaved using the ThrombinCleanCleavage Kit (Figure 3.3.4). After the cleavage, the purification of the native protein was performed

by ionic exchange chromatography using a Mono Q column, taking advantage of their different isoelectric points (Figure 3.3.5).
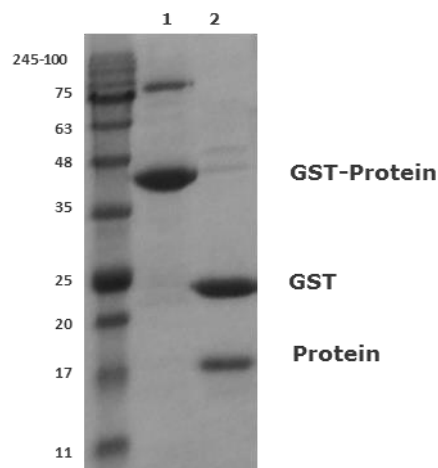
Figure 3.3.4: 1: SDS-PAGE after the GST cleavage, which was performed incubating the protein with Thrombin beads for 6 h at room temperature. Lane 1: protein before the cleavage; Lane 2: protein after the cleavage.
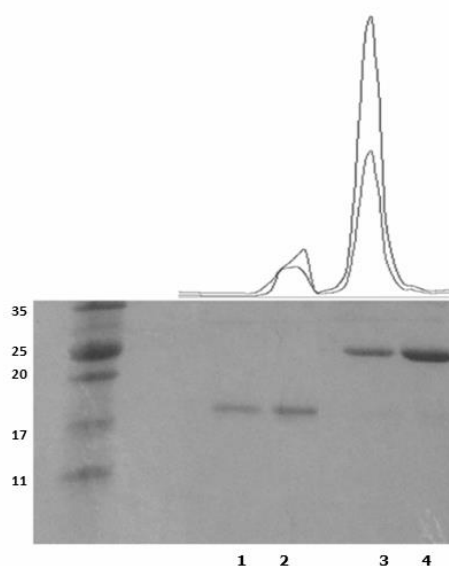
Figure 3.3.5: SDS-PAGE of the separation of the protein from GST by anionic exchange chromatography using a Mono Q column. Lanes 1-2: protein; Lanes 3-4: GST.

3.3.1.2 Biophysical Screening: nanoDSF

The cleaved protein was used in a biophysical assay with the aim to evaluate the interaction with UNC1215 analogues. This primary screening was performed

by nanoDSF that is an advanced Differential Scanning Fluorimetry method for measuring ultra-high resolution protein stability (Chapter 1.6.2).

All compounds were screened by nanoDSF at 100 μM concentration and if they exhibited a ΔTm ≥ 0.5 °C (chosen as cut-off), they were selected as potential modulators. Therefore, compounds EML637, EML639, EML644 and EML666 met the selection criteria exhibiting ΔTm values ranging from 0.5 - 1.1 °C at 100 μM (Table 3.3.1).

#	Start Temperature	End Temperature	Tm	ΔTm
Ctrl	20 °C	95 °C	69.59	0
UNC1215	20 °C	95 °C	70.09	0.50
EML635	20 °C	95 °C	69.17	-0.42
EML636	20 °C	95 °C	69.54	-0.049
EML637	20 °C	95 °C	70.66	1.1
EML638	20 °C	95 °C	69.56	-0.026
EML639	20 °C	95 °C	70.09	0.50
EML643	20 °C	95 °C	69.95	0.36
EML644	20 °C	95 °C	70.15	0.56
EML666	20 °C	95 °C	70.29	0.70

Table 3.3.1: nanoDSF assays were performed using the Prometheus. The small molecule screening was performed at the fixed dose of 100 μM, with a protein concentration of 20 μM. For the analysis, standard capillaries were used.

3.3.1.3 AlphaScreen assay: design, optimization and evaluation of UNC1215 analogues activity

In order to analyse the effect of UNC1215 analogues on the reader activity of Tudor domains of PHF20, an AlphaScreen assay was designed and set-up using streptavidin-coated donor beads and anti-GST antibody coated acceptor beads to measure binding of a GST-tagged protein to a biotinylated histone peptide.

With the aim to define the best conditions under which the assay delivered a high signal and low background, different buffer components were tested; first,

the impact of three detergents (Tween20, Triton-X100 and CHAPS) on assay signal was examined (Figure 3.3.6).
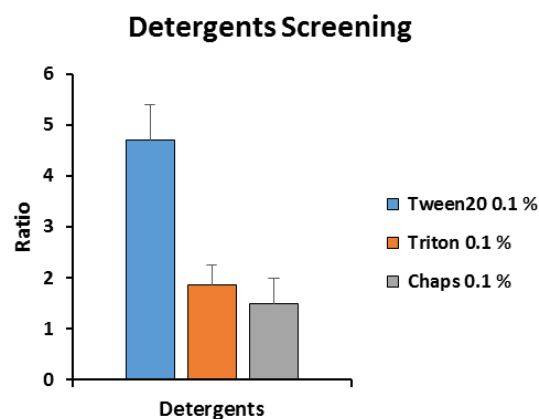
Figure 3.3.6: Effect of three detergents to decrease the nonspecific binding observed when the assay was performed in basic buffer 20 mM Tris-HCl pH 8. Each assay was performed in presence of NaCl 50 mM. The use of Tween 20 resulted in the best signal/noise ratio.

The use of Tween 20 yielded the best signal/background ratio, so this detergent was subjected to a 3-point titration to determine its optimal concentration in the assay buffer; in the same assay, 3 different concentration of NaCl were tested as well. Two combinations of reagents yielded similar profiles: NaCl 50 mM with Tween20 0.025% and NaCl 25 mM with Tween 0.05% (Figure 3.3.7).
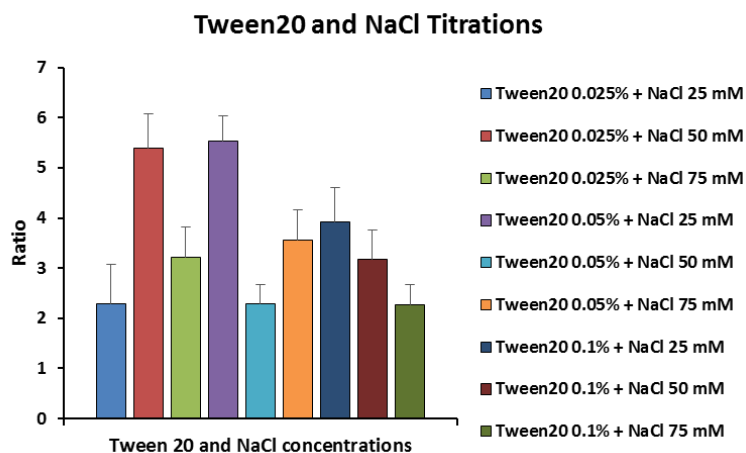
Figure 3.3.7: Optimization of the components for the assay buffer in order to facilitate the desired interaction between the binding partners. Tween 20 and NaCl were each titrated over 3 concentration points, and the relative effect, defined as the signal-to background window, is plotted.

To reduce assay background, the effect of 0.1% BSA in the two selected buffer was tested. As the addition of BSA caused no significant change in assay signal and the combination of 25 mM NaCl with 0.05% Tween 20 showed a slightly better ratio, these conditions were selected for subsequent experiments (Figure 3.3.8).
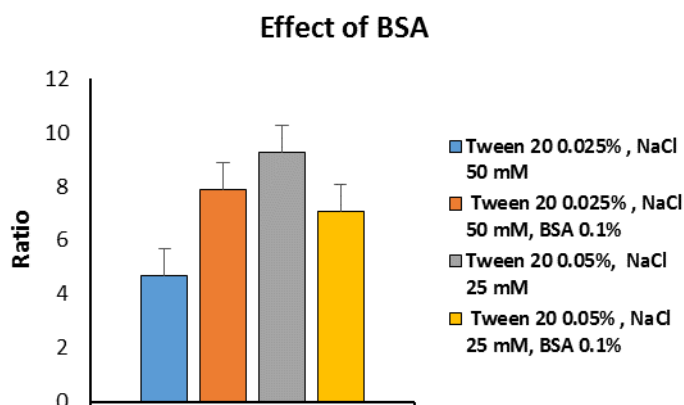
Figure 3.3.8: Effect of BSA and optimization of Tween20 and NaCl in the optimized assay buffer.

After the optimization of the assay buffer, the first experiment performed was a protein cross-titration in order to determine optimal concentrations of enzyme and substrate for the assay. In this experiment, while the concentrations of beads were kept constant, the concentration of the binding partners varied: GST-protein and H4K20me2 were titrated from 0 to 100 nM and 0 to 200 nM, respectively (Figure 3.3.9).

A hook point was reached at 100 nM H4K20me2, after which the signal begins to decrease because the protein concentration surpasses the binding capacity of the beads: determining where high concentrations of analyte lead to non-productive binding and loss of signal is essential in the optimization of AlphaScreen assays. The best signal/noise ratio was achieved using protein 25 nM and the substrate 100 nM so these concentrations were selected for further optimization and validation.
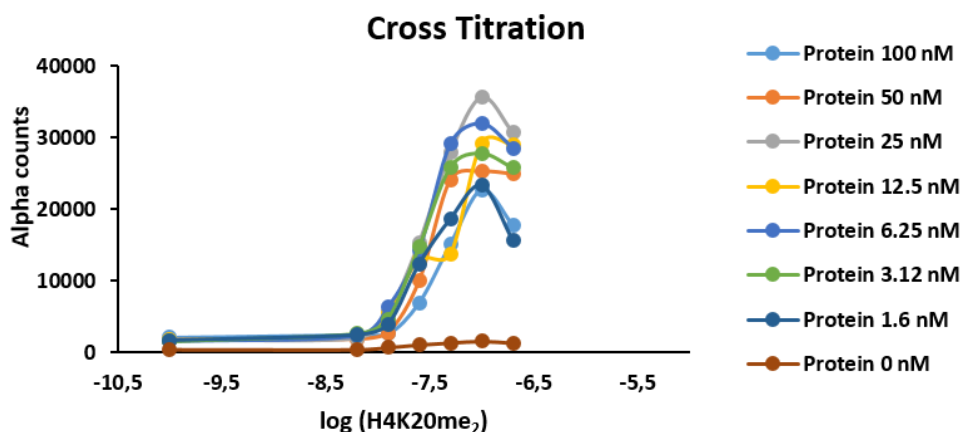
Figure 3.3.9: Cross-titration data for Tudors binding to biotinylated H4K20me2 peptide, using Streptavidin Donor Beads and anti-GST Acceptor beads.

Finally, a time course for protein-substrate interaction was performed to establish the optimal incubation time; anti-GST Acceptor beads were added after 30, 60 and 120 min. Because of the better signal/noise ratio, a 120 min interaction time was selected for all subsequent experiments (Figure 3.3.10).
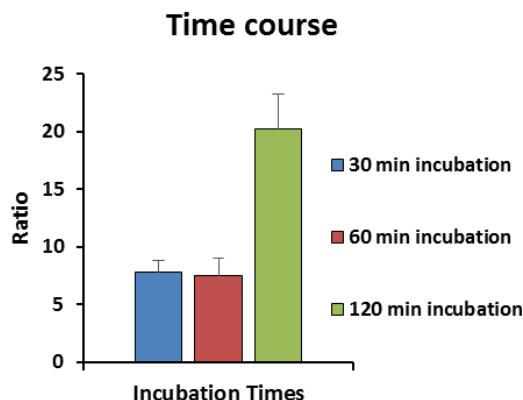
Figure 3.3.10: Time dependence of the Alphascreen signal. Three incubation times were examined: 30, 60 and 120 minutes.

After the optimization of assay conditions, this assay was used to evaluate the effect of UNC1215 analogues on Tudor domain reader activity; compounds activity was determined at a fixed concentration of 100 μM. As reported in Figure 3.3.11, the four molecules (EML637, EML639, EML644 and EML666), which were positive in the nanoDSF screening, were endowed with inhibitory activity ≥ 80%, confirming the validity of the nanoDSF biophysical assay as primary screening. Experiments are still in progress to evaluate the IC_{50} of these compounds, as well as to characterize in more details their inhibition mechanism.
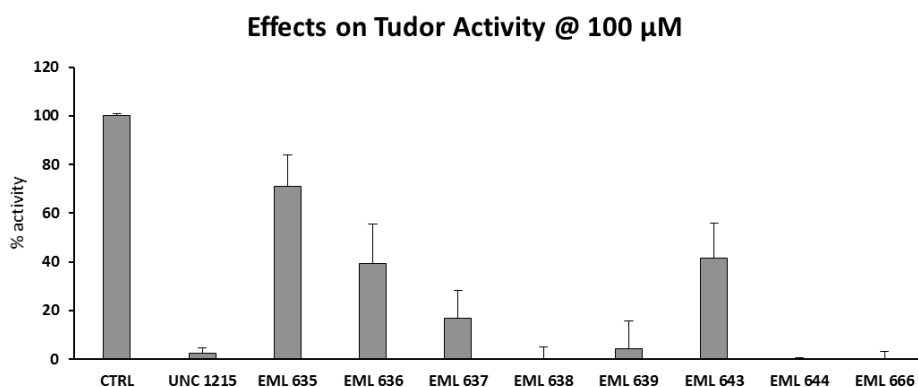
Figure 3.3.11: Effects of Compounds on the Activity of Tudor domains. Enzyme activity percentage determined at 100 μM with respect to DMSO.

Furthermore, the compound EML638, which did not cause a marked variation of the Tm measured in the nanoDSF experiments, strongly inhibited the reader activity of the protein in the Alphascreen assay. This compound could behave as a false negative in nanoDSF assay or a false positive in Alphascreen assay. Experiments are in progress to evaluate the real activity of this compound, which remains unclear and should be addressed.

4. CONCLUSIONS

It is widely reported that epigenetic proteins are involved in the development of several human diseases, with different mechanisms of action. Inhibitors of two classes of epigenetic enzymes, the DNMTs and HDACs, have already demonstrated to be useful chemotherapeutic agents for specific cancers, and they are approved drugs for these indications.

However, the number of reported modulators is limited and refers only to specific classes of epigenetic enzymes. As the availability of selective chemical probes against individual epigenetic enzymes is necessary for exploring their physiological and pathological activities, the lack of specific modulators is responsible for a poor knowledge of the biological roles of several epigenetic proteins.

The discovery of epigenetic modulators is affected by several problems. It is worth mentioning that these enzymes do not work alone but they participate in complex pathways and actively crosstalk with each other and with other proteins. Moreover, the lack of specific and robust screening methods to evaluate epigenetic enzymes activity get difficult to deeply understand this complex network.

This thesis reported on the application of biochemical and biophysical techniques to obtain a multiple screening platform for the study of specific epigenetic enzymes. This combined approach has been useful to overcome the limitations of each screening technique, allowing the identification and a deep characterization (defining potency, selectivity and mechanism of action) of several small-molecule modulators synthesized in the EMCL. In particular, among the different epigenetic enzymes, this approach was applied to the acetyltransferase p300, the methyltransferase SETD8 and the reader domains of PHF20.

Regarding p300, **SPV106** and garcinol were selected as lead compounds. Initially, a series of **SPV106** analogues was prepared and tested through an SPR-based filtering procedure to select compounds able to bind the acetyltransferase enzymes p300 and PCAF. Subsequently, it was reported that all the SPR+ derivatives markedly affected the catalytic activity of one or both enzymes in a radiometric assay. Finally, the effect of the most promising compounds was evaluated on the acetylation of lysine residues H4K5 and H3K9 in C33A, HeLa, and U937 cell lines and on the ability to alter the cell cycle. This approach allowed the identification of derivatives **2d**, **4b** and **5b** as modulators of p300 and PCAF.

Again regarding p300, the application of a molecular pruning approach to the garcinol core structure led to the identification of the barbituric acid moiety as a useful scaffold to easily prepare numerous analogues and achieve an inclusive SAR framework for p300 inhibition. In this case, the screening platform was first characterized by the application of a radioactivity-based assay to measure compounds potency, followed by an SPR method that highlighted the instability of the most promising compounds in aqueous solution. The chemical stabilization of the compound **15b** led to the identification of derivative **15h,** which retains the ability of selectively inhibit p300**.** Subsequently, it was evaluated the kinetic mechanism of p300 inhibition using an AlphaLISA homogeneous proximity immunoassay. The derivative **15h** was shown to be non-competitive versus both acetyl-CoA and a histone H3 peptide. Furthermore, in human leukemia U937 cells, it induced a marked and time-dependent reduction in the acetylation of lysine H4K5 and H3K9 and a marked arrest in the G_0/G_1 phase. Therefore, the derivative **15h** together with the **SPV106** analogues **2d**, **4b** and **5b,** may be used as invaluable chemical probes to further investigate the biological role of acetyltransferase enzymes and their implications in physiological and/or pathological processes.

Regarding the Tudor domains of PHF20, the nanoDSF biophysical assay was applied to evaluate the ability of the protein to bind a small pool of **UNC1215** analogues synthesized in EMCL. Afterwards an Alphascreen assay was designed and developed for the evaluation of the enzymatic activity of the synthesized compounds. The use of these techniques allowed the identification of the small-molecule compounds **EML637**, **EML639**, **EML644**, **EML666**, which are able to bind and inhibit Tudor domains of PHF20 and whose activity is still under characterization.

Finally, as regard to the methyltransferase SETD8, the preparation of a protein suitable for biophysical and biochemical assays needed more efforts than expected. For this reason, the development of a screening approach is still in progress.

In conclusion, this multiple approach proved to be widely usable because of its robustness and reliability. The application of this platform would provide new opportunities to increase drug discovery success and productivity in the epigenetic field.

5. MATERIALS AND METHODS

5.1 Chemistry: Synthesis of SPV106 Analogues

General directions: All chemicals were purchased from Aldrich Chimica (Milan, Italy) and were of the highest purity. All solvents were reagent grade and were purified and dried by standard methods when necessary. All reactions requiring anhydrous conditions were conducted under a positive atmosphere of nitrogen in oven-dried glassware. Standard syringe techniques were used for the anhydrous addition of liquids. Reactions were routinely monitored by TLC performed on aluminum-backed silica gel plates (Merck DC, Alufolien Kieselgel 60 F254) with spots visualized by UV light (λ= 254, 365 nm) or using a $KMnO_4$ alkaline solution. Solvents were removed using a rotary evaporator operating at a reduced pressure of $\approx$ 10 Torr. Organic solutions were dried over anhydrous Na_2SO_4. Chromatographic separations were performed on silica gel (silica gel 60, 0.015–0.040 mm; Merck DC) columns. Melting points were determined on a Stuart SMP30 melting point apparatus in open capillary tubes and were uncorrected. Infrared (IR) spectra were recorded neat with a Shimadzu IR Affinity-1 FTIR fitted with a MIRacle 10 single reflection ATR accessory at room temperature. ^1H and ^{13}C NMR spectra were recorded at 300 MHz and 75 MHz, respectively, with a Bruker Avance 300 spectrometer. Chemical shifts are reported in d (ppm) relative to the internal reference tetramethylsilane (TMS). Mass spectra were recorded with a Finnigan LCQ DECA TermoQuest (San Jose, USA) mass spectrometer in electrospray-positive and -negative ionization modes (ESI-MS). The purity of the test compounds was established by combustion analysis, confirming purity $\geq$95%.

A stirred solution of the appropriate alkyl aldehyde (4.00 mmol) and 2,4-pentanedione (acetylacetone) (4.40 mmol) in anhydrous methylene chloride (3 mL) was treated with piperidine (0.08 mmol) and acetic acid (0.08 mmol) at 0 °C. The reaction mixture was stirred at room temperature for 1 h (TLC monitoring), diluted with methylene chloride (50 mL), washed with brine (3_10 mL), and dried (Na$_2$SO$_4$). After removing the solvent, the crude residue was purified by column chromatography on silica gel (n-hexane/EtOAc) to afford the title compounds.

3-Pentylidenepentane-2,4-dione (**2a**, **EML319**): Colorless oil (619 mg, 92%): ^{1}H NMR (300 MHz, CDCl$_3$): δ = 6.67 (t, J=7.7 Hz, 1 H), 2.30 (s, 6H), 2.28–2.15 (m, 2 H), 1.52–1.42 (m, 2 H), 1.41–1.31 (m, 2 H), 0.92 ppm (t, J=7.1 Hz, 3H); ^{13}C NMR (75 MHz, CDCl$_3$): δ = 203.5, 197.2, 146.9, 145.4, 30.9, 29.5, 26.1, 22.5, 13.9 ppm IR (neat): $\bar{v}$=2959, 2932, 2862, 1705, 1667, 1628 cm^{-1}; ESI-MS m/z: 169 [M+H]$^+$; Anal. calcd for C$_{10}$H$_{16}$O$_2$: C 71.39, H 9.59, found: C 71.54, H 9.61.

3-Dodecylidenepentane-2,4-dione (**2b**, **EML318**): Colorless oil (991 mg, 93%): ^{1}H NMR (300 MHz, CDCl$_3$): δ = 6.71 (t, J=7.7 Hz, 1 H), 2.35 (s, 6H), 2.28–2.18 (m, 2 H), 1.53–1.42 (m, 2 H), 1.34–1.22 (m, 16H), 0.89 ppm (t, J=6.5 Hz, 3H); IR (neat): $\bar{v}$=2955, 2924, 2855, 1705, 1667, 1628 cm^{-1}; ESI-MS m/z: 267 [M+H]$^+$; Anal. Calcd for C$_{17}$H$_{30}$O$_2$: C 76.64, H 11.35, found: C 76.83, H 11.38.

3-Tetradecylidenepentane-2,4-dione (**2c**, **EML317**): Colorless oil (1095 mg, 93%): ^{1}H NMR (300 MHz, CDCl$_3$): δ = 6.66 (t, J=7.7 Hz, 1 H), 2.27 (s, 6H), 2.25–2.13 (m, 2 H), 1.51–1.40 (m, 2 H), 1.28–1.16 (m, 20H), 0.86 ppm (t, J=6.5 Hz, 3H); IR (neat): $\bar{v}$=2924, 2855, 1713, 1670, 1624 cm^{-1}; ESI-MS m/z: 295 [M+H]$^+$; Anal. calcd for C$_{19}$H$_{34}$O$_2$: C 77.50, H 11.64, found: C 77.69, H 11.67.

3-Pentadecylidenepentane-2,4-dione (**2d**, **EML76**): Colorless oil (1098 mg, 89%): ^{1}H NMR (300 MHz, CDCl$_3$): δ = 6.70 (t, J=7.7 Hz, 1 H), 2.34 (s, 6H), 2.28–2.19 (m, 2 H), 1.54–1.48 (m, 2 H), 1.38–1.26 (m, 22H), 0.99 ppm (t, J=6.3 Hz, 3H); ^{13}C NMR (75 MHz, CDCl$_3$): δ = 203.7, 197.2, 147.1, 145.3, 32.1, 31.8, 29.8, 29.6, 29.5, 28.8, 26.2, 26.2, 22.8, 14.3 ppm; IR (neat): $\bar{v}$=2916, 2851, 1701, 1664, 1636 cm^{-1}; ESI-MS m/z: 309 [M+H]$^+$; Anal. calcd for C$_{20}$H$_{36}$O$_2$: C 77.87, H 11.76, found: C 78.05, H 11.79.

3-Hexadecylidenepentane-2,4-dione (**2e**, **EML320**): Colorless oil (1238 mg, 96%): ^{1}H NMR (300 MHz, CDCl$_3$): δ = 6.66 (t, J=7.7 Hz, 1 H), 2.28 (s, 6H), 2.26–2.16 (m, 2 H), 1.53–1.43 (m, 2 H), 1.30–1.23 (m, 24H), 0.86 ppm (t, J=6.3 Hz, 3H); IR (neat): $\bar{v}$=2916, 2851, 1701, 1663, 1636 cm^{-1}; ESI-MS m/z: 323 [M+H]$^+$; Anal. calcd for C$_{21}$H$_{38}$O$_2$: C 78.20, H 11.88, found: C 78.41, H 11.91.

5.1.2 General procedure for the synthesis of derivatives 3a–d:

Derivatives **3a**–**d** were prepared by reacting the appropriate alkyl aldehyde and ethyl 3-oxobutanoate (for compounds **3a,b**) or tert-butyl 3-oxobutanoate (for compounds **3c,d**), according to the procedure used for derivatives 2a–e. The crude residue was purified by column chromatography on silica gel (n-hexane/EtOAc) to afford the title compounds as a mixture of E and Z isomers.

Ethyl 2-acetylhexadec-2-enoate (**3a**, **EML329**): Low-melting-point white solid (934 mg, 72%): 1:1 mixture of geometric isomersa and b; ^{1}H NMR (300 MHz, CDCl$_3$): δ = 6.92 (t, J=7.7 Hz, 1H, isomer **a**), 6.85 (t, J=7.7 Hz, 1H, isomer **b**), 4.31 (q, J=7.1 Hz, 2H, isomer **b**), 4.25 (q, J=7.1 Hz, 2H, isomer **a**), 2.36–2.27 (m, 5H, isomer **b** and 3H, isomer **a**), 2.25–2.21 (m, 2H, isomer **a**), 1.55–1.40 (m, 2H, isomer **a** and 2H isomer **b**), 1.30–1.21 (m, 23 H, isomer **a** and 23H

isomer **b**), 0.88 ppm (br t, J=6.3 Hz, 3H, isomer a and 3H, isomer b); IR (neat): $\bar{v}$=2922, 2853, 1728, 1701, 1638, 1622 cm^{-1}; ESI-MS m/z: 325 [M+H]$^+$; Anal. calcd for $C_{20}H_{36}O_3$: C 74.03, H 11.18, found: C 73.92, H 11.20.

Ethyl 2-acetylheptadec-2-enoate (**3b**, **EML330**): Low-melting-point white solid (1056 mg, 78%): 1:1 mixture of geometric isomers a and b; ^{1}H NMR (300 MHz, CDCl$_3$): δ = 6.91 (t, J=7.7 Hz, 1H, isomer **a**), 6.83 (t, J=7.7 Hz, 1H, isomer **b**), 4.29 (q, J=7.1 Hz, 2H, isomer **b**), 4.23 (q, J=7.1 Hz, 2H, isomer **a**), 2.36–2.27 (m, 5H, isomer **b** and 3H, isomer **a**), 2.27–2.18 (m, 2H, isomer **a**), 1.54–1.40 (m, 2H, isomer **a** and 2H isomer **b**), 1.34–1.16 (m, 25 H, isomer **a** and 25H isomer **b**), 0.86 ppm (br t, J=6.3 Hz, 3H, isomer **a** and 3H, isomer **b**); ^{13}C NMR (75 MHz, CDCl$_3$): δ = 201.2, 195.2, 166.7, 164.8, 149.2, 148.8, 137.7, 137.2, 61.3, 32.0, 30.1, 29.8, 29.6, 29.5, 28.7, 28.5, 27.0, 22.8, 14.3, 14.2 ppm; IR (neat): $\bar{v}$=2913, 2851, 1717, 1670, 1643 cm^{-1}; ESI-MS m/z: 339 [M+H]$^+$; Anal. calcd for $C_{21}H_{38}O_3$: C 74.51, H 11.31, found: C 74.37, H 11.33.

tert-Butyl 2-acetylhexadec-2-enoate (**3c**, **EML331**): Low-melting-point white solid (1072 mg, 76%): 1:1 mixture of geometric isomers a and b; ^{1}H NMR (300 MHz, CDCl$_3$): δ = 6.80 (t, J=7.9 Hz, 1H, isomer **a**), 6.75 (t, J=7.8 Hz, 1H, isomer **b**), 2.33–2.27 (m, 5H, isomer **b** and 3H, isomer **a**), 2.25–2.14 (m, 2H, isomer **a**), 1.55–1.40 (m, 11H, isomer **a** and 11H isomer **b**), 1.30–1.21 (m, 20 H, isomer **a** and 20H isomer **b**), 0.88 ppm (br t, J=6.5 Hz, 3H, isomer **a** and 3H, isomer **b**); IR (neat): $\bar{v}$=2924, 2855, 1724, 1701, 1636, 1620 cm^{-1}; ESI-MS m/z: 375 [M+Na]$^+$; Anal. calcd for $C_{22}H_{40}O_3$: C 74.95, H 11.44, found: C 74.79, H 11.43.

tert-Butyl 2-acetylheptadec-2-enoate (**3d**, **EML332**): Low-melting-point white solid (1056 mg, 72%): 1:1 mixture of geometric isomers a and b; ^{1}H NMR (300 MHz, CDCl$_3$): δ = 6.80 (t, J=7.9 Hz, 1H, isomer **a**), 6.75 (t, J=7.8 Hz, 1H, isomer **b**), 2.33–2.27 (m, 5H, isomer b and 3H, isomer **a**), 2.25–2.14 (m, 2H, isomer **a**),

1.55–1.40 (m, 11H, isomer **a** and 11H isomer **b**), 1.30–1.21 (m, 22 H, isomer **a** and 22H isomer **b**), 0.88 ppm (br t, J=6.5 Hz, 3H, isomer **a** and 3H, isomer **b**); IR (neat): $\bar{v}$=2913, 2851, 1717, 1686, 1620 cm^{-1}; ESI-MS m/z: 389 [M+Na]$^+$; Anal. calcd for $C_{23}H_{42}O_3$: C 75.36, H 11.55, found: C 75.21, H 11.54.

5.1.3 General procedure for the synthesis of derivatives 4a–b:

Derivatives **4a**–**b** were prepared by reacting the appropriate alkyl aldehyde and malonic acid according to the procedure used for derivatives **2a**–**e**. The crude residue was purified by column chromatography on silica gel (CH_2Cl_2/MeOH) to afford the title compounds.

2-Tetradecylidenemalonic acid (**4a**, **EML341**): White solid (991 mg, 83%): mp: 69–708C; ^{1}H NMR (300 MHz, [D$_6$]DMSO): δ = 6.99 (t, J=7.5 Hz, 1H), 2.42–2.29 (m, 2 H), 1.44–1.33 (m, 2H), 1.32–1.15 (m, 20H), 0.85 ppm (t, J=6.2 Hz, 3H); IR (neat): $\bar{v}$=2953, 2918, 2851, 1735, 1720, 1697, 1568 cm^{-1}; ESI-MS m/z: 297 [M-H]$^-$; Anal. calcd for $C_{17}H_{30}O_4$: C 68.42, H 10.13, found: C 68.27, H 10.15.

2-Pentadecylidenemalonic acid (**4b**, **EML264**): White solid (975 mg, 78%): mp: 73–758C; ^{1}H NMR (300 MHz, [D$_6$]DMSO): δ = 6.88 (t, J=7.6 Hz, 1H), 2.41–2.27 (m, 2 H), 1.49–1.38 (m, 2H), 1.34– 1.14 (m, 22 H), 0.85 ppm (t, J=6.3 Hz, 3H); ^{13}C NMR (75 MHz, DMSO): δ = 169.8, 167.1, 147.3, 129.8, 31.3, 29.1, 28.8, 22.1,
13.8 ppm; IR (neat): $\bar{v}$=2954, 2916, 2848, 1735, 1710, 1697, 1568 cm^{-1}; ESI-MS m/z: 311 [M-H]$^-$; Anal. calcd for $C_{18}H_{32}O_4$: C 69.19, H 10.32, found: C 69.05, H 10.34.

5.1.4 General procedure for the synthesis of derivatives 5a–b:

A mixture of TFA and CH_2Cl_2 (1:3, 12 mL) was added to ester derivatives **3c** or **3d** (1.00 mmol). The reaction was stirred at room temperature for 30 min and

then concentrated in vacuo to give the title compounds as a mixture of E and Z isomers.

2-Acetylhexadec-2-enoic acid (**5a**, **EML333**): Low-melting-point white solid (284 mg, 96%): 2:1 mixture of geometric isomers **a** and **b**; ^{1}H NMR (300 MHz, CDCl$_3$): δ = 10.90 (br s, 1H, isomer **a** and 1H isomer **b**), 7.41 (t, J=7.2 Hz, 1H, isomer **a**), 7.16 (t, J=7.8 Hz, 1H, isomer **b**), 2.88–2.78 (m, 2H, isomer **a**), 2.46 (s, 3H, isomer **a**), 2.40 (s, 3H, isomer **b**), 2.35–2.25 (m, 2H, isomer **b**), 1.62–1.40 (m, 2H, isomer **a** and 2H isomer **b**), 1.30–1.21 (m, 20 H, isomer **a** and 20H isomer **b**), 0.88 ppm (br t, J=6.3 Hz, 3H, isomer **a** and 3H, isomer **b**); IR (neat): $\bar{v}$=2916, 2851, 1713, 1682, 1624 cm^{-1}; ESI-MS m/z: 297 [M+H]+; Anal. calcd for C$_{18}$H$_{32}$O$_3$: C 72.93, H 10.88, found: C 72.80, H 10.90.

2-Acetylheptadec-2-enoic acid (**5b**, **EML334**): Low-melting-point white solid (292 mg, 94%): 2:1 mixture of geometric isomers **a** and **b**; ^{1}H NMR (300 MHz, CDCl$_3$): δ = 10.90 (br s, 1H, isomer **a** and 1H isomer **b**), 7.53 (t, J=7.1 Hz, 1H, isomer **a**), 7.38 (t, J=7.7 Hz, 1H, isomer **b**), 3.00–2.91 (m, 2H, isomer **a**), 2.50 (s, 3H, isomer **a**), 2.46 (s, 3H, isomer **b**), 2.45–2.35 (m, 2H, isomer **b**), 1.65–1.47 (m, 2H, isomer **a** and 2H isomer **b**), 1.40–1.15 (m, 22 H, isomer **a** and 22H isomer **b**), 0.88 ppm (br t, J=6.4 Hz, 3H, isomer **a** and 3H, isomer **b**); ^{13}C NMR (75 MHz, CDCl$_3$): δ = 201.9, 201.1, 169.0, 165.5, 164.0, 153.7, 134.4, 131.0, 32.0, 31.4, 31.3, 30.0, 29.8, 29.6, 29.5, 28.7, 26.7, 22.8, 14.2 ppm; IR (neat): $\bar{v}$ =2922, 2853, 1717, 1684, 1636 cm^{-1}; ESI-MS m/z: 311 [M+H]$^+$; Anal. calcd for C$_{19}$H$_{34}$O$_3$: C 73.50, H 11.04, found: C 73.35, H 11.06.

5.1.5 General procedure for the synthesis of derivatives 6a,b-8a–f:

To a solution of 3-(ethoxymethylene)-2,4-pentanedione **9** (1.00 mmol) in anhydrous THF (3 mL), the appropriate alkylamine (1.00 mmol) or alkylthiol (2.00 mmol) was added, and the reaction mixture was stirred at reflux for 2 h

(monitored by TLC). After cooling at room temperature, the solvent was removed, and the crude residue was purified by column chromatography on silica gel (CH_2Cl_2/EtOAc) to afford the title compounds.

Dodecanethiol, dodecanamine, and tridecanamine used for the preparation of derivatives **6a**, **8a**, and **8b**, respectively, were commercially available. Tridecanethiol used for the synthesis of **6b** and N-ethyldodecan-1-amine, N-ethyltridecan-1-amine, N-benzyldodecan-1-amine, and N-benzyltridecan-1-amine used for the synthesis of derivatives **8c**, **8d**, **8e**, **8f**, respectively, were prepared by standard synthetic procedures.

3-(Dodecylthiomethylene)pentane-2,4-dione (**6a**, **EML327**): Low-melting-point white solid (288 mg, 92%): ^{1}H NMR (300 MHz, $CDCl_3$): δ = 8.17 (s, 1 H), 2.83 (t, J=7.4 Hz, 2 H), 2.47 (s, 3 H), 2.38 (s, 3H), 1.79–1.63 (m, 2 H), 1.48–1.37 (m, 2H), 1.34–1.16 (m, 16 H), 0.88 ppm (t, J=6.5 Hz, 3H); IR (neat): $\bar{v}$ =2951, 2920, 2847, 1659, 1643 cm^{-1}; ESI-MS m/z: 313 [M+H]$^+$; Anal. calcd for $C_{18}H_{32}O_2S$: C 69.18, H 10.32, S 10.26, found: C 69.32, H 10.34, S 10.27.

3-(Tridecylthiomethylene)pentane-2,4-dione (**6b**, **EML328**): Low-melting-point white solid (307 mg, 94%): ^{1}H NMR (300 MHz, $CDCl_3$): δ = 8.16 (s, 1 H), 2.83 (t, J=7.4 Hz, 2 H), 2.47 (s, 3 H), 2.38 (s, 3H), 1.78–1.65 (m, 2 H), 1.48–1.37 (m, 2H), 1.33–1.19 (m, 18 H), 0.88 ppm (t, J=6.5 Hz, 3H); ^{13}C NMR (75 MHz, $CDCl_3$): δ = 197.7, 194.7, 162.6, 134.2, 38.3, 32.1, 31.1, 30.2, 29.8, 29.6, 29.3, 28.6, 27.8, 22.8, 14.2 ppm; IR (neat): $\bar{v}$=2951, 2917, 2847, 1659, 1643 cm^{-1}; ESI-MS m/z: 327 [M+H]$^+$; Anal. calcd for $C_{19}H_{34}O_2S$: C 69.89, H 10.50, S 9.82, found: C 70.05, H 10.52, S 9.84.

3-((Dodecylamino)methylene)pentane-2,4-dione (**8a**, **EML321**): Low-melting-point pale-yellow solid (287 mg, 97%): ^{1}H NMR (300 MHz, $CDCl_3$): δ = 11.07 (br s, 1H), 7.71 (d, J=12.3 Hz, 1H), 3.38–3.31 (m, 2H), 2.48 (s, 3H), 2.26 (s,

3H), 1.67–1.56 (m, 2 H), 1.41–1.19 (m, 18H), 0.88 ppm (t, J=6.4 Hz, 3H); IR (neat): $\bar{\nu}$=3202, 2916, 2847, 1651, 1605, 1582 cm^{-1}; ESI-MS m/z: 296 [M+H]$^+$; Anal. calcd for $C_{18}H_{33}NO_2$: C 73.17, H 11.26, N 4.74, found: C 73.33, H 11.28, N 4.75.

3-((Tridecylamino)methylene)pentane-2,4-dione (**8b**, **EML322**): Low-melting-point pale-yellow solid (303 mg, 98%): ^{1}H NMR (300 MHz, CDCl$_3$): δ = 11.07 (br s, 1H), 7.72 (d, J=13.7 Hz, 1H), 3.41–3.29 (m, 2H), 2.48 (s, 3H), 2.24 (s, 3H), 1.68–1.58 (m, 2 H), 1.34–1.19 (m, 20H), 0.88 ppm (t, J=6.5 Hz, 3H); ^{13}C NMR (75 MHz, CDCl$_3$): δ = 200.4, 194.4, 160.0, 111.5, 50.6, 32.0, 30.7, 29.8, 29.6, 29.5, 29.3, 27.5, 26.6, 22.8, 14.2 ppm; IR (neat): $\bar{\nu}$=3202, 2916, 2851, 1651, 1605, 1585 cm^{-1}; ESI-MS m/z: 310 [M+H]$^+$; Anal. Calcd for $C_{19}H_{35}NO_2$: C 73.74, H 11.40, N 4.53, found: C 73.94, H 11.42, N 4.54.

3-((Dodecyl(ethyl)amino)methylene)pentane-2,4-dione (**8c**, **EML323**): Low-melting-point pale-yellow solid (301 mg, 93%): ^{1}H NMR (300 MHz, CDCl$_3$): δ = 7.36 (s, 1 H), 3.32–3.20 (m, 4 H), 2.32 (s, 6H), 1.58–1.42 (m, 2 H), 1.33–1.20 (m, 18H), 1.19–1.03 (m, 3 H), 0.87 ppm (t, J=6.3 Hz, 3H); IR (neat): $\bar{\nu}$=2924, 2855, 1655, 1620, 1578 cm^{-1}; ESI-MS m/z: 324 [M+H]$^+$; Anal. calcd for $C_{20}H_{37}NO_2$: C 74.25, H 11.53, N 4.33, found: C 74.47, H 11.55, N 4.34.

3-((Ethyl(tridecyl)amino)methylene)pentane-2,4-dione (**8d**, **EML324**): Low-melting-point pale-yellow solid (317 mg, 94%): ^{1}H NMR (300 MHz, CDCl$_3$): δ = 7.36 (s, 1 H), 3.39–3.18 (m, 4 H), 2.32 (s, 6H), 1.62–1.37 (m, 2 H), 1.35–1.19 (m, 20H), 1.18–1.05 (m, 3 H), 0.87 ppm (t, J=6.4 Hz, 3H); IR (neat): $\bar{\nu}$=2920, 2851, 1659, 1612, 1578 cm^{-1}; ESI-MS m/z: 338 [M+H]$^+$; Anal. calcd for $C_{21}H_{39}NO_2$: C 74.72, H 11.65, N 4.15, found: C 74.94, H 11.68, N 4.16.

3-((Benzyl(dodecyl)amino)methylene)pentane-2,4-dione (**8e**, **EML325**): Pale-yellow solid (370 mg, 96%): mp: 53–568C; ^{1}H NMR (300 MHz, CDCl$_3$): δ = 7.49 (s, 1H), 7.38–7.27 (m, 3H), 7.18–7.10 (m, 2 H), 4.44 (s, 2H), 3.37–3.20 (m, 2 H), 2.15 (s, 6H), 1.62–1.46 (m, 2 H), 1.32–1.19 (m, 18H), 0.88 ppm (t, J=6.5 Hz, 3H); IR (neat): $\bar{v}$=2916, 2851, 1670, 1574 cm^{-1}; ESI-MS m/z: 386 [M+H]$^+$; Anal. calcd for C$_{25}$H$_{39}$NO$_2$: C 77.87, H 10.20, N 3.63, found: C 78.10, H 10.22, N 3.64.

3-((Benzyl(tridecyl)amino)methylene)pentane-2,4-dione (**8f**, **EML326**): Pale-yellow solid (388 mg, 97%): mp: 61–648C; ^{1}H NMR (300 MHz, CDCl$_3$): δ = 7.49 (s, 1 H), 7.39–7.28 (m, 3 H), 7.20–7.11 (m, 2 H), 4.43 (s, 2H), 3.34–3.17 (m, 2 H), 2.15 (s, 6H), 1.66–1.48 (m, 2 H), 1.31–1.20 (m, 20H), 0.88 ppm (t, J=6.4 Hz, 3H); IR (neat): $\bar{v}$=2916, 2851, 1674, 1574 cm^{-1}; ESI-MS m/z: 400 [M+H]$^+$; Anal. calcd for C$_{26}$H$_{41}$NO$_2$: C 78.15, H 10.34, N 3.51, found: C 78.38, H 10.36, N 3.52.

5.2 Surface Plasmon Resonance

SPR analyses were performed on a Biacore 3000 optical biosensor equipped with research-grade CM5 sensor chips (Biacore AB). Recombinant p300/KAT3B (Enzo Life Sciences, # BML-SE451; Gen-Bank accession no. NM_001429) and PCAF/KAT2B (Biovision, # 1137–100; GenBank accession n. NM003884) HAT domains were used in this analysis. Proteins (10 μg/mL in 100 mM sodium acetate, pH 4.5) were immobilized on individual flow cells of the sensor chip at a flow rate of 10 μL/min using standard amine coupling protocols to obtain densities of 8–9 kRU. Myoglobin was used as a negative control, and one flow cell was left empty for background subtraction. All compounds were dissolved in DMSO (100%) to obtain 50 mM solutions, and they were diluted in HBS-P (10 mM HEPES pH 7.4, 0.15 M NaCl, 0.005%

surfactant P20) while maintaining a final 0.2% DMSO concentration. Binding experiments were performed at 25 °C using a flow rate of 30 μL/min with 120 s association monitoring and 200 s dissociation monitoring.

Surface regeneration was performed when necessary by a 10 s injection of 5 mM NaOH. The simple 1:1 Langmuir binding fit model of BIAevaluation software (version 4.1) was used for determining equilibrium dissociation constants (KD) and kinetic dissociation (kd) and association (ka) constants using Equations (1) and (2), where R represents the response unit, and C is the concentration of the analyte.

$$dR/dt = Ka\, C\,(Rmax - R) - kd\, R \quad (1)$$
$$KD = Kd/Ka \quad (2)$$

5.3 Histone acetyl transferase IC$_{50}$ profiling

The effect of the derivatives on the catalytic activity of PCAF and p300 was determined with a HotSpot HAT activity assay by Reaction Biology Corporation (Malvern, PA, USA) according to the company's standard operating procedure. Briefly, the recombinant catalytic domains of PCAF (aa 492–658) or p300 (aa 1284–1673) were incubated with histone H3 as a substrate (5 μM) and [acetyl-^{3}H]-acetyl coenzyme A (3.08 μM) as an acetyl donor in reaction buffer (50 mM Tris-HCl (pH 8.0), 50 mM NaCl, 0.1 mM EDTA, 1 mM DTT, 1 mM PMSF, 1% DMSO) for 1 h at 30 °C in the presence or absence of a dose titration of the compounds. Histone H3 acetylation was assessed by liquid scintillation. Anacardic acid or curcumin served as controls that inhibit PCAF or p300 activity, respectively. Data were analysed using Excel and GraphPad Prism software (version 6.0, GraphPad Software) for IC$_{50}$ curve fits using sigmoidal dose-response (variable slope) equations.

5.4 Cell viability assay

The U937 cell line (derived from a human histocytic lymphoma) was cultured in RPMI-1640 medium (Sigma) supplemented with 10% (v/v) fetal bovine serum (Sigma), 100 U/mL penicillin, and 100 μg/mL streptomycin (Sigma) at 37 °C in a 5% CO_2 atmosphere. U937 cell viability was measured using a 3-(4,5-dimethylthiazol-2-yl)-2,5-diphenyltetrazolium bromide (MTT) assay. A total of 200 μL of cells seeded in 96-well microtiter plates (2.5x 10^5 cells/mL) were exposed for 24 h to different concentrations of selected compounds in media containing 0.2% DMSO. The mitochondrial-dependent reduction of MTT to formazan was used to assess cell viability. Experiments were performed in quadruplicate, and all values are expressed as the percentage of the control containing 0.2% DMSO.

5.5 Cell-cycle analysis

For cell-cycle analysis, 500 μL of U937 cells (2.5x 10^5 cells/mL) were seeded in 24-well plates and incubated with selected compounds at different concentrations. After 24 or/and 72 h of treatment, 500 μL of hypotonic buffer (33 mM sodium citrate, 0.1% Triton X-100, 50 μg/mL propidium iodide) was added to cell suspensions. Cells were analyzed with a FACScan flow cytometer (Becton Dickinson, CA), using Mod FitLT (version 3.2, Verity Software House, Inc., ME, USA) for quantitative analysis of cell-cycle distribution. All experiments were performed at least in triplicate.

5.6 Western blot analysis of acetyl-lysines

U937 (10 mL, 2.5x 10^5 cells/mL), HeLa and C33A (sub-confluent) cells were seeded and incubated with compounds at different concentrations, and after 24, 48 and 72h, the cells were harvested and washed three times with 1X PBS (Sigma) and then resuspended in lysis buffer (10 mM Tris pH 8, 1 mM KCl, 1.5 mM $MgCl_2$, and 1 mM DTT) supplemented with a protease inhibitor cocktail

(Sigma). All subsequent manipulations were performed at 4 °C. After incubation for 1 h on a rotator, nuclei were collected by centrifugation for 10 min at 10000g. The nuclear pellets were suspended in 0.4 N H_2SO_4, and after incubation for 2 h, were centrifuged for 15 min at 12000g. Histones contained in the supernatant were precipitated by adding TCA to a final concentration of 33% and incubating overnight at 4 °C. After centrifugation at 10000g for 30 min, the histone pellets were washed twice with acetone, air-dried, and finally redissolved in 50 µL of water. Protein concentrations were determined using the Bradford assay, and 1 µg of histones from each sample was loaded onto a 15% SDS-PAGE gel and transferred to a nitrocellulose membrane. The following primary antibodies were used: anti-histone H4 (acetyl K5) (Abcam, # ab61236); anti-histone H3 (acetyl K9) (Abcam, # ab10812); anti-histone H3 (Abcam, # ab1791).

5.7 Garcinol Derivatives Stability Assays

Compounds **15b–h**, **9a** and **12a** were dissolved in PBS to reach a final concentration of 100 µM (5% DMSO). 5 µL of the prepared solutions were analysed by HPLC after 2, 10, 30, 60 min and 24 h. Spectra were recorded on a Shimadzu SPD 20A UV/vis detector (λ = 220 nm) using C-18 column Phenomenex Synergi Fusion RP 80A (75mm × 4.60 mm; 4 µm) at 25 °C using a mobile phase A (water + 0.1% TFA) and B (MeCN + 0.1% TFA) at a flow rate of 1 mL/min.

5.8 Parallel Artificial Membrane Permeability Assay (PAMPA)

Donor solution (0.5 mM) was prepared by diluting 1 mM dimethyl sulfoxide (DMSO) compound stock solution using phosphate buffer (pH 7.4, 0.01 M). Filters were coated with 5 µL of a 1% (w/v) dodecane solution of phosphatidylcholine. Donor solution (150 µL) was added to each well of the filter plate. To each well of the acceptor plate were added 300 µL of solution

(50% DMSO in phosphate buffer). Compounds were tested in triplicate. The sandwich was incubated for 24 h at room temperature under gentle shaking. After the incubation time, the sandwich plates were separated and 250 μL of the acceptor plate were transferred to a UV quartz microtiter plate and measured by UV spectroscopy, using a Multiskan GO microplate spectrophotometer (Thermo Scientific) at 250-500 nm at step of 5 nm. Reference solutions (250 μL) were prepared diluting the sample stock solutions to the same concentration as that with no membrane barrier. The apparent permeability value P_{app} is determined from the ratio r of the absorbance of compound found in the acceptor chamber divided by the theoretical equilibrium absorbance (determined independently) applying the Faller modification of Sugano equation:

$$Papp = -\left(\frac{VD * VR}{(VD + VR)At}\right) * \ln(1 - r)$$

In this equation, VR is the volume of the acceptor compartment (0.3 cm^3), VD is the donor volume (0.15 cm^3), A is the accessible filter area (0.24 cm^2), and t is the incubation time in seconds.

5.9 Kinetic Characterization of 15h Inhibitor

To explore the mechanisms of p300 inhibition by **15h**, we took advantage of an AlphaLisa homogeneous proximity immunoassay. Reactions were performed as suggested by manufacturer, briefly each assay containing 5 nM p300 (Enzo LifeScience, # BML-SE451), 3 μM Acetyl CoA, and 50 nM biotinylated H3 (1−21) peptide (Anaspec, # 61702) in 10 μL of assay buffer (50 mM Tris-HCl, pH 8.0, 0.1 mM EDTA, 1 mM DTT, 0.01% Tween-20, 0.01% BSA, 330 nM TSA) was incubated at room temperature for 15 min in a White opaque OptiPlate-384 (PerkinElmer, # 6007299). Reactions were stopped by adding garcinol (final concentration 50 μM) and anti-acetyl histone H3 lysine 9 (H3K9Ac) acceptor beads (PerkinElmer, # AL114, final concentration 20

µg/mL). After 60 min of incubation at room temperature, 20 µg/mL final concentration of Alpha Streptavidin Donor beads (PerkinElmer, # 6760002) were added in subdued light and incubated in the dark for 30 min at room temperature. Signals were read in Alpha mode with a PerkinElmer EnSpire Multilabel plate reader. To determine the pattern of inhibition of **15h**, different set of assays were performed maintaining one substrate constant and varying the other in the presence of three different concentrations of inhibitor (0, 5, and 10 µM). In the first set of experiments, H3 peptide was varied from 1.5 to 50 nM while holding AcCoA constant at 3 µM, and in the second set AcCoA was varied from 15.6 nM to 1 µM while holding H3 peptide constant at 50 nM. Reactions were performed in duplicate and data were fitted to determine the kind of inhibition.

5.10 His-FLAG-SETD8 expression and purification

The DNA sequence encoding human SETD8 (residues 51-383) was cloned as His-FLAG fusion protein into the pET-28 b (+) vector. The vector, generously provided by D. Reinberg, was transformed into BLR(DE3)*pLysS* competent cells and the protein was overexpressed in 1 L of LB at 37 °C by the addition of 0.1 mM IPTG when the $OD_{600}= 0.6$. After 6 h at 25 °C, the cells harbouring the expressed protein were pelleted at 5000g for 15 min at 4 °C and resuspended in 40 mL of Lysis Buffer (Tris HCl 50 mM pH 8, NaCl 100 mM, DTT 0.1 mM), adding protease inhibitors cocktail (Sigma). Cells were lysed using a sonicator (Vibra-Cells, Sonics) and cell debris were pelleted at 10000g for 30 min at 4 °C. The clarified lysate was filtered using a 0,45 µm syringe filter and loaded onto a 1-mL HisTrap HP column (GE Healthcare, # 17-5247-01) using an AKTA FPLC (GE Healthcare) at the flow rate of 1 mL/min. The protein was eluted using the elution buffer (Phosphate Buffer 20 mM pH 7.4, NaCl 0.5 M, Imidazole 0.5 M) over 10 column volumes. Fractions containing the protein

were confirmed by sodium dodecyl sulfate-polyacrilamide gel electrophoresis (SDS-PAGE) and then pooled.

5.11 SETD8 Labelling and Microscale Thermophoresis experiments

Fluorescence labelling of SETD8 was performed following the protocol for N-hydroxysuccinimide (NHS) coupling of the dye NT647 (NanoTemper Technologies) to lysine residues. Briefly, 100 µL of a 10 µM solution of SETD8 protein in labelling buffer was mixed with 100 µL of 30 µM NT647-NHS fluorophore (NanoTemper Technologies) in labelling buffer and incubated for 30 min at room temperature (RT). Unbound fluorophores were removed by size-exclusion chromatography with MST buffer (50 mM Tris, pH 7.8, 150 mM NaCl, 10 mM MgCl$_2$) as running buffer. The degree of labelling was determined using extinction coefficients ε_{280} = 20800 M^{-1} cm^{-1} for SETD8 and ε_{653} = 250000 M^{-1} cm^{-1} for the NT647 fluorophore.

Prior to MST experiment, aliquots of NT647-SETD8 were thawed on ice and centrifuged for 15 min at 4 °C and 12000g to remove protein aggregates.

A Monolith NT.115 (NanoTemper Technologies) was used to measure equilibrium binding between SETD8 and EPI-009. Standard treated capillaries were obtained from NanoTemper Technologies. The sample tray format allowed to process automatically up to 16 capillaries for Kd determination in one experiment. Measurements were performed at 80% LED and 80% MST power.

For Kd determination, the non-fluorescent binding EPI-009 was titrated (highest concentration 500 µM) against a fixed concentration of 100 nM of the fluorescent partner SETD8. After preparing the serial dilution, samples were loaded into MST capillaries. Capillary scan control led to constant initial fluorescence intensity in the 16 capillaries throughout the titration series. After the measurement, the MO analysis software calculates the extent of binding by plotting the ratio between the fluorescence when the laser is on and the

fluorescence before the laser is turned on. The software automatically calculated the Kd by using the mass action equation via the NanoTemper tool.

5.12 SETD8 cloning in pGEX-4T-1

SETD8 nucleotide sequence from pET-28 b (+) was amplified by PCR, using the designed following primers:

BamHI

5'-ataggatccaagccctccgcggtg-3'   oligo FW-SETD8

XhoI

5'-atactcgagctaatgcttcagccacgg-3'   oligo REV-SETD8

The PCR reaction was carried out in a final volume of 50 µL, using 0.5 µL of vector, 1 µL of each primer (FW and REV) 10 µM, 1 µL of dNTPs 10 mM, 0,25 µL of Taq Polimerase (1U/ µL), using the following amplification program:

- 2 min 95 °C

  30 sec 95 °C
- 30 sec 65 °C   X 30 cycles
  1 min 72 °C

- 15 min 72 °C

To facilitate the cloning in the expression vector pGEX-4-T1, we used a cloning vector pGEM-T (Promega, # A1360): this linearized vector has a single 3´-terminal thymidine at both ends. The T-overhangs at the insertion site greatly improve the efficiency of ligation of PCR products by preventing recircularization of the vector. The ligase reaction was performed in a final volume of 10 µL, incubating the DNA of SETD8 and the vector with a molar ratio of 1:1 for 1h at 25 °C. For the ligase reaction it was used 1 µL of T4 DNA ligase (3 Weiss units/ µl) (Promega, # A1360) and 5 µL of Ligation buffer mix 2 X (Promega, # A1360). 1 µL of the ligase product was transformed into 50 µL JM109 high-efficiency competent cells (Promega, # L2001) with the heat-shock

method. Briefly, the mixture plasmidic DNA-competent cells were incubated for 30 minutes on ice, subsequently the cells were heat shocked for 45 sec at 42°C and then incubated for 2 min on ice. LB medium was then added to reach a final volume of 1 mL and the cells were incubated at 37 °C for 1h, the suspension was plated out on LB/ampicillin/IPTG/X-Gal agar plates. Blue/white screening allowed to identify recombinant colonies, after an incubation of the agar plates at 37 °C overnight.

The recombinant colonies were amplified and the plasmidic DNA was purified by Mini-Prep, afterwards the plasmid was digested by incubating it for 2 h at 37 °C with the restriction enzymes BamHI and XhoI, in order to separate the SETD8 DNA from the vector. After the digestion, the sample was loaded on an agarose gel and the electrophoresis of the DNA fragments was performed in order to separate the band of interest (SETD8). Then, this band was excised out from the agarose gel and placed into a dialysis bag with some TAE buffer. The bag was then placed into a gel box (also containing the same buffer) and an electric current of 100 V was applied. After the release of Ethidium Bromide from the dialysis bag, the solution inside the bag was removed and the DNA was precipitated from the solution by the addition of 3 volumes of ethanol and 1/10 of Sodium Acetate and storing the sample at -80 °C for 30 minutes. The sample was centrifuged at high speed and the pellet obtained air dried, then resuspended in 10 mM Tris HCl pH 8.0.

The DNA purified by electroelution was then used for a ligase reaction with the expression vector pGEX-4T-1, incubating them at 16 °C overnight. The ligase product was then transformed with the heat-shock method (as previously reported) in JM109 competent cells, the colonies obtained were amplified and the plasmidic DNA purified to detect the recombinant ones. Finally, the DNA of a single recombinant colony was transformed into BLR(DE3)*pLysS* competent cells to overexpress the protein.

5.13 GST-SETD8 Expression and Purification

The vector pGEX-4T-1 transformed into BLR(DE3)*pLysS* competent cells allowed the overexpression of the protein in 1 L of LB at 37 °C by the addition of 0.1 mM IPTG when the $OD_{600}= 0.6$. After 2 h at 37 °C, the cells harbouring the expressed protein were pelleted at $5000g$ for 15 min at 4 °C and resuspended in 40 mL of Lysis Buffer (Tris HCl 50 mM pH 8, NaCl 100 mM, DTT 0.1 mM), adding protease inhibitors cocktail (Sigma). Cells were lysed using a sonicator (Vibra-Cells, Sonics) and cell debris were pelleted at $10000g$ for 30 min at 4 °C. The clarified lysate was filtered using a 0.45 μm syringe filter and loaded onto a 1-mL GSTrap HP column (GE Healthcare, # 17-5281-01) using an AKTA FPLC (GE Healthcare) at the flow rate of 1 mL/min. GST-SETD8 was eluted using the elution buffer (Tris HCl 50 mM pH 8.0, glutathione reduced 10 mM) over 10 column volumes. Fractions containing the protein were confirmed by sodium dodecyl sulfate-polyacrilamide gel electrophoresis (SDS-PAGE) and then pooled.

5.14 GST-SETD8 Thrombin Cleavage

The cleavage of GST was performed using ThrombinCleanCleavage Kit (Sigma, # RECOMT), following the procedure of the technical datasheet. Each cleavage experiment was performed using 1 mg of GST-SETD8 in a final volume of 1 mL. 100 μL aliquot of a 50% (v/v) suspension of thrombin agarose resin was centrifuged at $500g$ and washed three times with 500 μL of Cleavage Buffer 1X, afterwards the resin was resuspended in 100 μL of Cleavage Buffer 10X, 1 mg of the protein was added and the final volume of 1 mL was reached with water. The cleavage reaction was incubated at two different temperatures (25 °C and 4 °C), with gentle agitation to keep beads in suspension, for different times. Analysis of cleavage reactions was performed by SDS-PAGE.

5.15 AlphaLISA SETD8 assay

The assays were performed in white Optiplate-384 (PerkinElmer, # 6007299) at room temperature in a final volume of 25 μL, using the following Assay Buffer: TrisHCl 50 mM pH 8.5, NaCl 50 mM, $MgCl_2$ 5 mM, DTT 1 mM, BSA 0.01%. His-SETD8 (Active Motif, # 31321) (20 nM, final concentration) and GST-SETD8 (expressed) (50 nM, final concentration) were diluted in Assay Buffer, then a mixture of SAM (Sigma, # A7007) (200 μM, final concentration) and Histone H4 (Active Motif, # 31223) (150 nM, final concentration) was added. The reaction was incubated for 1 h, afterwards it was stopped by adding 5 μL of High Salt Buffer (50 mM Tris-HCl pH 7.4, 0.1% Tween-20, 1 M NaCl, 0.3% poly-L-lysine). After an incubation of 15 min, a mixture of anti-Histone H4K20me1 Acceptor beads (PerkinElmer, # AL145) and biotinylated anti-H4 antibody (PerkinElmer, # AL146) was prepared in Epigenetic Buffer 1X and added in each well, to reach a final concentration of 20 μg/mL and 1 nM respectively. After an incubation of 1 h, Streptavidin Donor beads (PerkinElmer, # 6760002) were diluted in Epigenetic Buffer 1X and added in each well to reach a final concentration of 20 μg/mL. After 30 minutes of incubation, the Alpha signal was read with the EnSpire Multilabel plate Reader (PerkinElmer). All incubation steps with AlphaScreen beads were performed at room under subdued lighting condition.

5.16 Optimized Conditions for the Gene Reporter System

All transient transfections were carried out using 293-T-REx cells, which were cultured in DMEM high glucose medium supplemented with FBS 10% + 100 U/mL penicillin + 100 μg/mL streptomycin+ Neomicin 200 μg/mL + Blasticidin 5 μg/mL. 200 μL of cells (1.0×10^4) were seeded in 96-well plate and after 48 h the transfection was carried out adding in each well a transfection mix composed by 0.2 μL of Lipofectamine (Invitrogen, # A12621), 100 ng of vector pcDNA™4/TO (GAL4-SETD8) and 25 ng of β-gal for each well (the β-gal

reporter was used as a transfection control), diluted in Opti-MEM (Thermo Fisher). After 6h of incubation at 37 °C, the transfection mix was removed and in each well the growing medium was added, supplemented with 1 µg/mL of Tetracycline to induce SETD8 expression. The cells were incubated for 48 h at 37 °C, afterwards they were harvested, lysed and the lysate was transferred in a white plate for the luminesce assay, using the Kit Dual-Light System (Applied Biosystems, # T1003) and following the procedure reported in the technical datasheet. The luminescent signal was read with the EnSpire Multilabel plate Reader (PerkinElmer) and the levels of luciferase activity were recorded.

5.17 Tudor domains of PHF20 expression, purification and cleavage.

The DNA sequence encoding the Tudor domains of human PHF20 (residues 1-150) was cloned as GST fusion protein into the pGEX-4T-1 vector (GE Healthcare) using *BamHI/AvaI* restriction sites. The vector, generously provided by M. Bedford, was transformed into BLR(DE3)*pLysS* competent cells and the protein was overexpressed in 1 L of LB at 37 °C by the addition of 0.1 mM IPTG when the OD_{600}= 0.6. After 4 h at 37 °C, cells harbouring the expressed protein were pelleted at 5000g for 15 min at 4 °C and resuspended in 40 mL of Lysis Buffer (Tris HCl 50 mM pH 8, NaCl 100 mM, DTT 0.1 mM), adding protease inhibitors cocktail (Sigma). Cells were lysed using a sonicator (Vibra-Cells, Sonics) and cell debris were pelleted at 10000g for 30 min at 4 °C. The clarified lysate was filtered using a 0,45 µm syringe filter and loaded onto a 1-mL GSTrap HP column (GE Healthcare, # 17-5281-01) using an AKTA FPLC (GE Healthcare) at the flow rate of 1 mL/min. GST-protein was eluted using the elution buffer (Tris HCl 50 mM pH 8.0, glutathione reduced 10 mM) over 10 column volumes. Fractions containing the protein were confirmed by sodium dodecyl sulfate-polyacrilamide gel electrophoresis (SDS-PAGE) and then pooled.

The cleavage of GST was performed using ThrombinCleanCleavage Kit (Sigma, # RECOMT), following the procedure of the technical datasheet. Briefly, 100 μL aliquot of a 50% (v/v) suspension of thrombin agarose resin was centrifuged at 500g and washed three times with 500 μL of Cleavage Buffer 1X, afterwards the resin was resuspended in 100 μL of Cleavage Buffer 10X, 1 mg of the protein was added and the final volume of 1 mL was reached with water. The cleavage reaction was incubated at room temperature, with gentle agitation to keep beads suspended, for 6h. Analysis of cleavage reaction was performed by SDS-PAGE. The cleaved protein was then separated from the GST by anionic exchange chromatography using a Mono Q™ column (GE Healthcare, # 17-5166-01): a 1-mL bed volume of Mono Q™ 5/50 GL was equilibrated in buffer A (20 mM Tris-HCl pH 8.0); the cleaved protein was loaded onto the column at 1 mL/min. The column was washed with 5 column volumes of buffer A and eluted with buffer B (20 mM Tris-HCl pH 8.0 + 1 M NaCl), allowing the separation of the native protein from the cleaved GST.

5.18 nanoDSF

Protein thermal stability was measured in a label-free fluorimetric analysis using the Prometheus NT.48 (NanoTemper Technologies). Briefly, the shift of intrinsic tryptophan fluorescence of proteins upon temperature-induced unfolding was monitored by detecting the emission fluorescence at 330 and 350 nm. Thermal unfolding was performed in nanoDSF grade standard glass capillaries (NanoTemper Technologies) at a heating rate of 0.5 °C per minute in a range from 20 °C to 95 °C, using 20 μM of protein and 100 μM of compounds. Protein melting points (Tm) were calculated from the first derivative of the ratio of tryptophan emission intensities at 330 and 350 nm.

5.19 Tudor Alphascreen assay optimization

All AlphaScreen experiments described were performed at room temperature in white 384-well Opti-Plates (PerkinElmer, # 6007299) in a final volume of 25 µL. For the detection of GST fusion protein, the anti-GST coated Acceptor beads (PerkinElmer, # AL110C) were used, while the detection of biotinylated peptide [Lys(Me2)20] - Histone H4 (8 - 30) (Anaspec, # AS-65419-1) was performed using the Streptavidin Donor Beads (PerkinElmer, # 6760002S). Equal concentrations of Acceptor beads and Donor beads were used in every experiments (5 µg/mL final concentration of each bead). All incubation steps with AlphaScreen beads were performed at room temperature for 1 h under subdued lighting conditions, and finally, the assay plates were read in an EnSpire Multilabel plate reader (PerkinElmer).

The effect of UNC1215 analogues on Tudor activity was determined at a fixed 100 µM concentration, incubating the compounds with 25 nM of the protein and 100 nM of the substrate in reaction buffer (TrisHCl 20 mM pH 8.0, NaCl 25 mM, Tween20 0.05%) for 2 h.

ACKNOWLEDGMENTS

three years. For all the enthusiasm that we put in our work and the daily encouragements. Thanks to Roberta and Raffaella for the support, the endless conversations and for all the laughs together. Thanks to Vincenzo for his help in the PHF20 project and for the ability to tolerate my bad moods and my sound advices. Thanks to Donatella for all the tea times, the laughs, for being above all a good friend. Thanks to Ciro, for being always on my side and for his endless support.

Alessandra

REFERENCES

1.   Blancafort, P.; Jin, J.; Frye, S. Writing and Rewriting the Epigenetic Code of Cancer Cells: From Engineered Proteins to Small Molecules. *Molecular Pharmacology* **2013,** 83, 563-576.

2.   Musselman, C. A.; Lalonde, M.-E.; Côté, J.; Kutateladze, T. G. Perceiving the epigenetic landscape through histone readers. *Nature structural & molecular biology* **2012,** 19, 1218-1227.

3.   Simó-Riudalbas, L.; Esteller, M. Targeting the histone orthography of cancer: drugs for writers, erasers and readers. *British Journal of Pharmacology* **2015,** 172, 2716-2732.

4.   Hodawadekar, S. C.; Marmorstein, R. Chemistry of acetyl transfer by histone modifying enzymes: structure, mechanism and implications for effector design. *Oncogene* **2000,** 26, 5528-5540.

5.   Avvakumov, N.; Cote, J. The MYST family of histone acetyltransferases and their intimate links to cancer. *Oncogene* **2000,** 26, 5395-5407.

6.   Dancy, B. M.; Cole, P. A. Protein Lysine Acetylation by p300/CBP. *Chemical Reviews* **2015,** 115, 2419-2452.

7.   Castellano, S.; Milite, C.; Feoli, A.; Viviano, M.; Mai, A.; Novellino, E.; Tosco, A.; Sbardella, G. Identification of Structural Features of 2-Alkylidene-1,3-Dicarbonyl Derivatives that Induce Inhibition and/or Activation of Histone Acetyltransferases KAT3B/p300 and KAT2B/PCAF. *ChemMedChem* **2015,** 10, 144-157.

8.   Milite, C.; Feoli, A.; Sasaki, K.; La Pietra, V.; Balzano, A. L.; Marinelli, L.; Mai, A.; Novellino, E.; Castellano, S.; Tosco, A.; Sbardella, G. A Novel Cell-Permeable, Selective, and Noncompetitive Inhibitor of KAT3 Histone Acetyltransferases from a Combined Molecular Pruning/Classical Isosterism Approach. *Journal of Medicinal Chemistry* **2015,** 58, 2779-2798.

9.   Balasubramanyam, K.; Swaminathan, V.; Ranganathan, A.; Kundu, T. K. Small Molecule Modulators of Histone Acetyltransferase p300. *Journal of Biological Chemistry* **2003,** 278, 19134-19140.

10.   Balasubramanyam, K.; Altaf, M.; Varier, R. A.; Swaminathan, V.; Ravindran, A.; Sadhale, P. P.; Kundu, T. K. Polyisoprenylated Benzophenone,

Garcinol, a Natural Histone Acetyltransferase Inhibitor, Represses Chromatin Transcription and Alters Global Gene Expression. *Journal of Biological Chemistry* **2004,** 279, 33716-33726.

11.   Balasubramanyam, K.; Varier, R. A.; Altaf, M.; Swaminathan, V.; Siddappa, N. B.; Ranga, U.; Kundu, T. K. Curcumin, a Novel p300/CREB-binding Protein-specific Inhibitor of Acetyltransferase, Represses the Acetylation of Histone/Nonhistone Proteins and Histone Acetyltransferase-dependent Chromatin Transcription. *Journal of Biological Chemistry* **2004,** 279, 51163-51171.

12.   Ravindra, K. C.; Selvi, B. R.; Arif, M.; Reddy, B. A. A.; Thanuja, G. R.; Agrawal, S.; Pradhan, S. K.; Nagashayana, N.; Dasgupta, D.; Kundu, T. K. Inhibition of Lysine Acetyltransferase KAT3B/p300 Activity by a Naturally Occurring Hydroxynaphthoquinone, Plumbagin. *Journal of Biological Chemistry* **2009,** 284, 24453-24464.

13.   Lau, O. D.; Kundu, T. K.; Soccio, R. E.; Ait-Si-Ali, S.; Khalil, E. M.; Vassilev, A.; Wolffe, A. P.; Nakatani, Y.; Roeder, R. G.; Cole, P. A. HATs off: Selective Synthetic Inhibitors of the Histone Acetyltransferases p300 and PCAF. *Molecular Cell* **2000,** 5, 589-595.

14.   Bowers, E. M.; Yan, G.; Mukherjee, C.; Orry, A.; Wang, L.; Holbert, M. A.; Crump, N. T.; Hazzalin, C. A.; Liszczak, G.; Yuan, H.; Larocca, C.; Saldanha, S. A.; Abagyan, R.; Sun, Y.; Meyers, D. J.; Marmorstein, R.; Mahadevan, L. C.; Alani, R. M.; Cole, P. A. Virtual Ligand Screening of the p300/CBP Histone Acetyltransferase: Identification of a Selective Small Molecule Inhibitor. *Chemistry & biology* **2010,** 17, 471-482.

15.   Mantelingu, K.; Reddy, B. A. A.; Swaminathan, V.; Kishore, A. H.; Siddappa, N. B.; Kumar, G. V. P.; Nagashankar, G.; Natesh, N.; Roy, S.; Sadhale, P. P.; Ranga, U.; Narayana, C.; Kundu, T. K. Specific Inhibition of p300-HAT Alters Global Gene Expression and Represses HIV Replication. *Chemistry & Biology* **2007,** 14, 645-657.

16.   Arif, M.; Pradhan, S. K.; G R, T.; Vedamurthy, B. M.; Agrawal, S.; Dasgupta, D.; Kundu, T. K. Mechanism of p300 Specific Histone Acetyltransferase Inhibition by Small Molecules. *Journal of Medicinal Chemistry* **2009,** 52, 267-277.
17.   Martinez-Balbás, M. A.; Bannister, A. J.; Martin, K.; Haus-Seuffert, P.; Meisterernst, M.; Kouzarides, T. The acetyltransferase activity of CBP stimulates transcription. *The EMBO Journal* **1998,** 17, 2886-2893.

18.   Ogryzko, V. V.; Schiltz, R. L.; Russanova, V.; Howard, B. H.; Nakatani, Y. The Transcriptional Coactivators p300 and CBP Are Histone Acetyltransferases. *Cell* **1996,** 87, 953-959.

19.   Liu, X.; Wang, L.; Zhao, K.; Thompson, P. R.; Hwang, Y.; Marmorstein, R.; Cole, P. A. The structural basis of protein acetylation by the p300/CBP transcriptional coactivator. *Nature* **2008,** 451, 846-850.

20.   Copeland, R. A. Molecular Pathways: Protein Methyltransferases in Cancer. *Clinical Cancer Research* **2013,** 19, 6344-6350.

21.   Hamamoto, R.; Nakamura, Y. Dysregulation of protein methyltransferases in human cancer: An emerging target class for anticancer therapy. *Cancer Science* **2016**, n/a-n/a.

22.   Patel, A.; Vought, V. E.; Dharmarajan, V.; Cosgrove, M. S. A Novel Non-SET Domain Multi-subunit Methyltransferase Required for Sequential Nucleosomal Histone H3 Methylation by the Mixed Lineage Leukemia Protein-1 (MLL1) Core Complex. *Journal of Biological Chemistry* **2011,** 286, 3359-3369.

23.   Zhang, X.; Wen, H.; Shi, X. Lysine methylation: beyond histones. *Acta Biochimica et Biophysica Sinica* **2012,** 44, 14-27.

24.   Kaniskan, H. Ü.; Jin, J. Chemical Probes of Histone Lysine Methyltransferases. *ACS Chemical Biology* **2015,** 10, 40-50.

25.   Del Rizzo, P. A.; Trievel, R. C. Molecular basis for substrate recognition by lysine methyltransferases and demethylases. *Biochimica et Biophysica Acta (BBA) - Gene Regulatory Mechanisms* **2014,** 1839, 1404-1415.

26.   Nishioka, K.; Rice, J. C.; Sarma, K.; Erdjument-Bromage, H.; Werner, J.; Wang, Y.; Chuikov, S.; Valenzuela, P.; Tempst, P.; Steward, R.; Lis, J. T.; Allis, C. D.; Reinberg, D. PR-Set7 Is a Nucleosome-Specific Methyltransferase that Modifies Lysine 20 of Histone H4 and Is Associated with Silent Chromatin. *Molecular Cell* **2002,** 9, 1201-1213.

27.   Wu, S.; Rice, J. C. A new regulator of the cell cycle: the PR-Set7 histone methyltransferase. *Cell cycle (Georgetown, Tex.)* **2011,** 10, 68-72.
28.   Beck, D. B.; Burton, A.; Oda, H.; Ziegler-Birling, C.; Torres-Padilla, M.-E.; Reinberg, D. The role of PR-Set7 in replication licensing depends on Suv4-20h. *Genes & Development* **2012,** 26, 2580-2589.

29.   Blum, G.; Ibáñez, G.; Rao, X.; Shum, D.; Radu, C.; Djaballah, H.; Rice, J. C.; Luo, M. Small-Molecule Inhibitors of SETD8 with Cellular Activity. *ACS Chemical Biology* **2014,** 9, 2471-2478.

30.   Ma, A.; Yu, W.; Xiong, Y.; Butler, K. V.; Brown, P. J.; Jin, J. Structure-activity relationship studies of SETD8 inhibitors. *MedChemComm* **2014,** 5, 1892-1898.

31.   Ma, A.; Yu, W.; Li, F.; Bleich, R. M.; Herold, J. M.; Butler, K. V.; Norris, J. L.; Korboukh, V.; Tripathy, A.; Janzen, W. P.; Arrowsmith, C. H.; Frye, S. V.; Vedadi, M.; Brown, P. J.; Jin, J. Discovery of a Selective, Substrate-Competitive Inhibitor of the Lysine Methyltransferase SETD8. *Journal of Medicinal Chemistry* **2014,** 57, 6822-6833.

32.   Valente, S.; Lepore, I.; Dell'Aversana, C.; Tardugno, M.; Castellano, S.; Sbardella, G.; Tomassi, S.; Di Maro, S.; Novellino, E.; Di Santo, R.; Costi, R.; Altucci, L.; Mai, A. Identification of PR-SET7 and EZH2 selective inhibitors inducing cell death in human leukemia U937 cells. *Biochimie* **2012,** 94, 2308-2313.

33.   Williams, D. E.; Dalisay, D. S.; Li, F.; Amphlett, J.; Maneerat, W.; Chavez, M. A. G.; Wang, Y. A.; Matainaho, T.; Yu, W.; Brown, P. J.; Arrowsmith, C. H.; Vedadi, M.; Andersen, R. J. Nahuoic Acid A Produced by a Streptomyces sp. Isolated From a Marine Sediment Is a Selective SAM-Competitive Inhibitor of the Histone Methyltransferase SETD8. *Organic Letters* **2013,** 15, 414-417.

34.   Grant, S.; Easley, C.; Kirkpatrick, P. Vorinostat. *Nat Rev Drug Discov* **2007,** 6, 21-22.

35.   Bertino, E. M.; Otterson, G. A. Romidepsin: a novel histone deacetylase inhibitor for cancer. *Expert Opinion on Investigational Drugs* **2011,** 20, 1151-1158.

36.   Sawas, A.; Radeski, D.; O'Connor, O. A. Belinostat in patients with refractory or relapsed peripheral T-cell lymphoma: a perspective review. *Therapeutic Advances in Hematology* **2015,** 6, 202-208.

37.   Libby, E. N.; Becker, P. S.; Burwick, N.; Green, D. J.; Holmberg, L.; Bensinger, W. I. Panobinostat: a review of trial results and future prospects in multiple myeloma. *Expert Review of Hematology* **2015,** 8, 9-18.

38.   Filippakopoulos, P.; Knapp, S. Targeting bromodomains: epigenetic readers of lysine acetylation. *Nat Rev Drug Discov* **2014,** 13, 337-356.

39.   Patel, D. J.; Wang, Z. Readout of Epigenetic Modifications. *Annual Review of Biochemistry* **2013,** 82, 81-118.

40.   Taverna, S. D.; Li, H.; Ruthenburg, A. J.; Allis, C. D.; Patel, D. J. How chromatin-binding modules interpret histone modifications: lessons from professional pocket pickers. *Nat Struct Mol Biol* **2007,** 14, 1025-1040.

41.   Chen, C.; Nott, T. J.; Jin, J.; Pawson, T. Deciphering arginine methylation: Tudor tells the tale. *Nat Rev Mol Cell Biol* **2011,** 12, 629-642.

42.   Cui, G.; Park, S.; Badeaux, A. I.; Kim, D.; Lee, J.; Thompson, J. R.; Yan, F.; Kaneko, S.; Yuan, Z.; Botuyan, M. V.; Bedford, M. T.; Cheng, J. Q.; Mer, G. PHF20 is an effector protein of p53 double lysine methylation that stabilizes and activates p53. *Nat Struct Mol Biol* **2012,** 19, 916-924.

43.   Adams-Cioaba, M. A.; Li, Z.; Tempel, W.; Guo, Y.; Bian, C.; Li, Y.; Lam, R.; Min, J. Crystal structures of the Tudor domains of human PHF20 reveal novel structural variations on the Royal Family of proteins. *FEBS Letters* **2012,** 586, 859-865.

44.   Pande, V. Understanding the Complexity of Epigenetic Target Space. *Journal of Medicinal Chemistry* **2016**.

45.   Campbell, R. M.; Tummino, P. J. Cancer epigenetics drug discovery and development: the challenge of hitting the mark. *The Journal of clinical investigation* **2014,** 124, 64-69.

46.   Holdgate, G.; Geschwindner, S.; Breeze, A.; Davies, G.; Colclough, N.; Temesi, D.; Ward, L. Biophysical Methods in Drug Discovery from Small Molecule to Pharmaceutical. In *Protein-Ligand Interactions*, Williams, M. A.; Daviter, T., Eds. Humana Press: **2013**; Vol. 1008, pp 327-355.

47.   Nguyen, H.; Park, J.; Kang, S.; Kim, M. Surface Plasmon Resonance: A Versatile Technique for Biosensor Applications. *Sensors* **2015,** 15, 10481.

48.   Cooper, M. A. Optical biosensors in drug discovery. *Nat Rev Drug Discov* **2002,** 1, 515-528.

49.   Neumann, T.; Junker, H. D.; Schmidt, K.; Sekul, R. SPR-based Fragment Screening: Advantages and Applications. *Current Topics in Medicinal Chemistry* **2007,** 7, 1630-1642.

50.   Grøftehauge, M. K.; Hajizadeh, N. R.; Swann, M. J.; Pohl, E. Protein–ligand interactions investigated by thermal shift assays (TSA) and dual polarization interferometry (DPI). *Acta Crystallographica Section D* **2015,** 71, 36-44.

51.   Zhang, R.; Monsma, F. Fluorescence-based thermal shift assays. *Current opinion in drug discovery & development* **2010,** 13, 389-402.

52.   Alexander, C. G.; Wanner, R.; Johnson, C. M.; Breitsprecher, D.; Winter, G.; Duhr, S.; Baaske, P.; Ferguson, N. Novel microscale approaches for easy, rapid determination of protein stability in academic and commercial settings. *Biochimica et Biophysica Acta (BBA) - Proteins and Proteomics* **2014,** 1844, 2241-2250.

53.   Seidel, S. A. I.; Dijkman, P. M.; Lea, W. A.; van den Bogaart, G.; Jerabek-Willemsen, M.; Lazic, A.; Joseph, J. S.; Srinivasan, P.; Baaske, P.; Simeonov, A.; Katritch, I.; Melo, F. A.; Ladbury, J. E.; Schreiber, G.; Watts, A.; Braun, D.; Duhr, S. Microscale thermophoresis quantifies biomolecular interactions under previously challenging conditions. *Methods* **2013,** 59, 301-315.

54.   Jerabek-Willemsen, M.; André, T.; Wanner, R.; Roth, H. M.; Duhr, S.; Baaske, P.; Breitsprecher, D. MicroScale Thermophoresis: Interaction analysis and beyond. *Journal of Molecular Structure* **2014,** 1077, 101-113.

55.   Bisswanger, H. Enzyme assays. *Perspectives in Science* **2014,** 1, 41-55.

56.   Acker, M. G.; Auld, D. S. Considerations for the design and reporting of enzyme assays in high-throughput screening applications. *Perspectives in Science* **2014,** 1, 56-73.

57.   Reymond, J.-L.; Flux, V. S.; Maillard, N. l. Enzyme assays. *Chemical Communications* **2008**, 34-46.

58.   Eglen, R. M.; Reisine, T.; Roby, P.; Rouleau, N.; Illy, C.; Bossé, R.; Bielefeld, M. The use of AlphaScreen technology in HTS: current status. *Current chemical genomics*, **2008**, 1, 2-10.

59.   Wagner, E. K.; Albaugh, B. N.; Denu, J. M. Chapter Eight - High-Throughput Strategy to Identify Inhibitors of Histone-Binding Domains. In *Methods in Enzymology*, Carl, W.; Allis, C. D., Eds. Academic Press: 2012; Vol. Volume 512, pp 161-185.

60.   Taouji, S.; Dahan, S.; Bosse, R.; Chevet, E. Current Screens Based on the AlphaScreen Technology for Deciphering Cell Signalling Pathways. *Current Genomics* **2009,** 10, 93-101.

61.   Dal Piaz, F.; Tosco, A.; Eletto, D.; Piccinelli, A. L.; Moltedo, O.; Franceschelli, S.; Sbardella, G.; Remondelli, P.; Rastrelli, L.; Vesci, L.; Pisano, C.; De Tommasi, N. The Identification of a Novel Natural Activator of p300 Histone Acetyltranferase Provides New Insights into the Modulation Mechanism of this Enzyme. *ChemBioChem* **2010,** 11, 818-827.

62.   Milite, C.; Castellano, S.; Benedetti, R.; Tosco, A.; Ciliberti, C.; Vicidomini, C.; Boully, L.; Franci, G.; Altucci, L.; Mai, A.; Sbardella, G. Modulation of the activity of histone acetyltransferases by long chain alkylidenemalonates (LoCAMs). *Bioorganic & Medicinal Chemistry* **2011,** 19, 3690-3701.

63.   Sbardella, G.; Castellano, S.; Vicidomini, C.; Rotili, D.; Nebbioso, A.; Miceli, M.; Altucci, L.; Mai, A. Identification of long chain alkylidenemalonates as novel small molecule modulators of histone acetyltransferases. *Bioorganic & Medicinal Chemistry Letters* **2008,** 18, 2788-2792.

64.   Colussi, C.; Rosati, J.; Straino, S.; Spallotta, F.; Berni, R.; Stilli, D.; Rossi, S.; Musso, E.; Macchi, E.; Mai, A.; Sbardella, G.; Castellano, S.; Chimenti, C.; Frustaci, A.; Nebbioso, A.; Altucci, L.; Capogrossi, M. C.; Gaetano, C. N(ε)-lysine acetylation determines dissociation from GAP junctions and lateralization of connexin 43 in normal and dystrophic heart. *Proceedings of the National Academy of Sciences of the United States of America* **2011,** 108, 2795-2800.

65.   Wei, W.; Coelho, C. M.; Li, X.; Marek, R.; Yan, S.; Anderson, S.; Meyers, D.; Mukherjee, C.; Sbardella, G.; Castellano, S.; Milite, C.; Rotili, D.; Mai, A.; Cole, P. A.; Sah, P.; Kobor, M. S.; Bredy, T. W. p300/CBP-associated factor selectively regulates the extinction of conditioned fear. *The Journal of neuroscience : the official journal of the Society for Neuroscience* **2012,** 32, 11930-11941.

66.   Vecellio, M.; Spallotta, F.; Nanni, S.; Colussi, C.; Cencioni, C.; Derlet, A.; Bassetti, B.; Tilenni, M.; Carena, M. C.; Farsetti, A.; Sbardella, G.; Castellano, S.; Mai, A.; Martelli, F.; Pompilio, G.; Capogrossi, M. C.; Rossini, A.; Dimmeler, S.; Zeiher, A.; Gaetano, C. The Histone Acetylase Activator Pentadecylidenemalonate 1b Rescues Proliferation and Differentiation in the Human Cardiac Mesenchymal Cells of Type 2 Diabetic Patients. *Diabetes* **2014,** 63, 2132-2147.

67.   Milite, C.; Viviano, M.; Santoriello, M.; Arico, F.; Sbardella, G.; Castellano, S. Straightforward, metal-free, and stereoselective synthesis of 9-oxo- and 10-hydroxy-2(E)-decenoic acids, important components of honeybee (Apis mellifera) secretions. *RSC Advances* **2012,** 2, 5229-5233.

68.   Cernuchova, P.; Vo-Thanh, G.; Milata, V.; Loupy, A. Solvent-free synthesis of quinolone derivatives. *Heterocycles* **2004,** 64, 177-191.

69.   Navratilova, I.; Hopkins, A. L. Fragment Screening by Surface Plasmon Resonance. *ACS Medicinal Chemistry Letters* **2010,** 1, 44-48.

70.   Castellano, S.; Spannhoff, A.; Milite, C.; Dal Piaz, F.; Cheng, D.; Tosco, A.; Viviano, M.; Yamani, A.; Cianciulli, A.; Sala, M.; Cura, V.; Cavarelli, J.; Novellino, E.; Mai, A.; Bedford, M. T.; Sbardella, G. Identification of Small-Molecule Enhancers of Arginine Methylation Catalyzed by Coactivator-Associated Arginine Methyltransferase 1. *Journal of Medicinal Chemistry* **2012,** 55, 9875-9890.

71.   Gao, X.; Lin, J.; Ning, Q.; Gao, L.; Yao, Y.; Zhou, J.; Li, Y.; Wang, L.; Yu, L. A Histone Acetyltransferase p300 Inhibitor C646 Induces Cell Cycle Arrest and Apoptosis Selectively in AML1-ETO-Positive AML Cells. *PLoS ONE* **2013,** 8, e55481.

72.   Mateo, F.; Vidal-Laliena, M.; Canela, N.; Zecchin, A.; Martínez-Balbás, M.; Agell, N.; Giacca, M.; Pujol, M. J.; Bachs, O. The transcriptional co-activator PCAF regulates cdk2 activity. *Nucleic Acids Research* **2009,** 37, 7072-7084.

73.   Sun, P.-C.; Tzao, C.; Chen, B.-H.; Liu, C.-W.; Yu, C.-P.; Jin, J.-S. Suberoylanilide hydroxamic acid induces apoptosis and sub-G1 arrest of 320 HSR colon cancer cells. *Journal of Biomedical Science* **2010,** 17, 76.

74.   Zhao, X.; Yang, W.; Shi, C.; Ma, W.; Liu, J.; Wang, Y.; Jiang, G. The G1 phase arrest and apoptosis by intrinsic pathway induced by valproic acid inhibit proliferation of BGC-823 gastric carcinoma cells. *Tumor Biology* **2011,** 32, 335-346.

75.   Richon, V. M.; Emiliani, S.; Verdin, E.; Webb, Y.; Breslow, R.; Rifkind, R. A.; Marks, P. A. A class of hybrid polar inducers of transformed cell differentiation inhibits histone deacetylases. *Proceedings of the National Academy of Sciences of the United States of America* **1998,** 95, 3003-3007.

76.   LeRoy, G.; DiMaggio, P. A.; Chan, E. Y.; Zee, B. M.; Blanco, M. A.; Bryant, B.; Flaniken, I. Z.; Liu, S.; Kang, Y.; Trojer, P.; Garcia, B. A. A quantitative atlas of histone modification signatures from human cancer cells. *Epigenetics & Chromatin* **2013,** 6, 20-20.

77.   Poux, A. N.; Cebrat, M.; Kim, C. M.; Cole, P. A.; Marmorstein, R. Structure of the GCN5 histone acetyltransferase bound to a bisubstrate inhibitor. *Proceedings of the National Academy of Sciences of the United States of America* **2002,** 99, 14065-14070.

78.   Pinacho Crisóstomo, F. R.; Carrillo, R.; León, L. G.; Martín, T.; Padrón, J. M.; Martín, V. S. Molecular Simplification in Bioactive Molecules: Formal Synthesis of (+)-Muconin. *The Journal of Organic Chemistry* **2006,** 71, 2339-2345.

79.   Dreassi, E.; Zizzari, A. T.; Falchi, F.; Schenone, S.; Santucci, A.; Maga, G.; Botta, M. Determination of permeability and lipophilicity of pyrazolo-pyrimidine tyrosine kinase inhibitors and correlation with biological data. *European Journal of Medicinal Chemistry* **2009,** 44, 3712-3717.

80.   Clemons, K.; Kretsch, A.; Verbeck, G. Parallel artificial membrane permeability assay for blood-brain permeability determination of illicit drugs and synthetic analogues. *Science and Justice* **2014,** 54, 351-355.

81.   Dancy, B. M.; Crump, N. T.; Peterson, D. J.; Mukherjee, C.; Bowers, E. M.; Ahn, Y.-H.; Yoshida, M.; Zhang, J.; Mahadevan, L. C.; Meyers, D. J.; Boeke, J. D.; Cole, P. A. Live cell studies of p300/CBP histone acetyltransferase activity and inhibition. *Chembiochem : a European journal of chemical biology* **2012,** 13, 2113-2121.

82.   Yan, G.; Eller, M. S.; Elm, C.; Larocca, C. A.; Ryu, B.; Panova, I. P.; Dancy, B. M.; Bowers, E. M.; Meyers, D.; Lareau, L.; Cole, P. A.; Taverna, S. D.; Alani, R. M. Selective Inhibition of p300 HAT Blocks Cell Cycle Progression, Induces Cellular Senescence and Inhibits the DNA Damage Response in Melanoma Cells. *The Journal of investigative dermatology* **2013,** 133, 2444-2452.

83.   Iyer, N. G.; Xian, J.; Chin, S. F.; Bannister, A. J.; Daigo, Y.; Aparicio, S.; Kouzarides, T.; Caldas, C. p300 is required for orderly G1//S transition in human cancer cells. *Oncogene* **2006,** 26, 21-29.

84.   Simola, D. F.; Graham, R. J.; Brady, C. M.; Enzmann, B. L.; Desplan, C.; Ray, A.; Zwiebel, L. J.; Bonasio, R.; Reinberg, D.; Liebig, J.; Berger, S. L.

Epigenetic (re)programming of caste-specific behavior in the ant Camponotus floridanus. *Science* **2016,** 351.

85.   Copeland, R. A.; Solomon, M. E.; Richon, V. M. Protein methyltransferases as a target class for drug discovery. *Nat Rev Drug Discov* **2009,** 8, 724-732.

86.   Cheng, D.; Yadav, N.; King, R. W.; Swanson, M. S.; Weinstein, E. J.; Bedford, M. T. Small Molecule Regulators of Protein Arginine Methyltransferases. *Journal of Biological Chemistry* **2004,** 279, 23892-23899.
87.   Ragno, R.; Simeoni, S.; Castellano, S.; Vicidomini, C.; Mai, A.; Caroli, A.; Tramontano, A.; Bonaccini, C.; Trojer, P.; Bauer, I.; Brosch, G.; Sbardella, G. Small Molecule Inhibitors of Histone Arginine Methyltransferases: Homology Modeling, Molecular Docking, Binding Mode Analysis, and Biological Evaluations. *Journal of Medicinal Chemistry* **2007,** 50, 1241-1253.
88.   Castellano, S.; Milite, C.; Ragno, R.; Simeoni, S.; Mai, A.; Limongelli, V.; Novellino, E.; Bauer, I.; Brosch, G.; Spannhoff, A.; Cheng, D.; Bedford, Mark T.; Sbardella, G. Design, Synthesis and Biological Evaluation of Carboxy Analogues of Arginine Methyltransferase Inhibitor 1 (AMI-1). *ChemMedChem* **2010,** 5, 398-414.

89.   Reinberg, D.; Trojer, P.; Sbardella, G. Naphthalenecarboxylic acids and related compounds as selective inhibitors for transferases and their preparation. WO2007149782A2, **2007**.

90.   Young, C. L.; Britton, Z. T.; Robinson, A. S. Recombinant protein expression and purification: A comprehensive review of affinity tags and microbial applications. *Biotechnology Journal* **2012,** 7, 620-634.

91.   Waugh, D. S. Making the most of affinity tags. *Trends in Biotechnology* **2005,** 23, 316-320.

92.   Malhotra, A. Chapter 16 Tagging for Protein Expression. In *Methods in Enzymology*, Richard, R. B.; Murray, P. D., Eds. Academic Press: **2009**; Volume 463, pp 239-258.

93.   Costa, S.; Almeida, A.; Castro, A.; Domingues, L. Fusion tags for protein solubility, purification and immunogenicity in Escherichia coli: the novel Fh8 system. *Frontiers in Microbiology* **2014,** 5, 63.

94.   England, C. G.; Luo, H.; Cai, W. HaloTag Technology: A Versatile Platform for Biomedical Applications. *Bioconjugate Chemistry* **2015,** 26, 975-986.

95.   James, L. I.; Barsyte-Lovejoy, D.; Zhong, N.; Krichevsky, L.; Korboukh, V. K.; Herold, M. J.; MacNevin, C. J.; Norris, J. L.; Sagum, C. A.; Tempel, W.; Marcon, E.; Guo, H.; Gao, C.; Huang, X.-P.; Duan, S.; Emili, A.; Greenblatt, J. F.; Kireev, D. B.; Jin, J.; Janzen, W. P.; Brown, P. J.; Bedford, M. T.; Arrowsmith, C. H.; Frye, S. V. Discovery of a chemical probe for the L3MBTL3 methyl-lysine reader domain. *Nature chemical biology* **2013,** 9, 184-191.